

ÉCOLE DES PONTS ET CHAUSSÉES

**SUPPLY FUNCTION EQUILIBRIA ON THE ELECTRICITY
MARKET**

THÈSE

pour l'obtention du titre de Docteur en Sciences Économiques
présentée et soutenue publiquement le XXXXXXXXX

par

Alexis BERGÈS

Jury

XXXX, XXXX XXXXXX XXXXXXXX
XXXX, XXXX XXXXXX XXXXXXXX
XXXX, XXXX XXXXXX XXXXXXXX
XXXX, XXXX XXXXXX XXXXXXXX

Remerciements—Acknowledgements

Dedication

XXXXXXXXXXXXXXXXXXXX

XXXXXXXXXXXXXXXXXXXX

Contents

Remerciements—Acknowledgements	i
General introduction	1
Summary	5
Chapter 1: Dynamics of the Electricity Day-Ahead Market : Supply Function Equilibria and Ramping Costs	9
Appendix	30
Chapter 2: Investigating the Impact of Uncertainty on Firms with Dy- namic Costs : A Case Study of the French Electricity Market	35
References	109
List of Figures	112

General introduction:

ℓ

Summary

Chapter 1:

Chapter 2:

Chapter 3:

Chapter 1

Dynamics of the Electricity Day-Ahead Market : Supply Function Equilibria and Ramping Costs

1.1 Introduction

The electricity markets have flourished in Europe during the 1990s during the wave of privatisation. The argument for their creation was one of competition, that was supposed to bring lower prices to the end consumer of electricity.

An important specificity to the economics of electricity is that electricity cannot be stored in large amounts, which in turn implies that at every moment production and consumption have to match. This means that in order to have a working electric grid, that is one that can produce electricity for high levels during the winter and lower levels in summer, one has to have production units ready to be turned on if the demand is high enough, but turned off otherwise. This in turn means that although their existence is required, it is difficult to see how to marginal cost pricing can cover their investment costs, which has been a long running argument in the litterature [Boiteux, 1960].

For this reason, from the very beginning the issue of the market design was deemed to be crucial to insure that the wished for outcome of the privatization wave came to fruition [Green, 1991]. And there has been an active litterature trying to model and measure the market power of oligopolists on these newly created markets [Green and Newbery, 1992, Newbery, 1998, Wolfram, 1998, Green, 1999].

One traditional understanding for the role of markets is that a market allows to aggregate information that would be otherwise dispersed. When applying this view to the electricity markets, the litterature has regarded the existence of the capacity market as a way to aggregate information about sunk costs when building a plant, the existence of the forward market as a way to aggregate information about the fixed costs, and the existence of the spot market as a way to aggregate information about marginal costs.

At the same time, the litterature as well as the industry is well aware of the existence of ramping costs, that is costs that depend on the variation of production. We think that the two spot markets can be understood as aggregating information about marginal costs and ramping costs. In this paper we model the day-ahead market using the supply function equilibria framework and considering that there exists ramping costs. This allows us to obtain unique solutions, in contrast to the usual continuum, and to describe the dynamic evolution of the optimal bid in a symmetric oligopoly. It also opens the possibility to distinguish between day-ahead and intraday markets.

The supply function equilibria litterature has been active since the seminal paper by Klemperer and Meyer in 1989 [Klemperer and Meyer, 1989] (henceforth known as KM).

In the wake of the electricity industry liberalisation, authors, notably Green and Newbery in 1992 [Green and Newbery, 1992], have used this framework to evaluate the expected level of competition and argue for certain regulatory paths.

Groundbreaking and fertile, the original model by KM studied how demand uncertainty collapses dramatically the set of available supply function equilibria to a well defined continuum. This continuum collapses further to a single Nash equilibria by considering an infinite support of demand shocks. All of these equilibria are ex-post optimal, meaning that changes in anticipated demand shocks do not impact the actual solutions, but only the parts of the solutions that are actually explored as shocks realize. In this setup markets are always efficient, a very strong result.

On the electricity day ahead markets, producers are generally required to submit supply schedules once a day for all the auctions taking place during the next day. The APX (England) and the EPEX (Austria, France, Germany and Switzerland) markets allow hourly auctions [APX, 2017, EPEX, 2015], and EPEX allows for bids comprising up to 256 price quantity combinations, effectively approximating smooth supply functions. Producers can submit different supply schedules for each individual auction, but every bid must be placed at the same time one day in advance for each block of 24 hours. Customers go through the same process and submit their demand schedules, then the market operator matches supply and demand for each auction. Producers thus have to submit schedules facing uncertain demand, this is the reason for the popularity of supply function equilibria approaches to the electricity market.

However, on this market, bids change from auction to auction. From the point of view of KM's model, this should happen only through a coordination of agents agreeing to collectively swap from one Nash equilibrium to another in the available continuum. Describing these dynamics, however, is increasingly important as the energetic mix is bound to include an increasing fraction of renewables. Power production can be separated in two classes: dispatchable and non-dispatchable technologies. Nuclear, coal, land-fill gas or hydro power generation are mainly dispatchable as one can actually choose their level of production whereas the two rising stars of renewable energy, namely wind and solar, are non-dispatchable: they react to weather conditions. Having these technologies in the mix introduces uncertainty on the production side, which comes down to dispatchable units facing a more uncertain residual demand [Boyle, 2007]. In this paper we want to explore how to model these dynamics.

Electricity production faces very specific technological constraints. These constraints, generally labelled as ramping costs, vary across production technologies, and have yet to

be captured in a model. We propose to do so by introducing a multivariate cost function, depending as always on the quantity produced, but also on the rate at which production varies: $C(S, \frac{dS}{dt})$. We call this class of cost functions dynamic cost functions.

All power plants face maintenance costs. However part of these maintenance costs are induced by the dynamics of production, and can be seen as ramping costs. More precisely, whatever the production technology, fluctuations in production are costly. Indeed, they imply fluctuations in the temperature of the core of the power plant, thus dilation and contraction cycles of the different parts, which cause wear and tear. The industry is aware of these effects [GE, 2015], some B2B companies even specialize in minimizing the related long term costs. For example, Wortsilä Power Plants, a supplier of power plants and tools to forecast long term costs, explains in a white paper [Arima, 2012]:

Increased variability in net load demand means that dispatchable generating units have to ramp considerably more steeply and deeper than traditionally, thus increasing wear and tear to components.

We are going to model these ramping costs through a dynamic cost function, increasing in the absolute value of its second argument : any change in production is costly. This paper will focus on the implications of considering this type of ramping costs. Other types of ramping costs exist, for example startup costs, but they will not be studied in this paper.

These effects cannot be captured by traditional cost functions depending on the level of production alone. One needs to take into account the actual path leading to a given quantity produced. This implies that we need to impose structure on the dynamics of the system while retaining uncertainty, the key ingredient of KM's paper. To do so, we use stochastic dynamics.

This seemingly small addition to KM's framework has a lot of implications on the results obtained. The solutions are not ex-post optimal anymore, allowing to account more satisfactorily for the dynamics of optimal supply schedules, and our solutions are unique, even for bounded demand shocks. We also define a novel selection rule to choose from KM's continuum of equilibria. Finally these results open the possibility to distinguish intraday and day-ahead markets.

In section 1.2 we will present a heuristic approach to get the intuition of the model. Then, in section 1.3 we will introduce the mathematical tools needed to use stochastic dynamics in this context, in section 1.4 and section 1.5 we will solve the monopoly and the symmetric oligopoly cases while considering that producers have information about

the overall distribution of shocks during the day, but do not have information about differences in the shocks at different dates. Finally in section 1.6 we will discuss the dynamic variation of the optimal bids, while sections 1.7 and 1.8 will respectively cover a few implications of these results and conclude the paper.

1.2 Heuristic Description of the Model

In this section the essence of the model is presented before introducing the proper mathematical tools needed to treat this problem rigorously in the next section.

As in KM's setup, the producer faces uncertain demand, $D(\theta, p)$, with θ a stochastic shock to the demand and p the price, to which we add ramping costs and uncertain dynamics of demand: $\theta(t)$ is the time trajectory of a stochastic shock with stochastic dynamics. In the real market, bidders submit a finite number of bids once a day, and face the ramping costs inter-period, that is, when production has to be adjusted to reach the subsequent market outcome. Here we assume that time is continuous, that ramping costs are incurred continuously, and that bidders are allowed to submit a different supply schedule for every point in time. This amounts to being asked to submit a surface of strategy in the price-quantity-time space.

The producer maximises her expected profits, and we consider here the simplest case in which the distribution of shocks is static and the producer is asked by the market operator to submit a single supply schedule a day in advance. In an oligopoly the program maximised by producer i is therefore:

$$\max_{S_i(p)} \mathbb{E} \left[\int_0^T \left(p(\theta(t)) S_i(p(\theta(t))) - C \left(S_i(p(\theta(t))), \frac{dS_i(p(\theta(t)))}{dt} \right) \right) dt \right] \quad (1.1)$$

with $p(\theta(t))$ the price given the demand shock $\theta(t)$ at date t , $S_i(\cdot)$ the supply schedule of producer i and $C(\cdot, \cdot)$ the dynamic cost function.

The goal of this section is to provide the intuition of the model, therefore we will not describe here the conditions that must be verified by the different terms of the model. We will simply assume that the dynamic cost function is additively separable between a static and a ramping term, $C(S_i, \frac{dS_i}{dt}) = C_s(S_i) + C_r(\frac{dS_i}{dt})$, and that the demand shocks θ are bounded in $[\underline{\theta}, \bar{\theta}]$. Lastly we require the ramping term $C_d(\cdot) = \frac{\gamma}{2}(\cdot)^k$ for clarity, and $k \geq 2$ an integer. We distribute the expectation operator and write that $\frac{dS_i}{dt} = \frac{dS_i}{dp} \frac{dp}{d\theta} \frac{d\theta}{dt} = S'_i \cdot \dot{p} \cdot \frac{d\theta}{dt}$, with X' the derivative of univariate function X with respect to its argument, $\dot{X} = \frac{dX}{d\theta}$.

The maximisation program can then be written as follows :

$$\max_{S_i(p)} \int_{\underline{\theta}}^{\bar{\theta}} f(\theta) \left(p(\theta) S_i(p(\theta(t))) - C_s(S_i(p(\theta(t)))) - \frac{\gamma}{2} (S'_i \cdot \dot{p})^k \mathbb{E} \left[\left(\frac{d\theta}{dt} \right)^k \middle| \theta \right] \right) d\theta \quad (1.2)$$

with $f(\theta)$ the distribution of shocks, and γ the ramping cost parameter capturing the magnitude of the ramping costs.

Note that $\mathbb{E} \left[\left(\frac{d\theta}{dt} \right)^k \middle| \theta \right]$ depends only on θ , and that producer i faces a residual demand so that $S_i(p(\theta(t))) = D(\theta, p(\theta(t))) - S_{-i}(p(\theta(t)))$ which depends only on θ and p , with S_{-i} the aggregate supply schedule of all the other producers, taken as given by producer i . This implies that the integrand in eq. 1.2 depends only on three variables: θ , p and \dot{p} . The maximisation program is therefore equivalent to an Euler-Lagrange problem, a very well described mathematical object: $\max_p \int \mathcal{L}(\theta, p, \dot{p}) d\theta$.

The information obtained from taking the first-order condition of an Euler-Lagrange problem yields a second order differential equation as well as two boundary conditions: $\frac{\partial \mathcal{L}}{\partial p} = \frac{d}{d\theta} \frac{\partial \mathcal{L}}{\partial \dot{p}}$ and $\frac{\partial \mathcal{L}}{\partial \dot{p}} \Big|_{\underline{\theta}} = \frac{\partial \mathcal{L}}{\partial \dot{p}} \Big|_{\bar{\theta}} = 0$. This is why we obtain unique solutions: if the boundary conditions are not verified there exists profitable deviations. In less mathematical terms, taking ramping costs into account as specified above means that for a given level of shock, one not only cares about the optimal level of production for this shock, but also about the optimal slope of the supply schedule at this level of production. Effectively, this means that optimal levels of production cannot be chosen independently for different level of shocks anymore, thus shrinking the continuum of equilibria. The boundary conditions' argument explains why the continuum not only shrinks, but collapses to a unique equilibrium.

Note that if the ramping cost parameter γ is taken equal to 0 we are back to KM's model: one doesn't care about the slope of the supply schedule anymore, and the problem comes down to a pointwise maximisation which therefore yields ex-post optimal equilibria. We want to stress that this means that it is not sufficient to specify the dynamics of the shocks to obtain a dynamic model, one needs to take into account ramping costs.

The maximisation program 1.2 is a heuristic description of the situation. We want to model the stochastic nature of demand and of its dynamics. We do this by using Itô processes, a class of stochastic processes built through brownians, to describe the stochastic trajectory of the demand shocks with respect to time. The difficulty is that brownians are everywhere continuous but nowhere differentiable, therefore the way program 1.2 is written, with a term in $\frac{d\theta}{dt}$, is incorrect.

In the next section we introduce the stochastic dynamics properly without using the concept of derivative.

1.3 Stochastic Dynamics

As described in the previous section, we consider that bidders submit surfaces, that is supply schedules for every point in time. The reason to describe a discrete dynamic market as a continuous one is that although discrete time is conceptually more easily understood, continuous time allows to use much more powerful mathematical tools and to obtain closed form solutions, which we think are crucial in gaining intuitive insights about these dynamics. Therefore we consider that demand fluctuates continuously and that ramping costs are incurred instantaneously. This approximation would need to be tested, although it should be noted that day ahead markets operate with hourly or half-hourly periods and are therefore facing a reasonable amount of periods each day.

Our strategy to describe a discrete process as a continuous one is as follows. We approximate the stochastic process (continuous in time) that we want to use to describe the market by a random walk (discrete in time), and then decrease its timescale towards 0 to converge towards the stochastic process. We are first going to describe the target stochastic process that we will be using throughout this paper, before illustrating how we go from a discrete description to a continuous one.

In the electricity market, demand shocks, denoted $\theta(t)$, are bounded: there are no days for which demand is null nor are there days for which demand tends towards infinity. The structure to be imposed on the dynamics of the shocks has to imply bounded shocks.

1.3.1 The stochastic process

A simple Itô process one can consider that leads to bounded shocks is defined by the following stochastic differential equation (SDE):

$$d\theta(t) = -2\theta(t)dt + \sqrt{1 - \theta(t)^2}dB_t \quad (1.3)$$

with B_t a brownian and dX an infinitesimal variation of quantity X .

Observe that this SDE is formed by a deterministic mean-returning term $-2\theta(t)dt$

and a bounded stochastic one $\sqrt{1 - \theta(t)^2} dB_t$. As $\theta(t)$ approaches -1 or 1 the stochastic term goes to 0 , thus $\theta(t) \in [-1, 1]$. Without loss of generality we can restrain ourselves to this special case. Other bounded supports, $\theta \in [\underline{\theta}, \bar{\theta}]$, can be captured through renormalisations of θ .

Such a stochastic process has a distribution of probability $f(\theta)$ given by Fokker-Planck's equation, easily solved here. In the general case of an Itô process given by SDE 1.4, one obtains in 1.5 the generic Fokker-Planck equation for its distribution of probability $f(\theta, t)$:

$$d\theta = \mu(\theta, t)dt + \sigma(\theta, t)dB_t \quad (1.4)$$

$$\frac{\partial}{\partial t}f(\theta, t) = \frac{\partial}{\partial \theta}(\mu(\theta, t)f(\theta, t)) + \frac{1}{2}\frac{\partial^2}{\partial \theta^2}(\sigma(\theta, t)^2 f(\theta, t)) \quad (1.5)$$

Here, for SDE 1.3, this yields that $f(\theta) = \frac{3}{4}(1 - \theta^2)$ on $[-1, 1]$ and 0 elsewhere.

1.3.2 The ramping costs

In the rest of the paper we are going to consider quadratic ramping costs. More precisely we consider the costs induced by fluctuations in the production level. As described in the introduction, fluctuations imply increased wear and tear, whether the production is increasing or decreasing. In addition, these ramping costs are null in the absence of fluctuations. This means that they can be captured by a function $C_r(\cdot)$ verifying $C_r(0) = 0$, $C_r(\cdot) \geq 0$ and increasing in the absolute value of its argument. In the absence of more detailed knowledge about the actual shape of these ramping costs, it seems reasonable to consider a quadratic cost function, that is the first term in a Taylor expansion of the actual real ramping cost function.

We cannot compute $\frac{d\theta}{dt}$ as it appears in Eq. 1.2, as a stochastic process, although everywhere continuous, is nowhere differentiable. We are therefore going to consider a random walk of timestep Δt which converges towards the Itô process 1.4, using the Euler-Maruyama approximation, a generalisation of the Euler method to stochastic differential equations. We consider a Markov chain Y defined as follows :

$$\Delta Y_n = Y_{n+1} - Y_n = \mu(Y_n, n\Delta t)\Delta t + \sigma(Y_n, n\Delta t)\Delta B_n \quad (1.6)$$

where $\Delta B_n = B_{(n+1)\Delta t} - B_{n\Delta t}$. These ΔB_n are *i.i.d.* normal random variables of mean 0 and variance Δt . Note that as Δt is taken towards 0 , this Markov chain converges towards its underlying stochastic process defined by eq.(1.4).

The ramping costs are taken as quadratic in the variation of the production, and also depend on a ramping cost parameter $\Gamma(\Delta t)$, that is the cost per unit of quadratic variation at horizon Δt , so we compute the following quantity :

$$\mathbb{E} \left[\frac{\Gamma(\Delta t)}{2} \cdot \left(\frac{Y_{n+1} - Y_n}{\Delta t} \right)^2 \middle| Y_n \right] = \frac{\Gamma(\Delta t)}{2} \cdot \frac{\sigma(Y_n, n\Delta t)^2}{\Delta t} \quad (1.7)$$

For this quantity to converge to a finite value when the Markov chain is taken towards its underlying stochastic process we have to consider that for small enough timescales, the ramping cost parameter $\Gamma(\Delta t)$ is linear in Δt , i.e. $\Gamma(\Delta t) = \gamma\Delta t + o(\Delta t)$. Mathematically, if $\Gamma(\Delta t)$ had a slower than linear relationship at small timescales, the ramping costs would diverge, and if it was faster they would converge to 0. A physical constraint, namely thermal inertia, ensures that the ramping cost parameter does actually behave in this way¹.

Consider for now that the mean function μ and the variance function σ from eq. 1.4 do not depend on time explicitly and are therefore written $\mu(\theta)$ and $\sigma(\theta)$. Consider now a transformation $T(\cdot)$ that we apply to the Markov chain Y . Then:

$$\mathbb{E} \left[\frac{\Gamma(\Delta t)}{2} \cdot \left(\frac{T(Y_{n+1}) - T(Y_n)}{\Delta t} \right)^2 \middle| Y_n \right] = \mathbb{E} \left[\frac{\Gamma(\Delta t)}{2} \cdot \left(\frac{T(Y_{n+1}) - T(Y_n)}{Y_{n+1} - Y_n} \cdot \frac{Y_{n+1} - Y_n}{\Delta t} \right)^2 \middle| Y_n \right] \quad (1.8)$$

And in the limit where the markov process Y converges towards the Itô process θ of equation 1.4:

$$\lim_{\Delta t \rightarrow 0} \mathbb{E} \left[\frac{\Gamma(\Delta t)}{2} \cdot \left(\frac{T(Y_{n+1}) - T(Y_n)}{\Delta t} \right)^2 \middle| Y_n \right] = \frac{\gamma}{2} \cdot T'(\theta(t))^2 \cdot \sigma(\theta)^2 \quad (1.9)$$

We apply this result to the problem at hand, that is that we evaluate the ramping costs in the case where the demand shocks are given by eq. 1.3:

$$\lim_{\Delta t \rightarrow 0} \mathbb{E} \left[\frac{\Gamma(\Delta t)}{2} \cdot \left(\frac{\Delta S_i(p(\theta(t)))}{\Delta t} \right)^2 \middle| \theta(t) \right] = \frac{\gamma}{2} \cdot S'_i(p(\theta(t)))^2 \dot{p}(\theta(t))^2 (1 - \theta^2) \quad (1.10)$$

with X' the derivative of quantity X with respect to its argument and \dot{X} its derivative with respect to θ . Note that we considered here that the variance term $\sigma(\theta) = 1 - \theta^2$ depends only on θ and not explicitly on t , which in turn implies that the strategy S_i does

¹Ramping costs come from thermal fluctuations in the core of the plant. Therefore we have to describe how temperature responds to fluctuations in production. Thermal inertia acts as a low pass filter, meaning that it smoothes out fluctuations on short timescales. Think about heating a saucepan full of water: although lighting the stove is almost instantaneous, the temperature of the water being heated increases only progressively, in an exponential fashion that is therefore linear in time for short timescales.

not depend explicitly on t either.

Let us consider the case where the strategy and the variance depend explicitly on time, and are thus written $S_i(p(\theta(t), t), t)$ and $\sigma(\theta, t)$ respectively. By using a first order expansion as before, the ramping cost function can be approximated as follows:

$$\begin{aligned} \lim_{\Delta t \rightarrow 0} \mathbb{E} \left[\frac{\Gamma(\Delta t)}{2} \left(\frac{\Delta S_i(p(\theta(t), t), t)}{\Delta t_c} \right)^2 \middle| \theta(t) \right] &= \lim_{\Delta t \rightarrow 0} \mathbb{E} \left[\frac{\gamma}{2} (\partial_1 S(p(\theta(t), t), t) \partial_1 p(\theta(t), t))^2 \frac{\Delta \theta^2}{\Delta t} + \mathcal{O}(\Delta t) \right] \\ &= \frac{\gamma}{2} (\partial_1 S(p(\theta(t), t), t) \partial_1 p(\theta(t), t))^2 \sigma(\theta, t)^2 \end{aligned} \quad (1.11)$$

with $\partial_i X$ the partial derivative of quantity X with respect to its i^{th} argument.

Now, we can write down the instantaneous expected value of the profit of producer i if the demand shock is $\theta(t)$, $\pi_i^e(t)$, that is the profit that one expects to obtain when demand is at $\theta(t)$ given the expected value of the ramping costs:

$$\pi_i^e(t) = p(\theta(t), t) S_i(p(\theta(t), t), t) - C_s(S_i(p(\theta(t), t), t)) - \frac{\gamma}{2} \partial_1 S_i(p(\theta(t), t), t)^2 \partial_1 p(\theta(t), t)^2 \sigma(\theta, t)^2 \quad (1.12)$$

Lastly we have to write down the expected profit for a day's worth of submitted strategies. Let us consider that the chosen unit of time is the day. Therefore, the total expected profit Π_i^e writes:

$$\begin{aligned} \Pi_i^e &= \int_0^1 \mathbb{E}[\pi_i^e(t)] dt \\ &= \int_0^1 \int_{\underline{\theta}}^{\bar{\theta}} f(\theta, t) \left[p(\theta, t) S_i(p(\theta, t), t) - C_s(S_i(p(\theta), t)) \right. \\ &\quad \left. - \frac{\gamma}{2} \partial_1 S_i(p(\theta, t), t)^2 \partial_1 p(\theta, t)^2 \sigma(\theta, t)^2 \right] d\theta dt \end{aligned} \quad (1.13)$$

1.3.3 Discussion of the approximations

We want a tractable mathematical formulation of the dynamic problem faced by producers on the electricity market. To achieve this we seek to describe the discrete real life problem by an approximated continuous one. We first use two technological facts: fluctuations in production are costly and these costs decrease linearly in time for short timescales. We then rely heavily on first order expansions of the different terms we have to compute.

1.3.4 The maximisation program

Here, we consider that the dynamics of demand shocks are given by eq.(1.3), and that therefore $\sigma(\theta, t)^2 = \sigma(\theta)^2 = (1 - \theta^2)$.

We now introduce the different conditions that have to be satisfied by the various terms in this problem. First, on most electricity markets, schedules must be increasing, therefore here we take $S'_i(\cdot) \geq 0$. Second, the aggregate demand is non negative as consumers do not have production facilities at their disposal: $D(\theta(t), p(\theta(t))) = \sum_i S_i(p(\theta(t))) \geq 0$. Last, we consider that the shocks θ are ordered so that the demand is increasing in θ , i.e. $\frac{\partial D}{\partial \theta} \geq 0$, and that the price has to weakly increase with the shocks, i.e. $\dot{p} \geq 0$. Our initial stochastic maximisation program can thus be rewritten as a regular optimal control problem:

$$\max_{S_i(p)} \int_{-1}^1 f(\theta) \left(p(\theta) S_i(p(\theta)) - C_s(S_i(p(\theta))) - \frac{\gamma}{2} (1 - \theta^2) (S'_i(p(\theta)) \dot{p}(\theta))^2 \right) d\theta \quad (1.14)$$

$$\begin{aligned} s.t. \quad & S'_i(\cdot) \geq 0 \\ & \dot{p} \geq 0 \end{aligned} \quad (1.15)$$

$$D(\cdot, \cdot) \geq 0 \quad (1.16)$$

The next section solves this problem for a monopoly.

1.4 The Monopoly

Let us consider that the aggregate demand is linear, that is:

$$D(\theta(t), p(\theta(t))) = a\theta(t) + b - p(\theta(t))$$

with a and b parameters taken to describe any bounded support of shocks given the stochastic dynamics introduced in the previous section for which $\theta \in [-1, 1]$. Here $(a\theta + b) \in [b - a, b + a]$.

In a monopoly situation we have $S = D(\theta(t), p(\theta(t)))$, therefore the constraints reduce to:

$$\dot{p}(\theta) \in [0, a], \text{ and } p(\theta) \leq a\theta + b$$

where \dot{X} corresponds to $\frac{dX}{d\theta}$.

Consider in addition that the static cost function is also quadratic: $C_s(S_i) = \frac{\lambda}{2}S_i^2$. The maximisation program is rewritten as:

$$\max_{p(\cdot)} \int_{-1}^1 f(\theta) \left(p(\theta)(a\theta + b - p(\theta)) - \frac{\lambda}{2}(a\theta + b - p(\theta))^2 - \frac{\gamma}{2}(1 - \theta^2)(a - \dot{p}(\theta))^2 \right) d\theta \quad (1.17)$$

$$\begin{aligned} s.t. \quad & \dot{p}(\theta) \in [0, a] \\ & p(\theta) \leq a\theta + b \end{aligned}$$

Results

Proposition 1.4.1 *The solution exists, is unique, and has the following form:*

$$\forall \theta \in [-1, 1] \quad p^*(\theta) = a \frac{4\gamma + 1 + \lambda}{4\gamma + 2 + \lambda} \theta + b \frac{1 + \lambda}{2 + \lambda} \quad (1.18)$$

The optimal schedule is parametrised by θ so that $S(p(\theta))$ is formed by the points of coordinate $(a\theta + b - p(\theta), p(\theta))$. Its equation is given by:

$$S^*(p) = \frac{1}{4\gamma + 1 + \lambda} \left(p + \frac{4\gamma}{2 + \lambda} b \right) \quad (1.19)$$

Proof See annex 1.A. ■

We present in Fig. 1.1(a) the results obtained for increasing values of the ramping cost parameter γ , starting at $\gamma = 0$ in black and moving progressively from black to blue to red to green. The supply schedules are obtained by noting that the optimal solution

As expected, adding these inertial costs narrows down the domain of attainable quantities produced, as a larger quantity domain implies larger incurred dynamic costs.

More interesting is the way the quantity domain is narrowed down. The domain of prices increases conversely, so that the solutions are steeper than the traditional monopoly situation, bringing the schedules ever closer to a Cournot-like situation. In addition, the optimal supply schedules do not depend on a , the parameter determining the width of the possible shocks, but only on b which defines the average value of the shocks.

One can then study the comparative statics when the values for a and b are varied, as illustrated in Fig. 1.1(b). In particular, if we consider an increase in a without changing b , the solution is represented by the same “master” function, but the explored region expands. On the other hand, if we consider a fixed a but an increasing b , the explored

length is kept constant, but the optimal schedule is translated towards the north-east region of the plane as expected intuitively: more demand implies a given mix between higher quantities and prices, which is given by the direction of the vector of translation. Note that the independence of the solution on variations of a comes from the fact that we are considering comparative statics, which is very different from dynamically evolving values of a and b , case which will be treated in detail in section 1.6.

Lastly, note that all schedules cross at a single point. These quadratic ramping costs imply a symmetric deformation of the solution without ramping costs. The limit of extremely high ramping costs is a Cournot-like schedule, i.e. a vertical one, taken at this crossing point.

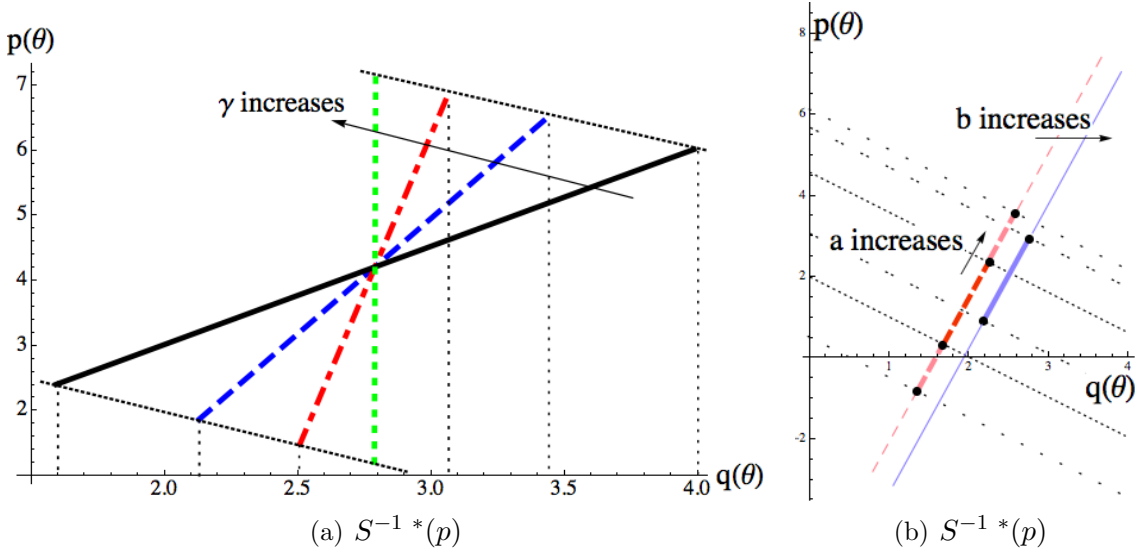


Figure 1.1: (a) Four optimal supply schedules are plotted. In black (full line) $\gamma = 0$. As γ increases we transition from the black curve to the blue curve (large dashes), then the red curve (mixed dashes) and then finally for $\gamma \rightarrow \infty$ to the green one (small dashes). The range of production is highlighted for each curve through the thin vertical dotted lines.

(b) The thin black dotted lines represent the extremal demand functions given a and b , i.e. $D(\underline{\theta}, p)$ and $D(\bar{\theta}, p)$. From ... to ... b is kept fixed while a is increased, and from ... to ... a is kept constant while b is increased. In red (dashed) the solution for a given value of b . As a increases, the solution widens from the thick deep red region to the thick light red one. In the case for which a is kept constant and b is increased the solution shifts from the dashed deep red region to the full thick blue one.

1.5 The Symmetric Oligopoly

We keep the same linear demand specification as in the monopoly, therefore, with n competitors one has to consider the residual demand faced by each producer:

$$S(p(\theta)) = a\theta + b - (n - 1)S(p(\theta)) - p \quad (1.20)$$

$$S(p(\theta)) = \frac{a\theta + b - p}{n} \quad (1.21)$$

$$S'(p(\theta)) = \frac{a - \dot{p}}{n\dot{p}} \quad (1.22)$$

$$S''(p(\theta)) = -\frac{a\ddot{p}}{n\dot{p}^3} \quad (1.23)$$

For concision, we drop the explicit dependencies of the different functions on their arguments in the following equations; $f(\theta)$, $p(\theta)$ and $S(p(\theta))$ will be noted f , p and S respectively. The maximisation program now writes:

$$\max_{p(\cdot)} \int_{-1}^1 f\left(p(a\theta+b-p-(n-1)S)-\frac{\lambda}{2}(a\theta+b-p-(n-1)S)^2-\frac{\gamma}{2}(1-\theta^2)(a-\dot{p}(1+(n-1)S'))^2\right)d\theta \quad (1.24)$$

$$\begin{aligned} s.t. \quad & \dot{p} \in [0, a] \\ & p \leq a\theta + b \end{aligned}$$

with, as before, $\dot{X} = \frac{dX}{d\theta}$ and X' is the derivative of function X with respect to its argument.

Results

Proposition 1.5.1 *The solution exists, is unique, and has the following form:*

$$\forall \theta \in [-1, 1], \quad p^*(\theta) = aK_1\theta + bK_2 \quad (1.25)$$

with

$$K_1 = \frac{n\sqrt{(4\gamma + \lambda + n)^2 - 4n + 4} - (4\gamma + \lambda + n)(n - 2)}{2(4\gamma + \lambda + 2n)} \quad (1.26)$$

$$K_2 = \frac{\lambda(n - 1) + K_1(\lambda + n)}{(\lambda + n)(n - 1) + K_1(\lambda + 2n)} \quad (1.27)$$

and the supply schedule has the following expression:

$$S^*(p) = \frac{1}{n} \left(p \left(\frac{1}{K_1} - 1 \right) + b \left(1 - \frac{K_2}{K_1} \right) \right) \quad (1.28)$$

Proof See Annex 1.B. ■

We are now going to focus on the graphical representation of these solutions. As in the monopoly case we obtain unique solutions of increasing steepness in the ramping cost parameter γ . When the ramping costs increase, it becomes more and more costly to allow for a large domain of potential quantities to be produced.

The black curve in Fig. 1.2 corresponds to the limit solution when $\gamma \rightarrow 0$, for which the problem gets closer to that of KM, i.e. no ramping costs. Note that as long as $\gamma \neq 0$ the solutions are unique, thus our framework does not converge to that of KM.

Proposition 1.5.2 *When $\gamma \rightarrow 0$, the solution remains unique and converges towards the linear schedule available in KM's set of solutions, that is the same schedule selected with KM's selection rule obtained when considering an infinite support for the shocks.*

Proof It is straightforward to check that K_1 and K_2 have the same values as KM for $\gamma \rightarrow 0$.

More intuitively the argument is as follows. When $\gamma \rightarrow 0$, with $\gamma > 0$, we retain a unique solution although the problem itself converges towards that of KM. We should select an equilibrium present in KM's continuum. When KM take the limiting case of an infinite support of shocks they select a unique equilibrium. In our case we can do the same thing by taking $a \rightarrow \infty$. In the limit, our solution being in their set which converges to a unique equilibrium, those two selected equilibria should be equal. Now note that our solution does not depend explicitly on a so that when the support is finite, we still select the same equilibria out of what is now a continuum of equilibria in KM's framework. ■

Intuitively, as we take γ to 0 we come closer to the situation captured in KM, but as long as $\gamma > 0$, the producer still faces dynamic costs, and therefore converges towards the only linear schedule available in KM's set, as shown in Fig. 1.2, in which we plot our solutions on top of KM's solution set in order to clarify the comparison.

Note that it isn't possible to transition smoothly from our model to that of KM, although they are obviously closely related. Indeed, $\forall \gamma > 0$, our model yields unique solutions, but for $\gamma = 0$ we return to KM's model for which there is a continuum of equilibria. There is an intrinsic discontinuity between these two models, namely, the correspondence $\Gamma(\gamma)$ associating the set of equilibria to the symmetric oligopoly problem obtained for a given value of the ramping cost parameter γ is not lower hemicontinuous at $\gamma = 0$.

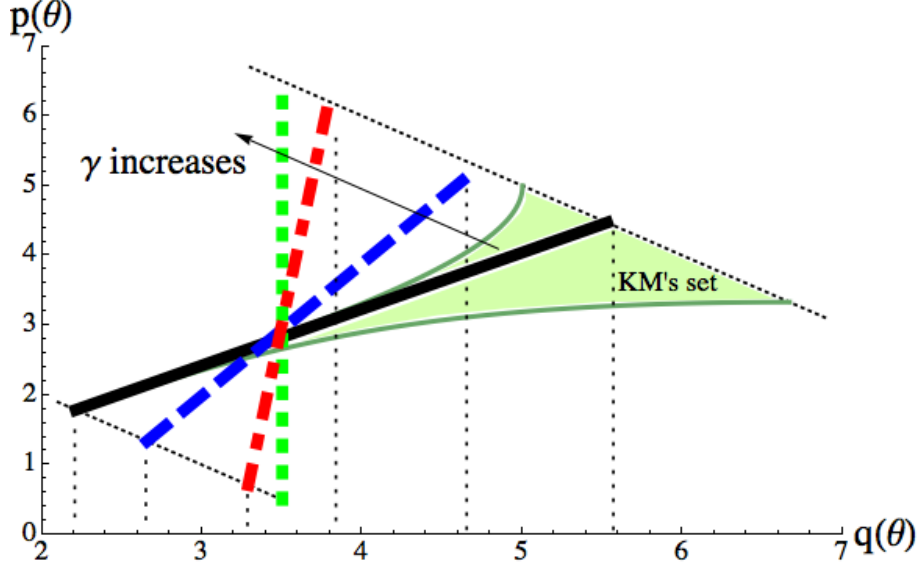


Figure 1.2: This graph plots $S^*(p)$ for different values of the ramping cost parameter, and compares them to the set of equilibria obtained in KM's framework. Four optimal supply schedules are plotted. The black curve (full line) corresponds to the case where $\gamma \rightarrow 0$. As before, as γ increases the optimal schedules get steeper and steeper until in the limit of $\gamma \rightarrow \infty$, the optimal schedule attains a vertical slope. In addition, we show the set of available equilibria in KM's model in light green, and the extremal demand schedules in dashed black.

In addition to proposing a way to take into account dynamic technological constraints, our model provides a selection rule to choose from the continuum of equilibria described in KM's seminal work, i.e. the solutions' stability to ramping costs.

We have here a model which solutions depend on the distribution of shocks, therefore we are able to capture the interday variation of bids by assuming that the distribution of shocks varies from day to day. In this case, there exists only one symmetric equilibria each day, function of the distribution of shocks.

In the next section we are going to present how to capture richer dynamics, and especially how the surface of bids should evolve with time when the producers have information about the anticipated variation of shocks during the day.

1.6 Dynamic behavior of the bids

On the day-ahead market, bids, although made once per day for each period included in the next 24 hours, vary from one another. This is because demand is expected to vary according to a daily cycle with, roughly speaking, low demand during the night and higher demand during the day. The model described above doesn't account for these hourly dynamics. Here we present a way to capture these intraday variations, by considering

bids that depend continuously on the date t .

Previously, the SDE defining the dynamics of the problem was written as:

$$d\theta(t) = -2\theta(t)dt + \sqrt{1 - \theta(t)^2}dB_t$$

This specification implies a stochastic trajectory for the shocks, bounded by a constant envelope.

To account for these intraday variations we define the envelope by two functions, $(\underline{\theta}(t), \bar{\theta}(t))$, respectively the lower and upper bounds of the shocks. These two functions, although very easy to comprehend, are not the most useful way to define the boundary. Instead we are going to use the average value of the shocks, and the half width of the envelope, $(\hat{\theta}(t), \omega(t))$. This means that $\underline{\theta}(t) = \hat{\theta}(t) - \omega(t)$ and $\bar{\theta}(t) = \hat{\theta}(t) + \omega(t)$. The only restriction we impose on the envelope is that we require it to be continuously differentiable, that is $(\hat{\theta}(t), \omega(t)) \in \mathcal{C}^1(\mathbb{R})$.

Consider the following SDE, in which we drop the explicit dependency of the different functions on time, that is $\theta(t)$, $\hat{\theta}(t)$ and $\omega(t)$ will be noted θ , $\hat{\theta}$ and ω :

$$\begin{aligned} d\theta = & \left[(\hat{\theta} - \omega - \theta) + \left(1 + \frac{\tau}{\omega} \frac{d\omega}{dt_r} \right) (\hat{\theta} + \omega - \theta) + \tau \left(\frac{d\hat{\theta}}{dt_r} - \frac{d\omega}{dt_r} \right) \right] \cdot dt_r \\ & + \sqrt{\left(1 + \frac{\tau}{\omega} \frac{d\omega}{dt_r} \right) (\theta - \hat{\theta} + \omega)(\hat{\theta} + \omega - \theta)} \cdot dB_{t_r} \end{aligned} \quad (1.29)$$

with τ a rescaling parameter allowing to change the rate at which the brownian process blurs information pertaining an initial condition. This parameter is of the order of the cutoff timescale Δt_c (a few seconds at most). We rescale time as we change this parameter, so that time t and the rescaled time t_r verify $t = \tau t_r$. By assumption, Δt_c is much smaller than the typical timescale of variation of strategies, therefore by hypothesis $\left(1 + \frac{\tau}{\omega} \frac{d\omega}{dt_r} \right) > 0$. The distribution of the shocks can be obtained through Fokker-Planck's equation 1.5 and we obtain:

$$f(\theta, t_r) = \frac{6}{\omega(t_r)^3} (\theta(t_r) - \hat{\theta}(t_r) + \omega(t_r)) (\hat{\theta}(t_r) + \omega(t_r) - \theta(t_r))$$

1.6.1 Results

Monopoly dynamics

Proposition 1.6.1 *In the case of an envelope evolving with time, that is shocks belong to the bounded support $[\hat{\theta} - \omega, \hat{\theta} + \omega]$, there exists a unique optimal solution to the monopoly*

problem. It can be expressed as:

$$p^* = \frac{4\gamma(1 + \frac{\tau}{\omega} \frac{d\omega}{dt}) + 1 + \lambda}{4\gamma(1 + \frac{\tau}{\omega} \frac{d\omega}{dt}) + 2 + \lambda} \cdot \theta - \frac{4\gamma(1 + \frac{\tau}{\omega} \frac{d\omega}{dt})}{(2 + \lambda)(4\gamma(1 + \frac{\tau}{\omega} \frac{d\omega}{dt}) + 1 + \lambda)} \cdot \hat{\theta} \quad (1.30)$$

The corresponding optimal supply schedule writes as:

$$S^*(p) = \frac{1}{4\gamma(1 + \frac{\tau}{\omega} \frac{d\omega}{dt}) + 1 + \lambda} \left(p + \frac{4\gamma(1 + \frac{\tau}{\omega} \frac{d\omega}{dt}) \cdot \hat{\theta}}{2 + \lambda} \right) \quad (1.31)$$

Proof See appendix 1.C, to be written. ■

We start by describing the dynamics of the monopoly case because the oligopoly case is not richer dynamically, but it is more complex to describe. Note that if $\frac{d\omega}{dt} = 0$ equations 1.30 and 1.31 are equal to equations 1.18 and 1.19 respectively as expected.

The optimal supply schedule depends on the relative rate of change of the width $\frac{1}{\omega} \frac{d\omega}{dt}$ and on the average shock $\hat{\theta}$. More precisely, with a constant width, the optimal supply schedule varies according to variations in the expected average value of the shocks. This is quite standard, if demand is higher, the price and quantities both increase, and here this increase occurs with a constant slope. The behavior of the supply schedule when the width varies is less trivial.

Remember that when describing the slope of the schedule, we are considering the plane (*quantity, price*) while the schedule as defined by $S^*(p)$ represents the same curve but in the plane (*price, quantity*). An increase in width is equivalent to a higher ramping cost parameter while a decrease in width is equivalent to a lower ramping cost parameter. These results are illustrated in Fig. 1.3.

To understand the economic intuition behind this result, consider first an increase in the width of the envelope at date t_1 . Consider now one possible value of $\theta(t_1)$. At $t_1 + dt$, had the width been constant there would have been a given level of uncertainty about the values that $\theta(t_1 + dt)$, and thus the ramping costs, could have taken. If the width of the envelope is increasing then there is more uncertainty regarding the potential values that could be taken by $\theta(t_1 + dt)$, therefore more expected ramping costs incurred, and a higher slope to hedge these costs. On the other hand, when the width decreases, the situation is reversed. In that case, we move towards a situation in which there is less uncertainty about the ramping costs, so that the slope is smaller than for a constant envelope. This difference between increasing and decreasing width is illustrated by comparing the two regions of the envelope displayed in (full) black line in Fig. 1.3. In addition, when contrasting the left and the right side of the figure one sees that the change

in the informativeness of the envelope is captured by the relative change of the width: for the same rate of change, if the width is larger (right) then the change in informativeness is smaller (the change in the area captured by the (dashed) red and (full) green arrows).

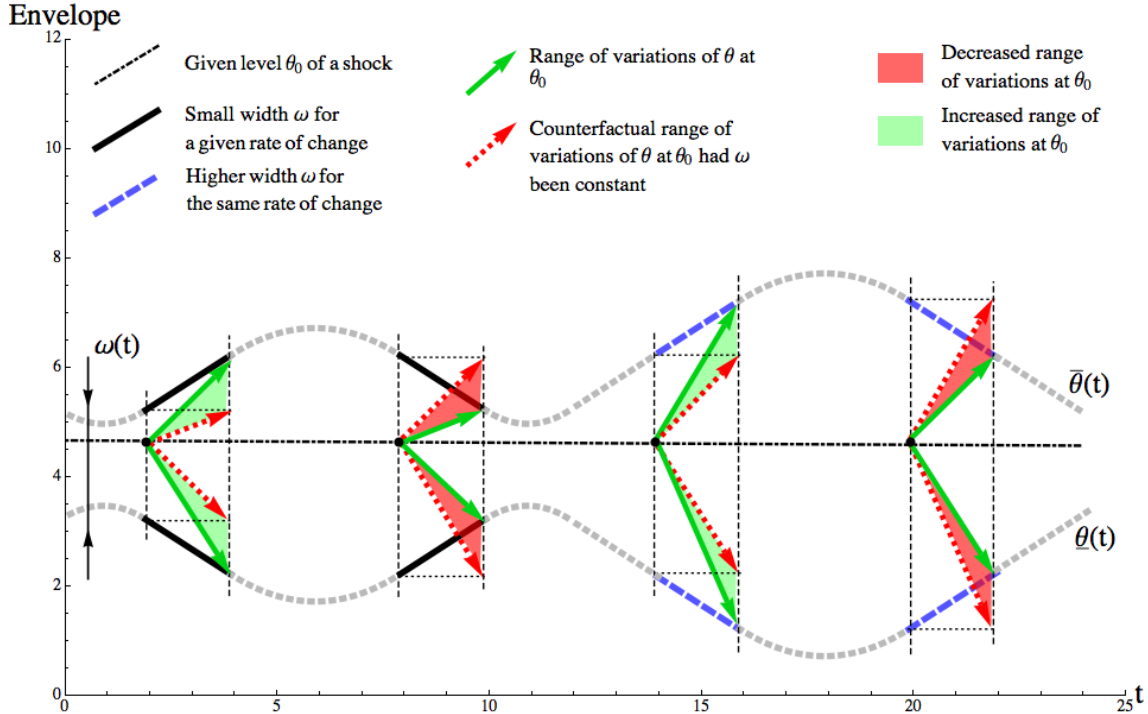


Figure 1.3: This graph plots an envelope of constant average value but varying width $\omega(t)$. By comparing regions of increasing or decreasing width, respectively the left or right side of a lobe, one sees that the informativeness of the envelope is being respectively reduced or increased with respect to a situation where the width would be kept constant. The change in informativeness is represented by the area between the (full) green arrows (observed level of informativeness) compared to the area between the (dashed) red arrows (level of informativeness had the width been constant). In addition, by comparing the left lobe to the right one, it is possible to see why the relative variation of the width, and not the absolute variation of the width, matters. For a larger width (right lobe) and the same rate of change in the width, there is less change in informativeness than for a smaller width (left lobe), i.e. the same rate of change matters less for the right lobe than for the left lobe.

Oligopoly dynamics

Proposition 1.6.2 *The solution exists, is unique, and has the following form:*

$$\forall \theta \in [-1, 1], p^*(\theta) = aK_1(t)\theta + bK_2(t) \quad (1.32)$$

with

$$K_1(t) = \frac{n\sqrt{\left(4\gamma\left(1 + \frac{\tau}{\omega} \frac{d\omega}{dt}\right) + \lambda + n\right)^2 - 4n + 4} - \left(4\gamma\left(1 + \frac{\tau}{\omega} \frac{d\omega}{dt}\right) + \lambda + n\right)(n - 2)}{2\left(4\gamma\left(1 + \frac{\tau}{\omega} \frac{d\omega}{dt}\right) + \lambda + 2n\right)} \quad (1.33)$$

$$K_2(t) = \frac{\lambda(n - 1) + K_1(t)(\lambda + n)}{(\lambda + n)(n - 1) + K_1(t)(\lambda + 2n)} \quad (1.34)$$

and the supply schedule has the following expression:

$$S^*(p, t) = \frac{1}{n} \left(p \left(\frac{1}{K_1(t)} - 1 \right) + \hat{\theta} \left(1 - \frac{K_2(t)}{K_1(t)} \right) \right) \quad (1.35)$$

Proof See Annex 1.D, to be written. ■

The dynamic behavior is the same as that of the monopoly situation presented above, and variations of the optimal schedule with respect to the other parameters are the same as in the case of a constant envelope, as described in section 1.5.

1.7 Discussion

DIFFERENTIATING DAY-AHEAD AND INTRADAY MARKETS.

TRANSITION BETWEEN KM AND THIS MODEL FOR DISCRETE TIME AND RAMPING COSTS: RATE OF CONVERGENCE TOWARDS THE UNIQUE SOLUTION OF THE CONTINUOUS CASE?

1.8 Concluding Remarks

By introducing technological constraints previously neglected we are able to take into account the effects of the dynamics of demand shocks on the supply function framework. We restrict ourselves to linear demand. The optimal supply schedules obtained are unique, and their slope increase with the ramping costs, congruent with the idea that too much variation in production is costly. We also capture the dynamics of the bids themselves.

Although mathematically more demanding than the traditional model by Klemperer and Meyer, we consider that this new model, while conceptually sparing (we only add

ramping costs) allows for a richer, more realistic description of the electricity market, and opens new research avenues. It yields precise and testable predictions on the dynamics of the electricity market with tractable functional forms, at least in the linear demand case. In addition, by explicitly modeling the dynamics, our work opens the possibility to explore interactions between intraday and day-ahead markets, markets that were indistinguishable in the previous framework. We are also able to account for negative prices which was impossible in the previous framework. Such negative prices are actually observed, although rarely, on the market: producers prefer to subsidize consumption instead of decreasing it by a lot.

Next, we want to generalize the existence and uniqueness results to non linear demand functions and develop more comprehensive comparative statics. It would also be important to study the robustness of our solutions to modifications of the general form of the stochastic differential equation governing the dynamics of the system. Finally, and more generally, we think that this concept of dynamic costs, the fact that change is costly, is ubiquitous and could fuel interesting research into the dynamics of a large range of markets. Such avenues have been pursued in the case of stochastic optimal control, that is, instantaneous reactions to stochastic shocks. Here we are describing a market on which agents are forced to optimize in advance, so that they have to react to continuous changes in the anticipated shocks, but not the shocks themselves, which can be understood as stochastic optimisation with periodic commitment.

Appendix

Appendix 1.A Proof of Proposition 1.4.1

Define the following Hamiltonian:

$$H(p(\theta), \dot{p}(\theta), \mu(\theta), \theta) = f(\theta) \left(p(\theta)(a\theta + b - p(\theta)) - \frac{\lambda}{2}(a\theta + b - p(\theta))^2 - \frac{\gamma}{2}(1 - \theta^2)(a - u(\theta))^2 \right) + \mu(\theta)u(\theta) \quad (1.A.1)$$

where $u(\theta)$ is the control variable defined through the following equation of motion: $u(\theta) = \dot{p}(\theta)$, $u(\theta) \in [0, a]$. We do not consider the non-negative demand constraint and will check ex-post that our solution verifies this condition.

Now note that:

$$\forall \theta \in (-1, 1), \quad \frac{\partial^2 H}{\partial p^2} = -(2 + \lambda)f(\theta) < 0 \quad (1.A.2)$$

$$\frac{\partial^2 H}{\partial u^2} = -\gamma(1 - \theta^2)f(\theta) < 0 \quad (1.A.3)$$

The Hamiltonian is therefore strictly concave in $p(\theta)$ and $u(\theta)$. Let $(p^*(\theta), u^*(\theta))$ be an admissible pair to the problem, that is a pair such that $u^*(\theta) = \dot{p}^*(\theta)$. If there exists a continuous and piecewise continuously differentiable function $\mu(\theta)$ such that:

$$\dot{\mu}(\theta) = -\frac{\partial H^*}{\partial p} \quad (1.A.4)$$

$$\mu(-1) = \mu(1) = 0 \quad \text{in order for prices to be free at the boundaries} \quad (1.A.5)$$

$$\forall (\theta, u) \in [-1, 1] \times [0, a], \quad \frac{\partial H^*}{\partial u} (u^*(\theta) - u) \geq 0 \quad (1.A.6)$$

with $\frac{\partial H^*}{\partial u} = \frac{\partial H}{\partial u}(p^*(\theta), u^*(\theta), \mu(\theta), \theta)$, then the Mangasarian sufficiency theorem ensures that $(p^*(\theta), u^*(\theta))$ is the optimal solution [Seierstad and Sydsæter, 1987, p.105]. Let us check that eq. 1.18 defines the optimal solution.

Equation 1.A.4 defines $\mu(\theta)$ up to a constant. Through direct integration we obtain:

$$\mu(\theta) = 3a \left((2 + \lambda) \frac{4\gamma + 1 + \lambda}{4\gamma + 2 + \lambda} - 1 - \lambda \right) (2\theta^2 - \theta^4) + \text{const.}$$

This expression is symmetric in θ therefore by choosing the adequate value for the constant, we ensure that eq. 1.A.5 is satisfied. The slope of the proposed p^* is in $[0, a]$ therefore eq. 1.A.6 requires $\frac{\partial H}{\partial u}$ to be null.

$$\begin{aligned} \forall \theta \in [-1, 1], \quad \frac{\partial H}{\partial u} &= 0 \implies \frac{d}{d\theta} \frac{\partial H}{\partial u} = 0 \\ \text{i.e. } \dot{\mu}(\theta) &= -\frac{4\theta}{1 - \theta^2}(a - u(\theta)) - \frac{(1 + \lambda)(a\theta + b)}{\gamma(1 - \theta^2)} + \frac{(2 + \lambda)p(\theta)}{\gamma(1 - \theta^2)} \end{aligned} \quad (1.A.7)$$

It is straightforward to see that the proposed solution satisfies this differential equation, thus we know that $\frac{\partial H}{\partial u}$ is a constant and as $\mu(-1) = 0$ it is in fact null. Lastly, we see that $p^*(\theta) \leq a\theta + b$.

The proposed $p^*(\theta)$ therefore defines the unique optimal supply function, i.e. the parametrized curve $(a\theta + b - p^*(\theta), p^*(\theta))$.

Appendix 1.B Proof of Proposition 1.5.1

As for eq. 1.24, for the sake of concision, we do not write the explicit dependencies of the different functions on θ , thus $f(\theta)$, $p(\theta)$, $u(\theta)$, $\mu(\theta)$ and $S(p(\theta))$ will be written as f , p , u , μ and S respectively. Define the following Hamiltonian:

$$H(p, u, \mu, \theta) = f \left(p(a\theta + b - p - (n-1)S) - \frac{\lambda}{2}(a\theta + b - p - (n-1)S)^2 - \frac{\gamma}{2}(1-\theta^2)(a - u(1 + (n-1)S'))^2 \right) + \mu u \quad (1.B.1)$$

where u is the control variable defined through the following equation of motion: $u = \dot{p}$, $u \in [0, a]$. We do not consider the non-negative demand constraint and will check ex-post that our solution verifies this condition.

If a symmetric equilibria exists, eqs. 1.20 through 1.23 imply that the regular conditions for an admissible pair to be optimal write :

$$u = \dot{p} \in [0, a] \quad (1.B.2)$$

$$\partial_u H < 0 \implies u = 0 \quad (1.B.3)$$

$$\partial_u H > 0 \implies u = a \quad (1.B.4)$$

$$\begin{aligned} \partial_u H = 0 &\implies u \in [0, a] \text{ and} \\ \ddot{p} &= -\frac{4\theta(a-\dot{p})}{1-\theta^2} - \frac{\lambda(a\theta+b-p)}{\gamma(1-\theta^2)} - n \frac{\dot{p}(a\theta+b-2p)-a(n-1)p}{\gamma(1-\theta^2)(a(n-1)+\dot{p})} \end{aligned} \quad (1.B.5)$$

$$\dot{\mu} = -\partial_p H \quad (1.B.6)$$

$$\mu(-1) = \mu(1) = 0 \quad (1.B.7)$$

It is easy to check that $(K_1, K_2) \in (0, 1)$ and that the solution 1.25 solves eq. 1.B.5 subject to the boundary conditions 1.B.7. The supply schedule is therefore also linear, with equation :

$$S(p) = \frac{1}{n} \left(p \left(\frac{1}{K_1} - 1 \right) + b \left(1 - \frac{K_2}{K_1} \right) \right) \quad (1.B.8)$$

We can now use the Mangasarian theorem to obtain that our admissible pair is indeed solution, $H(p, u, \mu, \theta)$ being concave in (p, u) for linear supply schedules. However the Mangasarian cannot yield that this solution is unique because for a symmetric equilibria, if supply schedules are modified, the hamiltonian changes alongside and we are faced with a new maximisation program.

To obtain that the solution is unique we are going to show explicitly that no other

candidate solution exists.

First, note that :

$$\begin{aligned}\dot{\mu} = & -f\left(\frac{a\theta + b - 2p}{n} - a\frac{(n-1)p}{n\dot{p}}\right. \\ & \left.+ \lambda\frac{a\theta + b - p}{n} \cdot \frac{a(n-1) + \dot{p}}{n\dot{p}} - \gamma(1-\theta^2)(n-1)\frac{a-\dot{p}}{n} \cdot \frac{a\ddot{p}}{n\dot{p}^2}\right)\end{aligned}\quad (1.B.9)$$

If (p^*, u^*) maximises the program then the maximum principle implies that there exists a continuous and piecewise continuously differentiable function μ , as shown in [Seierstad and Sydsæter, 1987, Theorem 2 p.85]. This combined with the above equation implies that $\dot{p} \neq 0$ a.e.

Assume now a solution of the form $\forall \theta \in [-1, 1], p = a\theta + \beta$, by injecting this expression in eq. 1.B.9 there is no β such that the boundary conditions 1.B.7 are verified.

In addition:

$$\forall \theta \in (-1, 1), \frac{\partial^2 H}{\partial u^2} = -f\gamma(1-\theta^2)(1+(n-1)S')^2 < 0 \quad (1.B.10)$$

The Hamiltonian is therefore strictly concave in u and $[0, a]$ is convex. These two properties yield that u^* is continuous, as shown in [Seierstad and Sydsæter, 1987, Note 2.b. p.86]. We have proved the following result :

Lemma 1.B.1 *For any symmetric equilibrium $\exists A \subseteq [-1, 1]$ s.t. A is the union of segments of $[-1, 1]$ and $\forall \theta \in A, \partial_u H = 0$*

Assume the following hypothesis is true, $H_1 : \exists \theta_c \in (-1, 1)$ s.t. $[-1, \theta_c] \subseteq A$, then knowing that $\dot{p} \in C^0([-1, 1], [0, a])$ we can rewrite differential equation 1.B.5 around the value $\theta = -1$ by defining $\theta = -1 + \epsilon$ with $\epsilon = o(1)$:

$$\frac{d^2 p}{d\epsilon^2} = \frac{C}{\epsilon} + o(1) \text{ with } C \neq 0 \text{ if } p(\theta) \neq aK_1\theta + bK_2 \quad (1.B.11)$$

This means that locally around -1 , any solution to eq. 1.B.5 but solution 1.25 diverges. Hypothesis H_1 is therefore wrong and $\exists \theta_c \in (-1, 1)$ s.t. $\forall \theta \in [-1, \theta_c], \exists \beta$ s.t. $p(\theta) = a\theta + \beta$.

At θ_c we have $\partial_u H = 0$ and as \dot{p} is continuous, $\dot{p}(\theta_c) = a$. For the solution to be interior we need $\ddot{p}(\theta_c) \leq 0$.

$$\partial_{\dot{p}} H(p, \dot{p}, \mu, \theta_c) = 0 \Leftrightarrow \mu(\theta_c) = 0 \quad (1.B.12)$$

$$\ddot{p}(\theta_c) \leq 0 \Leftrightarrow b(1+\lambda) - \beta(n+1+\lambda) \geq na\theta \quad (1.B.13)$$

Straightforward computations show that both conditions are mutually exclusive, therefore there doesn't exist another candidate symmetric equilibria, and our solution is unique.

Lastly, to compute the optimal supply function, we inverse the optimal price in order to get the shock as a function of the price at the equilibrium, and we inject this expression in Eq. 1.21.

Appendix 1.C Proof of proposition 1.6.1

Appendix 1.D Proof of proposition 1.6.2

Chapter 2

Investigating the Impact of Uncertainty on Firms with Dynamic Costs : A Case Study of the French Electricity Market

In the last chapter, we have given some attention to a methodology that allows us to use functional data for reduced form analysis. In this chapter, we focus on the economic questions that can be asked using such a methodology. Specifically, we focus on an investigation of the effect of uncertainty on the behaviour of electricity producers.

There exists a consensus that dynamic costs, also referred to as ramping or adjustment costs, are important on the electricity market¹. These are the costs incurred by a producer when production varies. The importance of uncertainty for the expectation of dynamic costs is shown in [Bergès and Martimort, 2014]. Uncertainty itself on the electricity market has been studied by [Wolak, 2007]. We focus on two sources of uncertainty for traditional electricity suppliers, namely uncertainty about the realisation of the market demand and uncertainty from the inherently unpredictable meteorological situation (which affects renewables generation). We propose a methodology to measure this uncertainty and its impact on firm strategies on the electricity market.

Electricity as a market is very important in and of itself (\$2 trillion in worldwide sales in 2010). It is also a crucial input for many industries; power outages induce very large costs to society ([LaCommare and Eto, 2004], [Reichl et al., 2013]). The electricity market is, however, quite different from the markets for other commodities in a few respects. First, electricity cannot be efficiently stored. As a consequence, electricity markets are high frequency (prices can update down to 15-min intervals) and firm strategies are purer as they are free of stock management considerations.

Second and in addition to non-storability, a generation surplus cannot be disposed of freely². Thus, generation of electricity must always be matched with consumption in real time (modulo a small tolerance). This represents a hard constraint on the market³ and forces suppliers to be reactive. However, this reactivity is costly as plant operators incur dynamic costs when adjusting production and the larger the adjustment made, the larger the cost. Hence, suppliers face a trade-off between cheap generation of electricity and costly reactivity to the demand realisation. Indeed, no single generation technology exists that satisfies both cheap generation and sufficient reactivity to allow production fluctuations at a reasonable price. Existing generation techniques are either cheap and unresponsive, e.g. nuclear plants, or expensive and flexible, e.g. gas turbines.

Interestingly, we also observe negative prices. In France for example, during the weekend of the 15th June 2013, the price per MWh dropped to -200€ . This contrasts to the yearly average of approx. $45\text{€}/\text{MWh}$ and is generally understood as a sign that subsidising consumption temporarily is cheaper for a supplier than shutting down a plant [EPEX, 2014]⁴. The increase of the share of renewable generation in the energy mix

¹ [Anderson and Xu, 2005], [Hobbs, 2001], [Hortacsu and Puller, 2008], [Reguant, 2011], [Sewalt and De Jong, 2003].

²The common assumption of free disposal as made in standard microeconomics is violated.

³Mismatches between consumption and generation ultimately result in power outages.

⁴“Negative prices are a price signal on the power wholesale market that occurs when a high inflexible

contributes to the occurrence of negative prices on the market. The intermittency of renewables causes large residual demand shocks [EPEX, 2014]. The unreliability of renewable generation also means that more flexible plants (i.e. plants with lower dynamic costs) are required to provide rapid responses to fluctuations in production from renewables [REN21, 2013].

Furthermore, uncertainty arises from the fact that renewable production is a local and dispersed production, but feeds into a national market with a single price. When meteorological conditions change, the geographic production profile also changes. This further complicates the predictability of renewables generation and contributes to the uncertainty that electricity producers face when playing on the electricity market [Meibom et al., 2009].

This paper explores the effect that the absolute level of uncertainty about residual demand has on players' strategies on the electricity market. In the light of the existence of dynamic costs, which are inherent to the production technologies, uncertainty is costly to suppliers [Bergès and Martimort, 2014]. Thus when faced with uncertainty, we expect that electricity producers smooth production volume over time in order to minimise dynamic costs. In a single market interaction with a symmetric oligopoly and linear demand functions this translates to playing a steeper supply function when uncertainty is high. The detailed intuition behind the predictions tested is given in section 2.0.2.

We show that uncertainty does impact supplier strategies. However, this prediction and result only apply locally to the central, flat and linear part of the supply bid function. Towards the high and low volume extremities of the bid functions when capacity constraints start to matter, bid functions become vertical and the effect of uncertainty vanishes. Furthermore, we observe results that indicate that demand-side bidding is also impacted by uncertainty.

We focus on the French one-day ahead market, EPEX Spot. This market is a divisible goods auction and particularly suited for our analysis as we observe data on the full aggregate bid functions for both supply and demand. We introduce the market's auction format and rules in section 2.1. The dataset and its sources are presented in section 2.2. We develop our identification methodology in section 2.3.1. Our empirical strategy relies on the non-parametric, comparable point selection technique presented in chapter 2.2. We reuse the selected points of the previous chapter for our analysis here. We present and interpret the results in section 2.4. Finally, we discuss some overarching points in section 2.5 and conclude in section 2.6.

power generation meets low demand. Inflexible power sources can't be shut down and restarted in a quick and cost-efficient manner. Renewables do count in, as they are dependent from external factors (wind, sun)."

2.0.1 Literature review and contribution

There exists a literature on supply function equilibria initiated by [Klemperer and Meyer, 1989]. In traditional models, firms choose between quantities (Cournot) or prices (Bertrand) as their strategic quantities. In the intermediate case, firms choose a relationship between quantities and prices, namely a supply function. This is the focus of the supply function equilibrium models. A key ingredient of these models is uncertainty.

Supply function equilibrium models are very relevant for the analysis of electricity markets, since many electricity market designs allow firms to submit a price-volume function rather than a specific price or quantity. [Green and Newbery, 1992], [Newbery, 1998] and [Bolle, 1992] have used these models to analyse competition on the electricity markets. These papers have contributed to a broader investigation of the competition on the electricity markets, which has also been looked at from empirical perspectives [Wolfram, 1998, Borenstein et al., 2002]. While those initial papers have focussed on the supply function equilibria of the market, they have abstracted from some technological specificities for the sake for simplification.

One such aspect that we are interested in and that has been the subject of research in recent years is the importance of dynamic costs for electricity production. [Bergès and Martimort, 2014] extend [Klemperer and Meyer, 1989] to derive predictions on firms facing dynamic costs in a supply function oligopoly under uncertainty. They find that when varying production is costly, suppliers take these costs into consideration by submitting steeper functions when facing more uncertainty, in order to limit the range of variation in production. [Reguant, 2011] develops a model and an empirical strategy to measure dynamic costs on the Spanish one-day-ahead electricity market. She finds that “complex bids”, which allow firms to minimise dynamic costs by linking production in one time period to production in a subsequent time period, reduce the volatility and the level of prices on the market. Her work is also unique in terms of data availability. By using individual bid functions she is able to produce estimates of start-up and ramping costs per production technology. In order to quantify dynamic costs on the Australian electricity market, [Wolak, 2007] derives a methodology to recover estimates of the parameters of parametric cost functions at the level of the production unit. His identification is based on the assumption that each profit maximising supplier knows the distribution of shocks on the demand function when playing on the market. Uncertainty is thus an explicit ingredient of his paper and he captures two sources of uncertainty in a single index: (i) the uncertainty from not knowing the aggregate supply function served by all other suppliers and (ii) the uncertainty about the realisation of the market demand. The recovered cost functions quantify the cost of varying output. Forward contracts are useful to avoid output variations. By comparing the observed level of forward contracting (assumed to be the profit maximising choice for production variation) with the theoretical minimum

cost production pattern, he does not find support for ramping costs.

We contribute to this literature by providing an empirical analysis of the French electricity market. Specifically, we look at the impact of uncertainty on supplier strategies and take this as evidence that dynamic costs matter. Our approach to separate out the uncertainty from market demand expectations and predictability of renewables generation is novel. Both proxies for uncertainty used are new, uncertainty from market demand is inferred from the prediction errors that firms make in a demand estimation and uncertainty from renewable production is computed in a bottom-up approach from local weather forecasts. Instead of opting for a time series regression, we understand all hourly auctions as a cross-sectional dataset and control for the time of the day by using continuous transition variables for daytime periods. Similarly, we control for seasonality using continuous variables rather than dummies. Thereby, we are able to leverage our dataset and increase the sample size for each of our regressions and improve the precision of our estimates.

Furthermore, our work contributes to the empirical literature testing strategic behaviour of market participants. Generally, these studies focus on point-wise analyses for reasons of data availability. Not only does this cause endogeneity problems when the data used is equilibrium data, but also the analysis is restricted to an understanding of the usually observed outcomes of the market. In our setting, we benefit from an interesting dataset in which we observe full aggregate bid functions of players. The functions describe the players' behaviour both in the region where the equilibrium is likely to occur as well as in regions that rarely have an impact on the equilibrium outcome. As such, they provide a much fuller description of the firms' strategies. The additional information contained in the full aggregate bid functions has been used extensively in theoretical work (notably in the supply function equilibria literature mentioned above). However, few papers exploit these full bid functions empirically. For the government bond market, [Préget and Waelbroeck, 2005] and [Özcan, 2004] use a parametric approach to this functional data for a description of the variation of bid functions with respect to exogenous factors and an investigation of the revenue superiority of the uniform or discriminatory multi-unit auction mechanism, respectively. On the electricity market, [Wolfram, 1999] leaves the analysis of equilibrium data to investigate duopoly power of firms on the UK day-ahead spot market. Instead, she uses information from the whole aggregate supply function to investigate the impact of price caps for electricity producers. Using an analysis conditioned on 25 different demand levels, she shows that the introduction of price caps resulted in a counter-clockwise rotation of the aggregate supply function. She relates these results to produce a lower bound on the extent to which firms can increase their prices above marginal costs when regulatory pressure makes it advantageous to do so. Thereby, she contributes empirical evidence for the distorting effects of price caps.

Our work adds to this empirical literature using the information contained in the full

bid functions by developing a non-parametric approach which allows to condition our analyses on multiple, representative points of the bid functions. The statistical ingredients rely on [Silverman and Ramsay, 2005] and are detailed in chapter 2.2. Thereby we are able to leverage our dataset, increase the sample size in individual regressions as well as obtain a fuller picture of the effects of exogenous variables on the behaviour of electricity producing firms. We emphasize that our approach allows to overcome structural restrictions underlying previous parametric approaches, e.g. the symmetry of the logistic function used in [Préget and Waelbroeck, 2005].

2.0.2 Theoretical prediction

We test the impact of uncertainty of supplier strategies by testing the prediction that suppliers bid steeper supply bid functions when faced with a larger uncertainty concerning the outcome of the (residual) demand realisation.

In a discontinuous setting, where the supplier produces volume Q_H of electricity in hour H , we assume that he faces a cost function $C_i(\cdot)$ for each production plant i . This cost function depends on both marginal costs of production as well as the dynamic costs for changing production rapidly: $C_i((Q_H), (Q_H - Q_{H-1})^2)$. The larger the variation in production between hours, the larger the dynamic costs. Even when the expected residual demand is constant, there are still fluctuations in the production due to possible shocks to the residual demand. The larger the shocks, the larger the change in production and thus the larger the dynamic costs. Consequently, increased uncertainty (as represented by shocks on the demand function) translates into increased expected dynamic costs. We assume that the profit maximising supplier knows the distribution of shocks on the demand function when choosing his supply function. In order to minimise these costs, the producer can choose a steeper supply function when uncertainty is high. We want to test this prediction.

We illustrate the intuition behind this prediction using a stylised case in figure 2.0.1. The graphs depict a situation in which a single, risk-neutral supplier bids a supply function to supply electricity in the hours 9 and 10 of the next day. For both hours, the supplier faces a constant expected residual demand function represented by $E(D)$. In a static optimisation problem, the supplier would bid a supply function S_0 in both auctions.

The uncertainty in the market is represented by the width of the envelope of shocks that affect the residual demand function (represented by the arrows on $E(D)$). Thus, in each hour, the residual demand fluctuates between D_{min} and D_{max} , where the range between the extremal demands may vary from one hour to the next.

Before submitting a supply function to the market, the supplier estimates the distribution of probabilities of demand shocks that he will face. In hour 9, the supplier is able to rather precisely predict the realisation of the demand function in the auction, i.e. it

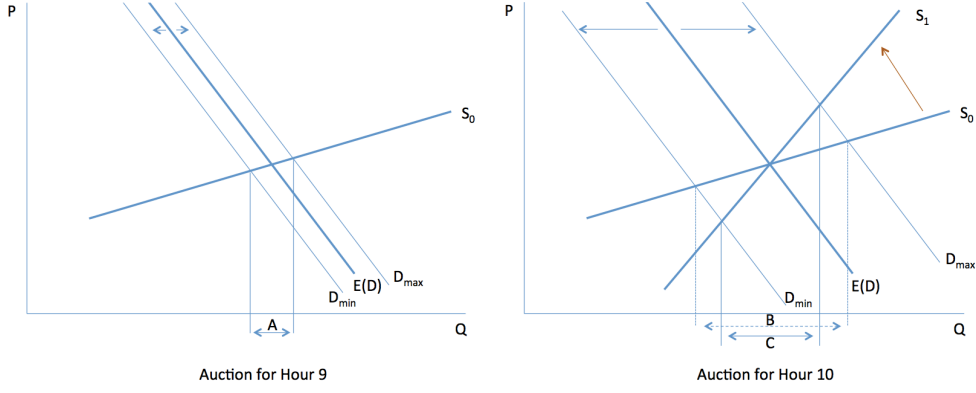


Figure 2.0.1: Illustrating the effect of increased uncertainty.

realises within a tight confidence interval. In hour 10, however, uncertainty in predicting the outcome of the demand realisation has grown strongly as represented by the much wider confidence interval on the demand realisation.

Given a fixed supply bid function S_0 , the possible range of quantities to be produced by the supplier when going from hour 9 to hour 10 has increased due to the increase in the size of the uncertainty (interval on the Q-axis has grown from length A for hour 9 to the dotted length B in hour 10).

Now, we assume that the supplier faces dynamic costs, i.e. it is costly for production to vary on top of any traditional marginal cost consideration and the larger the variation, the larger the cost. Then in the case of a fixed supply bid function (S_0 in both auctions), an increase in uncertainty implies an increase in expected dynamic costs.

The supplier's reaction to increased uncertainty is therefore to bid a steeper supply function S_1 in order to trade-off static optimality and dynamic effects. As a consequence, the range of volumes produced in equilibrium is reduced (the firm produces in the range C instead of B). When seen over time, these considerations lead to a smoother production as compared to a constant supply curve: demand shocks are absorbed through a higher price volatility and a lower production volatility.

If cautious behaviour under high uncertainty is true for all firms on the market and each firm has the same expectation of the probability distribution of the uncertainty, then the reaction of bidding a more price inelastic supply function to increased uncertainty should be observable on the aggregated supply function.

We emphasize that this prediction relies on linear demand and supply functions and does not incorporate capacity constraint considerations (both upper and lower bounds on the production volume of plants), which are also important on the market. Furthermore, we have outlined our prediction using a discrete time-setting. The continuous version of this analysis on dynamic costs is explored in detail by [Bergès and Martimort, 2014].

The present paper tests this mechanism empirically and understands an increase in the slope of aggregate supply bid functions due to an increased level of uncertainty as

evidence that firms minimise dynamic costs across auctions.

2.1 The EPEX spot market

2.1.1 General background

The EPEX Spot market is an auction market, which allows firms to trade electricity 12-36h ahead of delivery. It covers France, Germany with Austria and Switzerland. The volume traded on Epex Spot represents 12%, 40% and 30% of the total electricity consumption in these countries respectively in 2013 [EPEX, 2014].

The EPEX Spot market has considerably gained in importance over time and the daily trading volume has almost quadrupled since 2005, whereas the total electricity consumption has essentially remained constant. The graph in figure 2.1.1 shows these trends very clearly. Furthermore, it shows the significant volatility of the market trading volume (as indicated by the width of the grey-shaded confidence interval).

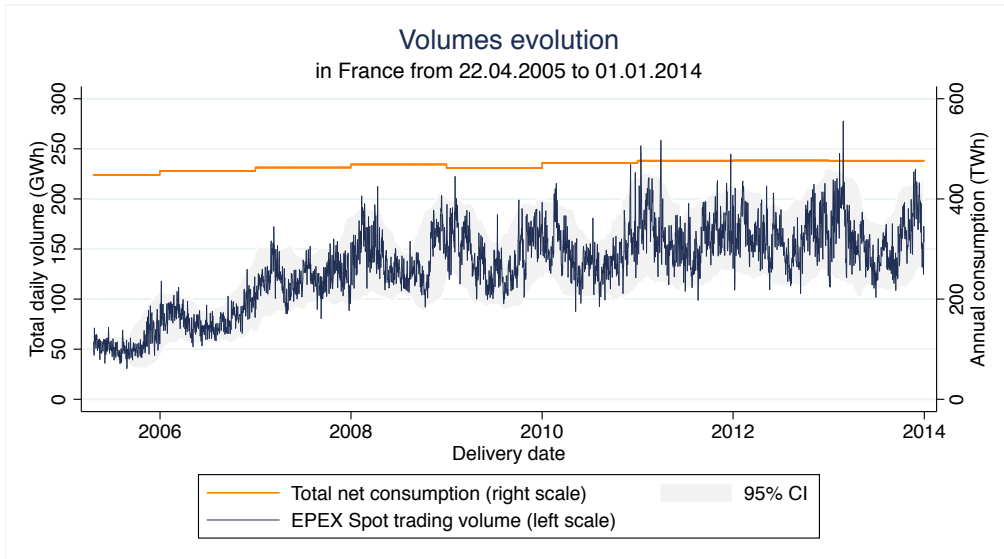


Figure 2.1.1: Traded volume plotted against total annual consumption

Note: Total consumption is netted of the electricity withdrawal at the level of the production unit. The 95% confidence interval is based on a 150-days moving window and assumes that volumes are normally distributed in the time window. GWh and TWh stand for giga and terawatt hours, respectively.

On the EPEX Spot market, the participants submit supply or demand bid functions to be able to meet their next day's supply commitment. This market is important, because it allows the firms to adjust their portfolio to the upcoming demand. The market matches business to business trades, where producers (the suppliers and transmission system operators) and industrial consumers may participate.

The EPEX Spot market settles in a three-pronged market that firms use to achieve their desired power position: The long-term bilateral contracting market, the day-ahead market and the intra-day market. Energy cannot be stored, thus an precise power position must be achieved at each point in time. Firms thus face a trade-off between cheap up-front sourcing and costly uncertainty. The closer the market gets to the delivery of its power, the less uncertainty does the firm face in determining its power requirements (pushing firms to wait until the last minute to fill their energy position). However, the imperfect flexibility of the electricity production landscape cannot satisfy the whole demand short-term at a reasonable price, hence firms must anticipate their requirements in order to obtain cheaper power. Consequently, these three markets complement each other to allow firms to gather a power position at a reasonable price.

2.1.2 Auction rules and mechanism

The EPEX Spot auction occurs daily, all year-round, and proceeds as follows: the order book closes every day at noon for contracts of the following day, results are published two hours later. Bids may be submitted 24/7 from 45 days prior until the closing of the books.

Tradable contracts exist for each hour of the day and firms submit an individual bid function for each of these hours, i.e. a separate, simultaneous auction is run for all hours of the following day and trading is specific for each of these hourly tranches.

The bid submission must be a supply function (or a demand function depending on the position of the firm) with at least 2 and at most 256 price/quantity combinations for single contract orders. The final bid function, thus, consists of the explicitly submitted points and all linearly interpolated points between them. The bid curves must be monotonically increasing for a supply function and vice versa for a demand function. Orders are transmitted via an online IT-platform and a redundant confirmation process aims to avoid erroneous bids. Bids are anonymous and the final electricity distribution is done via the French distribution network controlled by RTE EDF Transport SA.

Prices are specified in €/MWh with two decimal digits and must range from -3000€/MWh to +3000€/MWh. Quantities are specified in whole MWh. In addition to single contract orders for an individual hour, bidders may submit block orders. These are combined single contract orders with a minimum of two consecutive hours. The vital difference with multiple single contract orders is the "All-or-None" condition, namely that the executions of the individual contract orders forming the block are dependent on one another. That is for a block order covering hours 17 to 20, the quantity demanded for the hour 17 is only awarded if the corresponding quantity is also awarded for the hours 18, 19 and 20. Each registered bidder account is limited to a maximum of 40 block orders per delivery day, each of which is limited in volume to 400 MWh (approx. equal to 0.25% of total

daily volume traded on EPEX Spot).

The price-quantity determining mechanism is a uniform price, multi-unit auction mechanism: the summed demand and supply curves are computed and the intersection of these gives the equilibrium price and quantity pair. The market clearing mechanism takes into account single and block orders simultaneously and hence solves the corresponding programme by an algorithm of full enumeration of possible solutions, where each partial solution is verified to provide real, compatible prices. The mechanism works under a time limit. In the case of a curtailment, i.e. a disequilibrium with disproportionate prices due to unmatched supply and demand or an abnormal price for a specific hourly contract, the system proceeds to a second price fixing.

Of particular interest is the clear distribution of information. Ex-ante bidding, firms in the market know the identities of the rival bidders they face (but neither their individual bid functions nor their results in past auctions), the history of aggregated equilibrium prices and quantities up to that day, their clients' past demand realisations and their individual long term contracting position. Upon the clearing of the market, the aggregated supply and demand bid functions, equilibrium quantity and the equilibrium price become common knowledge. Each bidding account is informed of the contracts it has been awarded, i.e. the individual quantities to be sold and bought through the system.

2.2 Our data explained

Auction market data

We have data from the French EPEX Spot market for the period 01.01.2011 to 30.06.2013. This is the latest period, where no significant changes in the auction rules have occurred and where data for all variables can be observed.

We observe the full aggregate bid functions for the day-ahead auctions of each hourly contract for both supply and demand. We understand the dataset as a cross-section rather than a time-series⁵ and focus on weekday trading contracts only. This sums up to about 31 500 observations⁶. A single aggregate bid function is the sum of the individual bid functions, which are not available. We also observe the equilibrium price and quantity for each auction.

Moreover, we observe the block bidding results at the equilibrium solution only. We ignore the blocked aspects and treat subsequent auctions as independent from one another.

⁵This is supported by the graph in figure 2.1.1, which shows a flat total consumption and average trading volume on EPEX Spot since 01.01.2011.

⁶31 500 observations \approx 2.5 years of hourly ($*365 * 24$) demand and supply ($*2$) functions for weekday trading ($*5/7$).

The two graphs in figure 2.2.1 show the aggregate supply and demand bid functions for the same hour of the same day. For a glimpse at the variation of bid functions over time, see figure 2.2.2. The table 2.1 sheds some light on the raw data. For further details as well as the plotted distribution of realised market equilibria, refer to appendix 2.9.2.

Finally, we reuse the data output from chapter 2.2. Specifically, we reuse the specific points extracted from the aggregate demand and supply bid functions, which are comparable across auctions. Why these points are useful for our analysis is explained in the methodology (section 2.3.1).

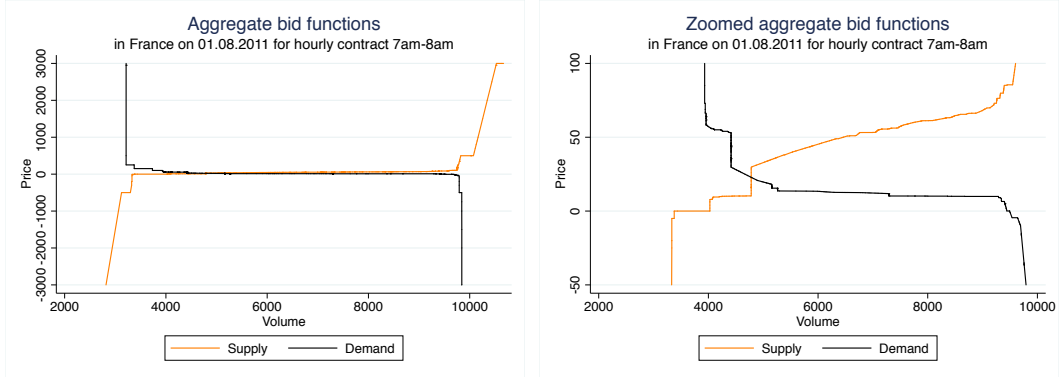


Figure 2.2.1: Example aggregate demand and supply bid functions

Note: The right-hand-side graph is a zoom of the left graph on for the price range $-50\text{ €}/\text{MWh}$ to $+100\text{ €}/\text{MWh}$.

	Mean	Median	Std. Dev	Min	Max
Total daily volume	161,912	159,313	25,059	99,054	277,531
Average realised daily price ⁷	46.6	48.3	17.2	-39.0	381.2
Minimum demanded agg. volume ⁸	5,030	4,968	1,467	914	11301
Maximum demanded agg. volume	13,327	13,222	2,212	4,990	23,254
Minimum supplied agg. volume	3,721	3,526	1,344	618	10594
Maximum supplied agg. volume	14,390	14,142	3,051	6,580	35,356
Bid points per demand function	543	531	163	115	1,253
Bid points per supply function	640	632	143	184	1,283
Bidders per auction ⁹	-	-	-	1	101

Table 2.1: Some descriptive statistics

⁷Average price is volume weighted over the 24 hourly contracts of the delivery day.

⁸Minimum and maximum volumes for both demand and supply refer to the aggregate volume bid on the market for a single hour contract at the extremal prices of $+3000\text{ €}/\text{MWh}$ or $-3000\text{ €}/\text{MWh}$.

⁹Due to the anonymity of the auction procedure, it is unknown which bidders submitted bids. Consequently, it cannot be deduced how many bid steps a typical bidder submits. Number of registered bidders for the French EPEX Spot market as of 01.10.2014.

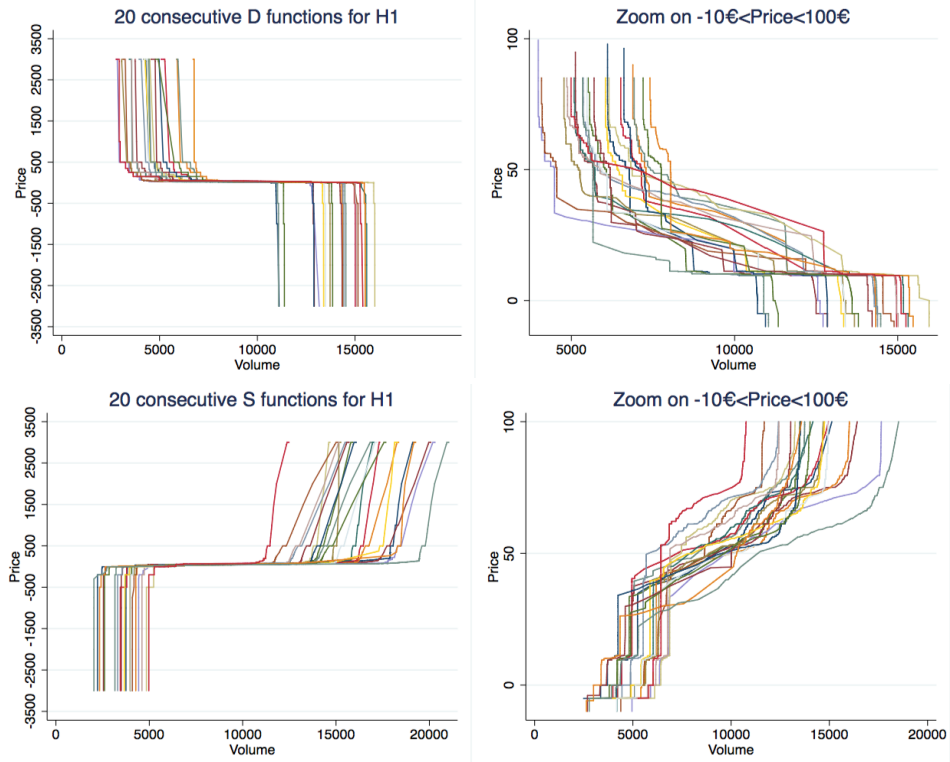


Figure 2.2.2: Aggregate bid functions for 20 consecutive days

Note: The graph shows 20 consecutive aggregate demand and supply functions for the contracts on hour 1 (between 12am and 1am) for the time period 11/12/2011 to 31/12/2011. The graph on the right is a zoom on the price elastic region of the curves on the left.

Exogenous factors

Regarding weather statistics, we have hourly previsions for temperature, wind and cloudiness from the GFS (Global Forecast System) as well as hourly observations for these quantities and luminosity from MétéoFrance . The previsions from the GFS are in the form of weather maps that are outputted from simulations that run one-day ahead at 6 am. This is the weather information that market participants have access to when bidding on EPEX Spot¹⁰. The weather observations are in the form of tables for specific weather stations (between 100 and 200 depending on the specific parameter of interest).

Moreover, we have the location of the total installed capacity per generation type (i.e. wind turbines, solar panels, etc.) at the level of the postcode, that is roughly a 3km precision. We obtain this data from the SOeS, a branch of the French government producing data on environmental issues at large.

¹⁰The next weather simulation run takes place at 12 noon, and is therefore not being used by the bidders on the EPEX day-ahead market, as the deadline for submitting bids is precisely 12 noon.

Population data and data on the level of the domestic production from the manufacturing industry is obtained in monthly steps from the French National Institute of Statistics and Economic Studies (INSEE). From the same source, we obtain the spot prices for petrol and natural gas as well as the import prices at the border for coal, which we use as a proxy for the domestic prices. Prices for the European CO₂ emission certificates are taken from the Portuguese secondary market (SENDECO₂) for European Unit Allowances (EUA)¹¹.

As a very coarse proxy for generation from hydro power plants, we have the total weekly stock of water in domestic dams (in the form of the summed height of all dam water levels in France) from RTE the grid operator.

2.3 Methodology

We want to identify the impact that the level of uncertainty has on the price elasticity of the aggregate supply function. In data terms, this means that we aim to regress the slope of (aggregate) supply bid functions on a proxy corresponding to the uncertainty that existed at the time of bidding. The uncertainty may come from two different sources: (i) uncertainty about the realisation of market demand and (ii) uncertainty on the generation from renewables. Both types of uncertainty affect the residual demand curve faced by each supplier¹².

This regression is able to explain how supply firms adjust their bidding strategies to the expectation of demand shocks that they face. Statistical significance of the level of uncertainty on the slope of the supply function would be evidence that firms take the strategic considerations of dynamic costs into account.

First, in section 2.3.2 we show the final regression of interest. Sections 2.3.2 and 2.3.2 then detail the theory and empirics underlying the variables that feed into the final regression.

Some of the information used in our analysis is drawn from the bid functions of the EPEX Spot market. As introduced in section 2.2, we observe the full aggregate bid functions for both supply and demand, the shape of which (and thus the information that we aim to extract from them, e.g. their slope) varies differently at different points (recall the graphs in figure 2.2.2). Generally speaking, a regression aims at quantifying the impact of some independent variables on a dependent one. The dependent variable is most frequently numerical, and the independent variables explain part of its value. Here the dependent variable is functional in nature, that is that we aim to describe how the supply function changes shape with respect to some independent variables. One

¹¹Each unit EUA permit allows one tonne of CO₂ emissions.

¹²Renewable generation benefits from a feed-in guarantee on the market and thus reduces the residual demand for all traditional electricity producers.

observation is formed of one function coupled to the value of some independent variables. We therefore adopt a functional data analysis approach, which allows us to condition our analysis at specific points $k = 1, \dots, K$ of the functions. This approach allows to define comparable points across auctions, that is different functions, in order to derive insights.

More precisely we want to quantify how uncertainty affects the strategy of bidders from one hour to the next. For this we cannot rely on a standard estimation of the overall demand or supply functions from market outcomes, we want to actually measure how the functions that we observe change shape.

The methodology to select comparable points across auctions is presented in section 2.3.1 and discussed in more detail in Appendix 2.7. This appendix also evaluates the results when applying the technique to our data from the Epex Spot market. Figure 2.3.1 shows the selected points on an example of demand and supply curve.

The different types of points selected capture different information of the aggregate bid functions. The most important point is the one we label $k = 3$, which corresponds to the central part of the bids. This point is most relevant for equilibrium determination¹³. The points $k = 2, 4$ are the points of maximum curvature and represent the transition points between the central (very price elastic) region and the outer (very price inelastic) regions of the bid function. Last, we have the points $k = 1, 5$ which are imposed by the auction rules and are the endpoints of the bid functions.

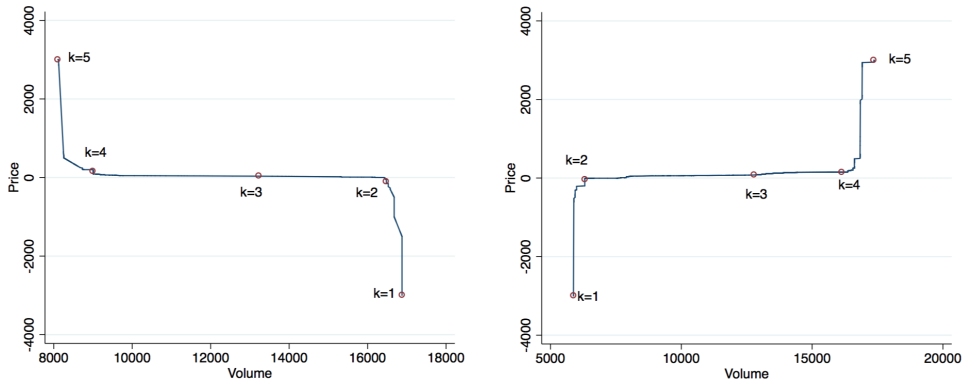


Figure 2.3.1: Selected points on original bid functions

Note: The demand function left, the supply function right, the graph superposes and names the points selected according to the methodology of section 2.3.1.

In Appendix 2.7, we also detail the choice of setting $K = 5$ and show that this choice allows us to improve the precision of our analysis by a factor of 50 when it is conducted on the 5 points simultaneously¹⁴.

¹³See figure 2.9.2 for a glimpse at the distribution of equilibrium outcomes.

¹⁴We briefly mention that the evaluation of the point selection has revealed focal price points for the points $k = 2, 4$. These points are however rarely relevant for equilibrium determination.

2.3.1 Point selection

We develop a methodology to analyse data of a specific format. The focus lies on the methodological details. The evaluation of the performance of our technique is detailed in appendix 2.7. The aim of this methodology is to extract points of interests from functional data. The economic interpretation is secondary in this section.

More precisely, we use a non-parametric, functional data analysis approach to select comparable data points from the original bid functions. These selected points can then be used to run a cross-sectional reduced form model. The utility of this approach is threefold. First, it aims to use as much of the original information as possible without distorting it into parameters of a logistic function. Also, information of different parts of the bid function is not mixed. Second, our approach is “scalable” and as many points as necessary can be extracted. The cross-sectional analyses are then conditioned on the type of comparable points selected. Third, we do not need to assume a specific functional form nor impose overly simplistic assumptions, such as symmetry on the functional forms, to ensure convergence of the estimator.

Reduced form models often rely on exploiting market outcomes, i.e. equilibrium prices and quantities, for their analysis in order to identify the determinants of firm behaviour and test predictions of the theory. On a few markets, we observe sufficient information to get around the problem of using endogenous equilibrium data. For example on the treasury bond markets, we observe both the full aggregate demand and supply functions. This market is of a specific type, it is a divisible goods auction¹⁵. The exact quantity is not predetermined, but endogenous and depends on the price. Furthermore, the auction format requires that buyers submit full demand functions for the goods, i.e. multiple price-quantity combinations at which each bidder is willing to buy electricity. The market price and quantity are determined by the intersection of the aggregate demand and supply functions.

The aggregate bid functions are very rich in information and the reduced form models can be adapted to use this data. However, the literature on working exploiting functional data is limited. [Préget and Waelbroeck, 2005] do this to investigate the determinants of demand bid functions in French treasury bond auctions. They rely on the propositions first put forward by [Boukai and Landsberger, 1998] and [Berg et al., 1999], who identified that aggregate bid functions in divisible goods auctions follow an S-shaped curve that can be estimated by a logistic function. [Préget and Waelbroeck, 2005] shows that across auctions, variation of the demand functions arises from differing auction covariates. [Özcan, 2004] applies the methodology to investigate the revenue superiority of the discriminatory price auction format over the uniform price auction format for the Turkish Treasury bonds market.

¹⁵ Also called multi-unit auctions or share auctions.

More generally, their methodology consists of a two-stage regression. The first stage summarises the (presumably functional) data of the aggregated demand function as parameters of an estimated smooth logistic function. The second stage reuses the information (concentrated in the estimated parameters) for cross-sectional analyses.

This method has worked remarkably well in the context of treasury auctions¹⁶. The logistic function approach does not suit the context of the electricity market because it assumes a strong symmetry in the shape of the functions, whereas we observe in our dataset that a lot of the functions are highly asymmetric, as can be seen in the example of Figure 2.3.2.

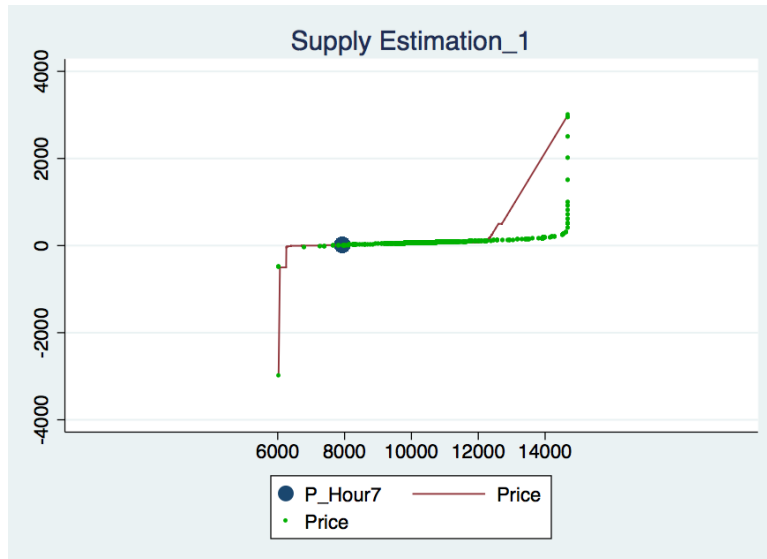


Figure 2.3.2: Example of an assymetric aggregate supply function. In red is the actual aggregate function, in green is an estimated logistic function showcasing the large discrepancies that can arise with this parametric approach. The blue point is the market outcome.

The heterogeneity arises from the fact that the bid functions for the electricity auctions are much richer since we have multiple, strategic players on both the demand and the supply side of the market (unlike the market of Treasury bonds, where the supply is monopolistically determined by the Treasury itself). Furthermore, supplier bidding is strongly influenced by the underlying (step-function-like) marginal cost of the production technology - in particular towards the extremities of the bid functions¹⁷. The observed data is consequently less homogeneous and the fitting of the logistic model not convinc-

¹⁶As an example, [Préget and Waelbroeck, 2005] results provide a forecasting tool of remarkable fit for upcoming treasury auctions. Their correlation coefficient between the observed and estimated stop out rates is 0.99997. This forecasting tool is still in use by the French Treasury (Source: Personal discussions with one of the authors, June 2014).

¹⁷Low volume bids are strongly impacted by ramping costs of base load production technologies (e.g. nuclear), while high volume bids are driven by peak-load production technologies (e.g. gas) which motivate bids closer to linear function and not an S-shaped form.

ing. Furthermore, the economic interpretation of the logistic function parameters is very difficult and reducing the whole bid function to two parameters of interest discards a lot of the original information of the bid functions. Finally, we are uncomfortable with the strong assumption of smooth underlying functions and want to circumvent the problems of fitting these.

Purpose

To briefly fix ideas, let's assume that we are interested in a regression à la:

$$S' = \alpha + \beta \mathbf{X} + \epsilon$$

where S' is the steepness of the bid function, \mathbf{X} the stacked vector of exogenous variables (not specified further here), α the regression constant, β the stacked vector of regression coefficients and ϵ the error term.

The information S' is drawn from the bid functions of a market, which have the specificities as detailed in Section 2.2. As mentioned, we observe the full aggregate bid functions for both supply and demand, the shape of which (and thus the information that we aim to extract from them, i.e. the slope S') varies differently at different points (recall the graph in figure 2.2.1).

For comparability, we require that a chosen point k from a supply function must be comparable to the k^{th} point from the supply functions of another auction. The same goes for chosen points of the demand functions. Note that we do not impose comparability between a pair k of points from a supply and a demand function of the same auction. The reason for this assumption is that comparing those points accross auction allows us to describe how the functions, that is the aggregate strategies, change shape when our independant variables vary.

Non-parametric technique to compare bid functions

Consider two demand functions (as shown in figure 2.3.3). One could compare the k^{th} point of each function to one another. Unfortunately the number of points varies from one auction to another, so this approach would be meaningless. Instead we have to identify "features" of the different functions in order to determine which points can be compared to one another. We aim to reproduce the type of analysis that the brain performs automatically when faced with such curve: we clearly identify three regions of different slope, where the central region is less steep than the left and right regions.

To recognise these features, we perform two successive kernel density analyses¹⁸. For details on the bandwidth and kernel selection as well as algorithm specificities, see ap-

¹⁸Bandwidth in the first estimation = 45, bandwidth in the second estimation = 2, kernels: epanechnikov.

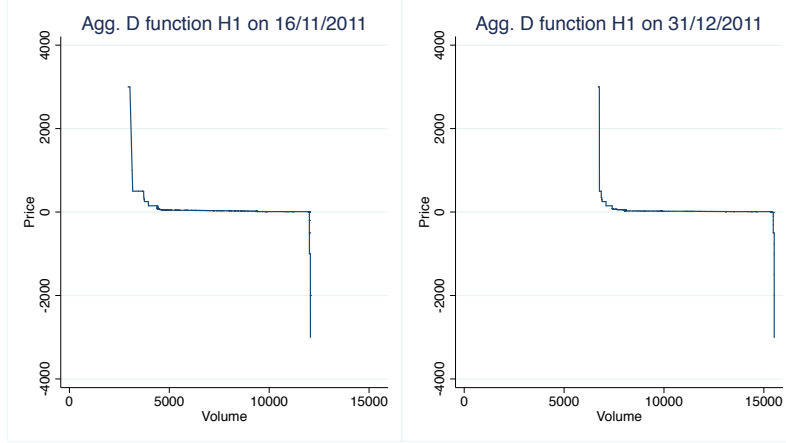


Figure 2.3.3: Comparison of two aggregate demand functions for the same hour

pendix 2.7. This allows us to access estimates of the absolute values of the first and second derivatives of the demand functions as shown in graphs B and C of figure 2.3.4.

From the bid function to the point selection

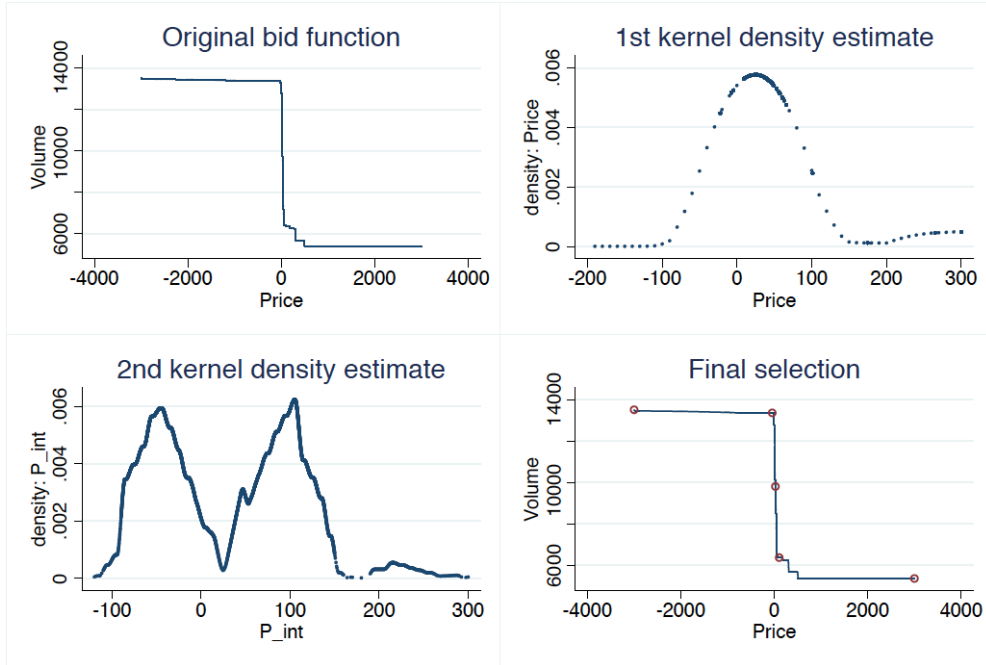


Figure 2.3.4: Steps of the point selection process

Top left (A): The full original aggregate demand bid function for hour 8 on 15.01.2011 in the quantity - price dimension. Top right (B): Kernel density estimates of the first derivative, zoomed on the relevant price range. Bottom left (C): Zoomed kernel density estimates of the second derivative. Bottom right (D): The full original bid function with the $K = 5$ selected points.

We are therefore able to identify the regions of very high curvature, which define the transition between the three characteristic regions of these functions. We assume that these maxima can be compared across different auctions. This hypothesis is commonly

made in functional data analysis and known under the method of landmark registration [Silverman and Ramsay, 2005].

We can develop this method further and define intermediary points¹⁹ that can again be compared to one another. This method allows to define as many points as needed, for computational reasons we limit ourselves to $K = 5$ points²⁰.

Graph D of figure 2.3.4 visualises an original demand bid function and the selected points that we retain as an informative summary of the original curve. Once this work is done we are left with $K = 5$ points per observed aggregate function, those points defined in such a way that they can be compared from one auction to another.

In our setting, the selected points are the two end-points of the curves (where bidding is imposed by the auction rules at the minimum ($k = 1$) and maximum ($k = 5$) Price), the point corresponding to the point of inflection were a smooth functional form imposed (determined by the maximum of the first derivative, ($k = 3$)) and the points separating the regions of high and low elasticity in price (determined by the maximum second derivatives to the left ($k = 2$) and right ($k = 4$) of the POI).

We described the technique here for the case of a demand function. The information measured at these points can thereby be compared across demand bid functions of different auctions. The method is used analogously for selecting comparable points on the supply function. We are hence able to extract slopes at these selected supply bid points, which are again comparable across auctions.

As the focus of this paper is not on this methodology but on what it allows us to study, we describe the results of this specific methodology in appendix 2.7 as well as a discussion of their robustness.

2.3.2 Regression methodology

Identification

At each of these comparable points, we want to identify the effect of uncertainty on the slope of the supply function.

Defining $S'_{i,k}$ the slope of the supply function of auction i at point k in the quantity (X-axis) - price (Y-axis) dimension, \mathbf{X}^S being the vector of exogenous variables, $PLU_{i,k}^D$ being the proxy for the level of demand uncertainty, PLU_i^R being the proxy for the level of uncertainty from renewables, α being the regression constant and ϵ being the error

¹⁹As an example, we could extract those points corresponding to half the density value of the maximum density of the second order derivative. The four points selected (one for each monotone portion of the graph of second derivative estimates) would then correspond to those where the curvature of the function is halved. Together with the maximum, the additional point would contain information on the speed (radius of the curvature) at which the function changes.

²⁰The point selection algorithm took 2 weeks runtime to complete its task of selecting 5 points per function. Defining intermediary points would have taken disproportionately more time since many sorting and interpolation steps are necessary for each intermediate point.

term, we estimate the following:

$$S'_{i,k} = \alpha_k^S + \beta_k^S \text{PLU}_{i,k}^D + \gamma_k^S \text{PLU}_i^R + \delta_k^S \mathbf{X}_i^S + \epsilon_{i,k}^S \quad (2.3.1)$$

We are interested in the sign and magnitude of the coefficients β^S and γ^S , which identify the effects of the PLUs (PLU_i^D and PLU_i^R , respectively) on the shape of the supply bid function. From the predictions outlined in section 2.0.2, we expect a positive coefficient when uncertainty levels increase²¹.

Left-hand-side variables

We extract the slope of the aggregate supply function at any given point k from a kernel density estimation with a bandwidth of 45 units²².

Effectively, this is a smoothed version of the slope. This makes our slope estimates robust to steps in the bid function²³, which in turn allows us to test the predictions from the theoretical paper. Steps in the bid functions mostly are much larger towards the extremities of the bid functions and probably arise from capacity constraints considerations. Working with smoothed slopes is in line with previous work à la [Préget and Waelbroeck, 2005] and [Özcan, 2004], who also apply reduced form models to aggregate bid function data.

Right-hand-side variables

We are regressing an ex-post measure of the auction market (realised slope of the supply bid function) on ex-ante information that bidders have at the time of bidding, i.e. which is available at midday of the day ahead of delivery. We thus keep a strict separation of the ex-post and ex-ante information to the left and right hand side of equation 2.3.1, respectively. This separation allows us to circumvent endogeneity problems and validates the use of simple OLS regressions.

For this reason, we construct our PLUs on the basis of predicted uncertainty. However, for data availability reasons we cannot exclude endogeneity problems completely. For details, see the discussion in section 2.5.3.

²¹Specifically, we want β^S to be positive, γ_1^S positive and γ_2^S negative. For details on γ^S , see section 2.3.2.

²²The slope is a by-product of the point selection mechanism and the bandwidth selection for the smoothing thus follows the same considerations as for the latter. The details of this choice are specified in appendix 2.7.

²³In our data, we observe that bid functions are effectively step functions. On EPEX spot 256 price-quantity combinations are allowed per bidder. When additional bid points are costly, then stepwise bidding behaviour may be very different from a setting where continuous functions can be bid [Kastl, 2011]. Due to the fact that, on average, we do not observe that firms use up all available price-quantity combinations, the cost argument of an additional bid point seems weak. Hence, by smoothing the slope we approximate the unconstrained, continuous bid function.

In this subsection, we first outline how we generate the proxies for the level of market demand uncertainty (PLU^D) in section 2.3.2. Second, we construct the proxies for the level of uncertainty from renewables energies (PLU^R) in section 2.3.2. Third, we detail how the vector of exogenous variables (\mathbf{X}) is constructed in subsection 2.3.2.

Generating proxies for uncertainty from market demand (PLU^D) We construct a proxy for the level of the demand uncertainty (PLU^D) by using the residuals from a demand estimation on exogenous parameters as a measure of the uncertainty that bidders face in an auction. Specifically, our PLU^D is the expected squared level of the prediction errors that firms expect to make when anticipating the demand level of the day ahead. We assume that the ex-post prediction errors give a reasonable estimate of the uncertainty at the time of bidding.

The uncertainty proxy is obtained as detailed next in a three-step procedure. In the first step, we explain what kind of uncertainty our PLU^D refers to. The second step details the conceptual details of constructing the PLU^D . The third step computes the PLU^D .

In the first step, we focus the analysis to a fixed number K of comparable points across auctions by using the non-parametric point selection technique outlined in section 2.3.1. Each k^{th} point is defined by a price and a quantity, which we regress independently on the exogenous variables.

Let us call $P_{i,k}^D$ and $Q_{i,k}^D$ the price and quantity of point k of the realised demand function in auction i , \mathbf{X}_i^D the vector of exogenous variables relevant for the demand estimation.

$$P_{i,k}^D = \alpha_k^{D,P} + \beta_k^{D,P} \mathbf{X}_i^D + \epsilon_{i,k}^{D,P} \quad (2.3.2)$$

$$Q_{i,k}^D = \alpha_k^{D,Q} + \beta_k^{D,Q} \mathbf{X}_i^D + \epsilon_{i,k}^{D,Q} \quad (2.3.3)$$

In regressions 2.3.2 and 2.3.3, firms try to anticipate the realisation of the demand using the exogenous information available. We consider that the producers are able to do such an analysis at the time of bidding.

The prediction errors $\epsilon_{i,k}^{D,J}$, $J = \{Q, P\}$ are a consequence of the stochastic nature of the demand and hence a manifestation of the uncertainty. We consider that more uncertainty will lead to larger prediction errors being made in equilibrium and adopt the square of the residuals $(\epsilon_{i,k}^{D,J})^2$ as our measure for the realised level of demand uncertainty.

In the second step, we recover the residuals from the demand estimation in regressions 2.3.2 and 2.3.3 and test for heteroskedasticity using [White, 1980], which is clearly confirmed (see tables 2.3 and 2.4).

Heteroskedasticity means here that the variation of error terms varies conditional on the levels of the exogenous factors: $E(\epsilon_i^2 | \mathbf{X}_i) = g(\mathbf{X}_i)$. However, they are still orthogonal: $E(\epsilon_i | \mathbf{X}_i) = 0$, thus ensuring that the prediction is unbiased, but not “best” in the sense of the best linear unbiased estimator (BLUE). Thus, heteroskedasticity results in inefficient regressions where the estimator is not minimum variance. Since we do not interpret regressions 2.3.2 and 2.3.3 for causality, but only for predictive purposes, we stick to the unbiased OLS.

The heteroskedasticity regression is given for $J = \{P, Q\}$ by

$$(\epsilon_{i,k}^{D,J})^2 = \alpha_k^{U,J} + \beta_k^{U,J} \mathbf{X}_i^D + \epsilon_k^{U,J} \quad (2.3.4)$$

In the third step, we compute the predicted $\text{PLU}_{i,k}^D$ that firms use when bidding in the auction as:

$$\underbrace{(\widehat{\epsilon}_{i,k}^{D,J})^2}_{\widehat{\text{PLU}}_{i,k}^D} = \alpha_k^{U,J} + \beta_k^{U,J} \mathbf{X}_i^D \quad (2.3.5)$$

The idea is that by experience, firms in the market know that their predictions are more or less accurate depending on the environmental conditions (in the sense of realisations of exogenous factors). In other words, firms can use the realisations of \mathbf{X}^D to infer the accuracy of their demand predictions. Technically speaking, they can use the heteroskedastic nature of the residuals to forecast the level of uncertainty that they face.

The PLU^D subs into regression 2.3.1. For simplicity, we do not include the uncertainty proxies $\text{PLU}_{i,k}^D$ measured at all $K = 5$ points in regression 2.3.1 simultaneously, but only a single $\text{PLU}_{i,k}^D$ at a time. Therefore in the final regression 2.3.1, we regress the slope at a point of the supply function on the $\text{PLU}_{i,k}^D$ estimated at the corresponding point on the demand function. The pairing is done in the quantity dimension. This means that the slope of the supply function at point $k = 2$ is regressed on the uncertainty measured at point $k = 4$ of the demand function (recall the labelling of the points as given in figure 2.3.1). We indicate this quantity paring in the index k^{-1} of the PLU:

$$\text{PLU}_{i,k}^D = \widehat{\text{PLU}}_{i,k^{-1}}^D \quad (2.3.6)$$

An increase in PLU_i^D corresponds to an increase in the uncertainty about the market demand realisation. We thus expect β^S to be positive in regression 2.3.1.

Generating proxy for uncertainty from renewable energies (PLU^R) We have already referred to the statement that the intermittency of renewables causes large residual demand shocks [EPEX, 2014]. Suppliers are thus wary of the expected production of renewables generation.

Given that renewable generation is an exogenous source of supply, it affects the resid-

ual demand curve for each supplier, but does not enter the PLU^D , which captures the uncertainty on market demand only.

In predicting the generation from renewables, we assume that suppliers are able to infer renewables generation from meteorological forecasts²⁴. When forecasting the residual demand shocks due to generation from renewables, we consider that suppliers have an idea of the precision of their estimate based on the “look” of the meteorological forecasts that they have. By look, we mean the geographical heterogeneity or homogeneity of the forecasts. Depending on the disparity of local weather forecasts, inference of the national level of renewables generation is more or less difficult. The geographical disparity of the forecasts is captured by the characteristic length of autocorrelation of weather forecasts, which feeds into our proxy for the level of uncertainty from renewables production (PLU^R).

Intuitively, the characteristic lengthscale of autocorrelation represents the distance required between two geographical points on a map of weather forecasts to observe a decorrelation of half of its maximum value. For example on the wind speeds prediction, a characteristic length of 80 km means that if we observe two very distant points (say 1000km) to have a difference in wind speeds of, on average, 50km/h (this being the maximum difference), then we will observe, on average, wind speed differences of 25km/h for points distant from each other by 80km.

We compute this characteristic lengthscale (L) as described in appendix 2.8. Our PLU^R is defined as the two proxies

$$\text{PLU}_{1,m}^R = \frac{1}{L_m}, \quad \text{where } m = \{\text{Wind, Solar, Temperature}\} \quad (2.3.7)$$

$$\text{and} \quad \text{PLU}_{2,m}^R = \left(\frac{1}{L_m}\right)^2 \quad (2.3.8)$$

Generally, we expect firms to face less uncertainty in predicting weather conditions when the lengthscale of autocorrelation L is longer since the overall weather conditions will be more homogenous. A longer length L (less uncertainty), will yield a smaller PLU^R and we expect a flattening of the supply curve. I.e. we expect a positive coefficient γ_1^S on the $\text{PLU}_{1,m}^R$ variables in the final slope regression.

However, we also expect the effect of L on the slope to be attenuated, if not counterbalanced, by the squared term²⁵. This means that for very short or long L , we expect an additional effect, which signifies reduced uncertainty. In the latter case, exponentially less uncertainty results from very homogenous weather conditions. In the former case, we observe a higher amount of noise in weather predictions. According to the law of large numbers, these errors should cancel out and we thus expect a negative

²⁴We specify the technique in appendix ?? and use it to construct our controls in section 2.3.2.

²⁵We expect the effects of L on the slope to be of the shape of a Laffer curve.

coefficient γ_2^S on the squared PLU^R term in the final slope regression (equation 2.3.1).

Controls This section details the exogenous variables, which we use for our study. The stacked vector of exogenous variables is not identical for the supply and demand regressions of equations 2.3.1 and 2.3.2.

The vector \mathbf{X}^D for the demand equation includes the variables: Tempeff15, Roll_Temp24, Roll_Temp240, suncycle, morning, deltasun, EWH, SolarRest, RteBlackBox.

For the supply regression we include in \mathbf{X}^S the following variables²⁶: Coal, Brent, Gas, IT2, EUA, Wind1DA, Hydro.

Table 2.2 gives a brief overview of the controls used. Details on the computation of some variables are given in the appendix (see links in table). The last column indicates the frequency with which we observe the variable in question.

Name	Explanation	Unit	Frequency
Wind1DA	The day-ahead predicted electricity volume generated from wind turbines. Details on p. 95.	MWh	Hourly
Solar	The electricity volume generated from photovoltaic sources. Details p. 99	MWh	Hourly
Tempeff15	Effective predicted temperature in France (with a cutoff point at 15°C to reflect demand patterns), aggregated on a national level. Details on p. 98.	°C	Hourly
Roll_Temp24	Mean of <i>Tempeff15</i> over the last 24 consecutive hours.	°C	Hourly
Roll_Temp240	Mean of <i>Tempeff15</i> over the last 240 consecutive hours.	°C	Hourly
suncycle	Luminosity as a percentage of maximum luminosity of the day. <i>Midday</i> defined as <i>suncycle</i> =1. Details on p. ??.	%	Hourly
morning	Indicator variable for hours before <i>Midday</i> .	{0, 1}	Hourly
deltasun	Absolute value of the change in <i>suncycle</i> . Details on p. ??.	[0, 1]	Hourly

Continued on next page...

²⁶We do not include the variables used for the demand estimation as they indirectly feed into the final regression via the PLU^D .

... table 2.2 continued

Name	Explanation	Unit	Frequency
EWH	Indicator variable for hours between 10pm and 4am.	{0, 1}	Hourly
SolarRest	The unexplained component of photovoltaic generation. Specifically, the residuals from a regression of <i>Solar</i> on <i>suncycle</i> . Details on p. 100.	MWh	Hourly
RteBlackBox	The unexplained component of the day ahead prediction of total consumption in France issued by the grid operator (RTE). Specifically, the residuals from a consumption estimation. Details on p. 101.	MWh	Hourly
Coal	Average coal import prices at the French border.	€/ton	Monthly
Brent	Average of spot prices for crude oil on the London based stock exchange.	\$/bl	Monthly
Gas	Average of closing prices for natural gas at 1 month on the London market (NBP).	£/Therm	Monthly
IT2	Interaction term: <i>Gas</i> weighted by an hourly index for the demand level. Details on p. ??.	£/Therm	Hourly
EUA	Price of CO ₂ emissions.	€/ton	Daily
Hydro	Sum of dam level heights on a national level.	%	Weekly

Table 2.2: Overview of exogenous variables.

The rationale for the included variables is the following: First, Wind1DA and Solar control for the expected level of renewables generation²⁷ on the day ahead market. These are computed using a novel bottom-up methodology described in the appendix 2.8.1. Second, Tempeff15 controls for the demand patterns as a function of the temperature²⁸. Tempeff15 includes a cut-off at 15°C in order to take into account the demand pattern as a

²⁷For data availability reasons, Solar is computed on realised luminosity values rather than forecasts of luminosity.

²⁸Note that electric heating is widely spread in France. It is used in 32% of principal residences (INSEE, RP2011 exploitation principale).

function of temperature according to [RTE, 2014]. Table 2.15 reveals the improved fit over a simple temperature variable without respecting the demand cut-off (Tempeff). Third, Roll_Temp24 and Roll_Temp240 capture the demand seasonality via the temperature. The former gives the daily average temperature, while the latter captures the average temperature over the last 10 days. The demand cut-off at 15°C for Tempeff15 is respected for these means. Including these as seasonality controls allows to get away from using dummy variables for the seasonality. In short, avoiding dummies yields more transparency of the results as we do not have the problem of interpreting the dummies, which are often black boxes²⁹. Fourth, we use the four variables suncycle, morning, deltasun and EWH

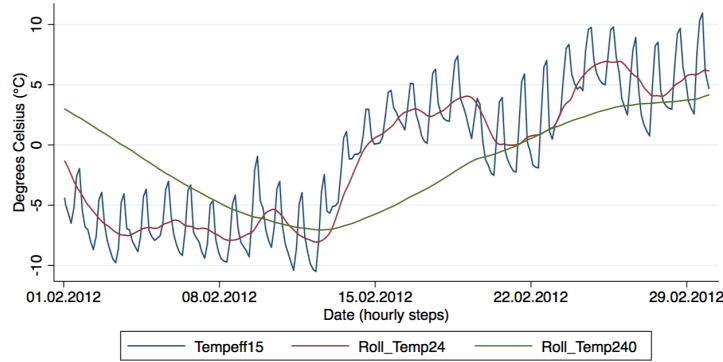


Figure 2.3.5: Temperature based seasonality controls

Note: The graph shows the evolution of the temperature based controls for seasonality for the month of February 2012. The graph shows the lagged nature of the rolling average temperature controls.

collectively to continuously control for the time of the day. The reasoning is again the ability to get away from using dummies and being able to interpret the results. Figure 2.3.6 shows how the controls describe the daily patterns continuously. Fifth, SolarRest and RteBlackBox are the residual information gained from the variables Solar and the day ahead consumption prediction of RTE (PrevConsoH) over other variables included in \mathbf{X}^D or \mathbf{X}^S , respectively³⁰. Sixth, Coal, Brent, Gas, IT2 and EUA are rough proxies for the input prices for electricity suppliers. Hydro is used as a crude proxy for dam operator's ability to generate short term electricity using hydro reserves.

We briefly emphasize that novel methodologies have been used to compute all variables derived from weather forecasts or observations. When tracing back the shape of aggregate bid functions on exogenous factors in the second stage estimation, we use aggregated statistics (at the national level) for the exogenous variables. We thus use an aggregation

²⁹See section 2.5.2 for a full discussion on the advantage of avoiding dummies.

³⁰E.g. Solar is strongly correlated with suncycle, thus SolarRest is the residual from a regression of the former on the latter. RteBlackBox is computed as the residuals from regressing PrevConsoH on Tempeff15, Roll_Temp24, Roll_Temp240, suncycle, morning, deltasun and EWH. See appendix 2.8.1 and 2.8.1 for details.

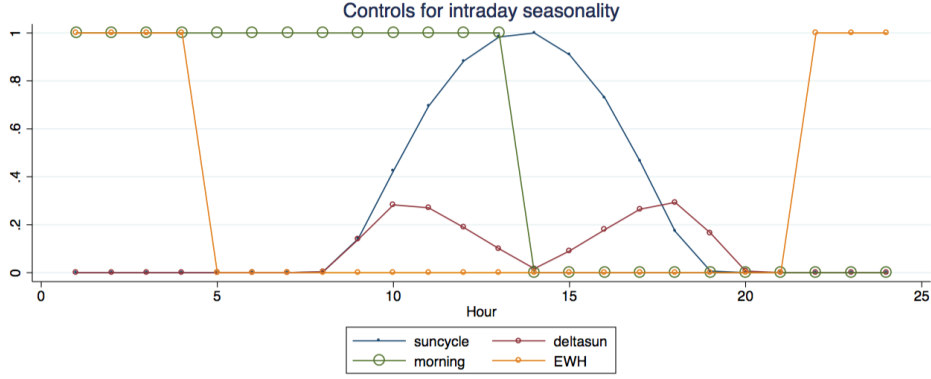


Figure 2.3.6: Continuous controls for daily patterns

Note: With the exception of EWH, all intraday seasonality controls (suncycle, morning, deltasun) are determined endogenously by the prevalent luminosity as captured by Solar.

methodology to summarise local information (collected at the level of the individual postcodes) in order to generate an aggregate statistic at the national level. The general methodology for the aggregation is explained using the example of Solar and as follows: We observe the value of a weather parameter (e.g. luminosity) every hour at known weather stations in France. We apply an interpolation technique in order to obtain parameter values for all possible geographic locations in France. At any local point, we can thus infer the electricity volume generated by using the information of the locally installed capacity (of solar panels) and the renewable energy available (i.e. sunlight inferred by the inverse of nebulosity). We then take the sum of all solar generated electricity per hour in France and use this as our aggregate statistic at the national level in our regression analyses. We used forecast data wherever possible in order to approximate the level of information that bidders have at the time of bidding and circumvent endogeneity problems. For cases where forecast data was not available, e.g. Solar, realised weather data was used.

Extensions and robustness checks

In order to test the robustness of our results and circumvent some drawbacks of the baseline model, we use a few alternative specifications of our empirical model.

Bootstrapping standard errors

The set-up of our empirical analysis relies on stochastic variables, e.g. PLU^D , which are computed in the first stage of our identification. The assumption made for an OLS regression of normally distributed residuals is a very strong one (particularly with the forecast variable) and one which can flaw the precision of estimates in the second stage regression. We therefore bootstrap the standard errors of the final regression by using

random sampling with replacement at each stage of the analysis, i.e. for both the PLU computation and the final slope regression with 300 repetitions.

Bootstrapping allows us to non-parametrically approximate the distribution of the forecast PLUs and thus enables us to correct the standard errors of our coefficient estimates.

Kernel based uncertainty forecasts (PLU^D) The PLU^D computed as described in section 2.3.2 is noisy since we assume a linear forecast model to be valid for any combination of realisations of exogenous parameters, i.e. the same model applies winter and summer, day and night. While the results are as desired for the baseline PLU^D , a bootstrapping of the standard errors indicates that the first stage forecast is too imprecise for effects of a satisfactory significance level.

We therefore develop an extension of the uncertainty prediction model in which we use the idea of demand forecasts (equation 2.3.5) only locally, i.e. for a limited range of variation in the exogenous parameters. In other words, we estimate the PLU^D corresponding to an auction only in the neighbourhood of this auction, i.e. over all auctions that occurred in similar conditions. By conditions, we mean realisations of exogenous parameters and the neighbourhood refers to the concept of measuring the similarity of these realisations by means of a range. The next step explains how this is done formally.

We consider that firms predict the level of the uncertainty by comparing it with the level of uncertainty in past³¹ auctions of similar exogenous conditions. The methodology is analogous to the computation of the baseline PLU^D . The suppliers forecast the precision (squared residuals) of their demand estimation as before, but only on a subsample of the data. The subsample is defined as all observations which lie within a distance b_{X_e} of the observation of interest with respect to each control variable X_e , $\forall e = \{1, \dots, E\}$. Effectively, this is a multi-variate kernel regression and subsequent forecast with a rectangular (also called “boxcar”) weighting function. Observations within the kernel window are given equal weight, while observations outside the kernel window are given zero weight. We set the bandwidth b_{X_e} with respect to each variable equal to $\frac{1}{3}$ of the range of that variable³².

At any arbitrary observation (auction) with the realisation $\tilde{\mathbf{X}}$ for the stacked vector of exogenous variables (X_e), the simple weight function is

$$W(\mathbf{X}) = \prod_e W(X_e) , \quad \text{where } W(X_e) = \begin{cases} 1, & \text{if } |\tilde{X}_e - X_e| \leq b_{X_e} \\ 0, & \text{otherwise.} \end{cases} \quad (2.3.9)$$

³¹For data availability reasons, we pool all (past and future) auctions for the computation of this PLU. This introduces some endogeneity. For a discussion of this choice, please see section 2.5.3.

³²See appendix 2.9.1 for details. Column 2 of table 2.16 indicates the choice of b_{X_e} for each exogenous variable considered.

and the subsample based regressions are then

$$P_k^D(\mathbf{X}) = \alpha_{k,\tilde{\mathbf{X}}}^{D,P} + \beta_{k,\tilde{\mathbf{X}}}^{D,P} W(\mathbf{X}) + \epsilon_{k,\tilde{\mathbf{X}}}^{D,P} \quad (2.3.10)$$

$$Q_k^D(\mathbf{X}) = \alpha_{k,\tilde{\mathbf{X}}}^{D,Q} + \beta_{k,\tilde{\mathbf{X}}}^{D,Q} W(\mathbf{X}) + \epsilon_{k,\tilde{\mathbf{X}}}^{D,Q} \quad (2.3.11)$$

and the local uncertainty regressions and forecasts $\forall J = \{P, Q\}$ are given by

$$(\epsilon_{k,\tilde{\mathbf{X}}}^{D,J})^2 = \alpha_{k,\tilde{\mathbf{X}}}^{U,J} + \beta_{k,\tilde{\mathbf{X}}}^{U,J} W(\mathbf{X}) + \epsilon_{k,\tilde{\mathbf{X}}}^{U,J} \quad (2.3.12)$$

$$\underbrace{(\epsilon_{k,\tilde{\mathbf{X}}}^{D,J})^2}_{\widehat{\text{PLU}}_{k,\tilde{\mathbf{X}}}^D} = \alpha_{k,\tilde{\mathbf{X}}}^{U,J} + \beta_{k,\tilde{\mathbf{X}}}^{U,J} \tilde{\mathbf{X}} \quad (2.3.13)$$

When firms infer the upcoming uncertainty by looking at the uncertainty in past auctions, the precision of their estimate depends on the number of comparable auctions available, i.e the sample size. Given that the sample size varies greatly across auctions, we use a sample-size-weighted OLS regression in the final estimation of equation 2.3.1. Finally, we bootstrap the standard errors on the kernel-based PLUs using 50 repetitions³³.

2.4 Results

We first present the results for the demand estimation in both the Price and Volume dimension since this step is identical for all PLU specifications. We then present the results of the final regression in the baseline and alternative specifications.

2.4.1 Demand estimation

Table 2.3 gives the results for the demand estimation on volumes (equation 2.3.3). Table 2.4 shows the results for the demand estimation on prices (equation 2.3.2).

These tables are interesting for two reasons. First, they provide the basis for our computation of the PLU^D . Second and the reason why we disclose them in such detail, they are already a result in themselves.

It is comforting to see that all variables used are significant and, more importantly, of the expected sign. Thus, these results provide support for our specification of the demand estimation. For the interpretation here, we focus on the effects at the point of inflection³⁴ ($k = 3$).

³³For computational reasons, we only bootstrap the kernel based PLUs for the point of inflection ($k = 3$). We choose only 50 repetitions for the same reason. Given the size of our dataset, we consider it acceptable. The general criterion for convergence is that each observation is selected at least once in the bootstrapping exercise.

³⁴As mentioned, the point of inflection is the centre point of the bid curves and the most relevant for equilibrium determination.

First, looking at the volume effects of the exogenous variables: All variables included in the regression are highly significant at the 1% level. All temperature statistics (Temp_eff15, Roll_temp24, Roll_temp240) bear coefficients with a negative sign and confirm that electricity demand falls with increasing ambient temperature. All daytime controls show up the expected sign as well: suncycle and deltasun have positive coefficients. This is sensible as electricity demand is higher during the day than at night (proxied for by suncycle) and rush or activity hours (proxied for by deltasun) in the morning and evening are also characterised by increased demand. The variables morning and EWH have coefficients of a plausible negative sign. The morning as controlled for by our indicator variable³⁵ is shorter than the afternoon and evening together, thus total electricity consumption is lower as well. EWH stands for the deep night between 10pm and 4am and thus also corresponds to low demand periods. SolarRest controls for selfgeneration to cover own consumption and has a plausible negative coefficient. RteBlackBox on the other hand has a very sensible positive coefficient and confirms that actual demand is higher when the grid operator expects it to be the case.

The analysis of the price effects of these controls on demand functions is in line with the analysis of volume effects. This is coherent since for a linear downwards sloping demand curve, a left shift (volume decrease) is synonymous for a downwards shift (price decrease) of the curve. We consider that at the point $k = 3$, the demand functions are locally linear. We note the only exception for the coefficient of SolarRest which has a positive price effect, while a negative volume effect³⁶.

Second, these tables already give a descriptive analysis of the effects of exogenous variables on the shape of the demand bid function: We now compare all coefficients for a specific variable on the $K = 5$ different points on the demand function (we read the table horizontally and compare sign changes across columns). In table 2.3, we observe for each row at most a single sign change across the coefficients for the different points. Furthermore (and with few exceptions), the magnitudes of the coefficients generally increase or decrease monotonically along a row. This is very convincing as it suggests that exogenous variables have a monotone effect on the shape of the bid function. We thus only observe one-directional shifts (e.g. a unilateral left shift) or two-directional shifts (extension or contraction) in the volume dimension induced by the variation in exogenous variables. While the unilateral effects are explained analogously to our point specific interpretation on the point $k = 3$ above, we do not have a story to tell about two-directional effects. Tempeff15 results in a contraction of the bid function in terms of

³⁵The morning is defined as the hours before midday, which occurs when luminosity is at its daily maximum.

³⁶We emphasize in the construction of our variable (appendix 2.8.1) that it is not possible to build a proxy for lighting consumption that would allow us to decorrelate the effects from photovoltaic production and lighting consumption. We therefore stick to the SolarRest proxy, which aims to capture the effect of Solar which is not captured by suncycle.

volumes (right shifts on low volume points, $k = 5, 4$ and left shifts on high volume points $k = 3, 2, 1$). Roll_Temp24 has the opposite effect and results in a volume extension of the curve. Roll_Temp240 induces a pure left shift of the whole function.³⁷. For the intraday seasonality controls, the results are very clear. While suncycle results in an extension of the demand function³⁸, all other intraday controls (morning, deltasun, EWH) have unilateral effects. When the indicators morning and EWH are positive, we observe volume decreases at all points and thus a left shift of the function. Higher values of deltasun induces volume increases at all points of the bid function. Finally, we have SolarRest which induces an expansion of the curve and RteBlackBox which has a unilateral right shifting effect on the aggregate demand bid function.

The price variation of the demand bid function yields interesting results, too. Given that the prices of points $k = 1, 5$ are fixed, we only observe effects for the interior points. We thus focus on the effects on the points $k = 4, 3, 2$ only (called the “central demand function” here). Again, we only observe at most a single sign change across columns for any exogenous variable. Both Tempeff15 and Roll_Temp240 lead to an extension of the central demand function (we are now looking at vertical variation of the bid function as shown in fig. 2.3.1), while Roll_Temp24 causes a unilateral downwards shift. For intraday seasonality controls, we see that suncycle and deltasun have a contracting effect on the central demand function and morning a unilaterally negative effect. EWH leads to an expansion of the central demand function. SolarRest and RteBlackBox indicate an extension of the central demand function in the price dimension.

³⁷Excluding interaction effects, we note that the net effect of a simultaneous 1°C increase for all three temperature variables results in a net left shift of the function. In the price dimension (table 2.4) we observe a net downwards shift. Both effects suggest that electricity demand decreases with the prevailing temperature.

³⁸Combined with the observed price effects from table 2.4, this suggests that demand is more price elastic during the day.

	$k = 5$ Volume	$k = 4$ Volume	$k = 3$ Volume	$k = 2$ Volume	$k = 1$ Volume
Tempeff15	50.72*** (9.942)	38.58*** (10.13)	-130.3*** (10.94)	-189.3*** (13.32)	-204.0*** (13.20)
Roll_Temp24	-63.57*** (11.78)	-67.13*** (12.06)	-48.87*** (13.14)	19.76 (15.83)	34.16** (15.76)
Roll_Temp240	-60.15*** (6.655)	-68.38*** (6.867)	-78.49*** (7.450)	-78.44*** (10.05)	-87.38*** (10.00)
suncycle	-894.0*** (44.27)	-652.1*** (45.50)	508.2*** (48.52)	1,351*** (56.36)	1,400*** (55.73)
morning	-101.2*** (27.52)	-220.3*** (28.33)	-814.8*** (30.44)	-872.2*** (37.71)	-885.8*** (37.28)
deltasun	2,659*** (153.5)	2,850*** (158.5)	3,201*** (166.1)	1,721*** (197.8)	1,821*** (196.5)
EWH	-803.1*** (30.74)	-833.1*** (31.91)	-782.7*** (33.15)	-354.7*** (42.09)	-322.8*** (41.78)
SolarRest	-0.595*** (0.0282)	-0.363*** (0.0305)	-0.145*** (0.0342)	-0.0137 (0.0418)	0.246*** (0.0407)
RteBlackBox	-0.00259 (0.00235)	0.0127*** (0.00243)	0.105*** (0.00255)	0.107*** (0.00316)	0.0979*** (0.00317)
Constant	6,054*** (33.71)	7,086*** (35.04)	11,446*** (37.15)	15,215*** (48.68)	15,502*** (48.27)
Observations	14,691	14,691	14,691	14,690	14,691
R^2	0.201	0.219	0.478	0.344	0.346
White	548.6	524.9	407.9	961.8	944.8

Robust standard errors in parentheses

*** p<0.01, ** p<0.05, * p<0.1

Table 2.3: Estimation results for demand volumes

Note: The estimated constants of this table or the left graph of fig. 2.3.1 indicate to which portion of the demand function the types of points $k = 1, \dots, 5$ refer.

	$k = 5$ Price	$k = 4$ Price	$k = 3$ Price	$k = 2$ Price	$k = 1$ Price
Tempeff15	0 (0)	4.675*** (1.523)	-0.969*** (0.0599)	-1.308*** (0.0980)	0 (0)
Roll_Temp24	0 (0)	-10.07*** (2.233)	-0.124* (0.0713)	-0.0470 (0.116)	0 (0)
Roll_Temp240	0 (0)	4.250*** (1.147)	-0.0901** (0.0404)	-0.353*** (0.0607)	0 (0)
suncycle	0 (0)	-10.98** (5.020)	6.870*** (0.258)	11.60*** (0.445)	0 (0)
morning	0 (0)	-0.226 (4.133)	-5.748*** (0.173)	-9.009*** (0.285)	0 (0)
deltasun	0 (0)	-16.54 (19.16)	10.60*** (0.881)	18.72*** (1.497)	0 (0)
EWH	0 (0)	5.136 (4.448)	-1.756*** (0.192)	-3.014*** (0.302)	0 (0)
SolarRest	0 (0)	0.000532 (0.00307)	0.00192*** (0.000193)	0.00253*** (0.000326)	0 (0)
RteBlackBox	0 (0)	9.91e-05 (0.000301)	0.000906*** (1.47e-05)	0.00147*** (2.26e-05)	0 (0)
Constant	3,000 (0)	131.3*** (4.210)	39.45*** (0.217)	-39.43*** (0.319)	-3,000 (0)
Observations	14,691	14,691	14,691	14,690	14,691
R^2		0.005	0.463	0.420	
White		138.2	640.9	761.2	

Robust standard errors in parentheses

*** p<0.01, ** p<0.05, * p<0.1

Table 2.4: Estimation results for demand prices

Note: The estimated constants of this table or the left graph of fig. 2.3.1 indicate to which portion of the demand function the types of points $k = 1, \dots, 5$ refer.

Overall, we take away a solid R^2 with coefficients of the correct sign. We furthermore have disclosed the White statistic which unanimously confirms heteroskedasticity in these regressions. The significance levels have been measured using robust standard errors. We point to the fact that the explanatory power of our demand estimations is highest for the point of inflection, in line with our expectations. Points of maximum curvature $k = 2, 4$ reveal lower R^2 statistics. This is likely due to the underlying data patterns that arise from bidding frictions, e.g. focal price points. For these points, it is thus not surprising that we do not observe convincing demand estimates - we note in particular the lack of explanatory power for the demand estimation in the price dimension for points of type $k = 4$.

2.4.2 Final regression

For the final regression, we first lay the focus on the point of inflection ($k = 3$) for a detailed interpretation of our results. We choose the point $k = 3$, because this type of point is the most relevant for equilibrium determination. We then disclose the results for all other points $k \neq 3$ to give an overview of the effects of uncertainty on the whole aggregate supply bid function.

Each result table has four (three³⁹) columns to show the results for different estimators and two specifications of the PLU^D . All other variables remain unchanged across the columns. In the tables, column 1 refers to the baseline specification of the $PLU^{D,J}$, where standard errors are calculated using the Huber-White sandwich estimator. Column 2 reports the results for the baseline model using bootstrapped standard errors with 300 repetitions. Column 3 reports the results for the regression on the kernel based $PLU_{\tilde{X}}^{D,J}$, using the sample size of each kernel as weights in the regression. Column 4 reports the results of the kernel based model using bootstrapped standard errors using 50 repetitions⁴⁰.

Regarding notation: In the results tables, $PLUvRvar'm'$ stands for $PLU_{1,m}^R$ with ‘m’

³⁹For computational reasons, we do not run the bootstrapping of the kernel based PLU^D for the points $k \neq 3$, thus we only have three columns for these tables.

⁴⁰Coefficients vary slightly ($< \pm 20\%$, no sign change), because the bootstrapping loop includes the kernel-based prediction of the uncertainty and thus varies the kernel sample sizes, which are used as weights in the final regression. Furthermore, the estimator has probably not yet fully converged with 50 repetitions, however for computational reasons we stick to this choice.

being replaced by the initial of the variable in question (W, S and T, respectively). $\text{PLU}_{2,m}^R$ is indicated by the extension “sq”. $\text{PLUvDvar}'J'$ stands for $\text{PLU}^{D,J}$ with $J = \{P, Q\}$ representing the dimension in which the demand uncertainty is measured. The kernel based $\text{PLU}_{\tilde{X}}^D$ are given by $\text{PLUvDvarK}'J'$ in the tables. To facilitate the reading of the tables, we adopt this notation for the discussion of the results.

For the point of inflection ($k = 3$), the results are shown in table 2.5. Regarding uncertainty from renewables production, only that of wind has a significant and robust impact. PLUvRvarW has a positive effect (significant at the 1% level) on the slope in all specifications. PLUvRvarWsq has a negative effect on the slope in all specifications, however this second effect is not robust to bootstrapping the standard errors. The signs of the estimated coefficients are in line with our expectations. To show this, we recall that both versions of the PLUvRvarW are based on the inverse of the characteristic lengthscale L_W of autocorrelation of the wind speed measurements. Thus, when L_W increases (it represents a decrease in the uncertainty since wind speeds are homogenous over longer distances), the PLU decreases (corresponding to a decrease in uncertainty). While an increase in the PLUvRvarW leads to an increase in the slope of the supply function, the effect is attenuated by the squared term PLUvRvarWsq for very small and large L_W ⁴¹. The estimated coefficient for the latter is negative and suggests that for very short L_W (i.e. very heterogeneous wind speeds over the country), prediction errors cancel out. For very long L_W (i.e. very homogeneous wind speed profile), the marginal impact of L_W on the level of uncertainty decreases.

With respect to the uncertainty from temperature forecasts, the results are insignificant (although of the anticipated sign). We expect the impact of temperature uncertainty goes via the demand response, which we account for in our proxy for the uncertainty from demand realisation (PLUvD). Similarly, uncertainty from Solar production is attributed no effect. This is not surprising as generation from solar is only a fraction of that generated from wind power and thus negligible. Furthermore, we are unable to disentangle the effect of solar generation from the reduced demand effect from high luminosity (which result in low demand for lighting). We do not find evidence for a direct response from

⁴¹By looking at the variation of our data, we see that the negative effect of the PLUvRvarWsq term merely attenuates, rather than overrides, the positive effect of the PLUvRvarW term on the slope since in our dataset we very rarely observe PLUvRvarW values sufficiently large to exceed the maximum of the Laffer curve of the impact on the slope.

suppliers to uncertainty in temperature or solar predictions.

Uncertainty from the realisation of market demand has a negative and significant effect when proxied for by price-based PLUvDvarP (see table 2.5) as opposed to a positive and significant effect when proxied for by a volume-based PLUvDvarQ (see table 2.5). The positive effect on PLUvDvarQ is in line with our prediction made in section 2.0.2. This results supports the theory that firms take uncertainty when bidding into account and consequently adjust their bidding strategy in order to minimise dynamic costs. However, our theory produces a prediction for volume based uncertainty only. We include the uncertainty proxy for price PLUvDvarP as a control and its effect seems rather robust. The effects of PLUvD in either the price or volume dimension are robust to the exclusion of the other⁴². We do not have a story to explain the opposing signs for the coefficients of the two proxies⁴³.

Furthermore, table 2.5 gives support to our extension using kernel based PLUvDs. Column 2 shows that the effects of the baseline PLUvD are not significant when bootstrapped. Our alternative is to use a more elaborate uncertainty prediction model. These kernel based PLUvD are more sophisticated in two respects: (i) the forecasting model is only applied locally, that is auctions are only compared to similar auctions and (ii) the obtained forecast is weighted by the sample size used for its prediction. Thereby, we control for the confidence of the firms in making those predictions. The results of the weighted regression are given in column 3. The results using the more elaborate prediction model are in line with those from the baseline regression, while being more accurate as indicated by the improved explanatory power of our model (we see a 16.5% increase of the R² from columns 1-2 to columns 3-4). Finally, the results of our kernel based model are more precise as indicated by the higher significance level for the PLUvDvarKP and PLUvDvarKQ, which are now also robust to a bootstrap (column 4).

Finally, we explicitly include the controls for the levels of the input prices of electricity producers (\mathbf{X}^S). We do not interpret these coefficients since there are no ex-ante expectations of their levels to affect the slope of the supply bid function. We briefly mention that intraday seasonality controls as well as other demand related variables are not

⁴²Results available from the authors.

⁴³The net effect cannot be precisely computed as the conversion of the PLUvD from the price dimension to the quantity dimension is not possible. We approximate the comparison however, by including both PLU^D simultaneously in the regression. All PLUvD are rescaled by their respective means to allow some degree of comparison.

included in this regression to avoid multicollinearity problems with the PLUvD, which are themselves computed as a linear combination of the demand control variables (\mathbf{X}^D).

Overall, we take away a goodness of fit of $\geq 20\%$ for our empirical model as well as the robust positive coefficients for both the demand based uncertainty proxy (PLUvDvarQ) and the weather based uncertainty proxies (PLUvRvarW and PLUvRvarWs). We note the puzzling result for the PLUvDvarP.

For the other points ($k = 1, 2, 4, 5$), the results are given in tables 2.6, 2.7, 2.8 and 2.9, respectively⁴⁴. We comment on the effects over all points collectively in order to give an overview of the full bid function behaviour.

The specification of the proxies for the uncertainty from renewables as well as of the controls does not vary across columns, we thus focus on column 2 for these (in order to take bootstrapped standard errors into account). While we observe in table 2.5 a convincing effect for the uncertainty from wind predictions on the slope of the point of inflection ($k = 3$), we cannot observe this effects on the other points of the bid function⁴⁵. No other proxy for the uncertainty from renewables has a significant effect on the slope at any point.

The proxies for uncertainty from market demand produce opposing effect depending on the prediction model. PLUvDvarP has a negative and significant effect on all points (with the exception of points $k = 1$ and $k = 5$ of course, which do not exhibit variation in prices due to the auction rules). PLUvDvarQ has a positive effect, when significant⁴⁶, on all points ($k = 2 - 5$), but not on $k = 1$.

On the remaining controls, we do not observe a clear patterns on the effects at the different points. We run the analysis without these controls and note that the signs of all significant variables remain unchanged⁴⁷.

⁴⁴Variables marked “(omitted)” are drop due to perfect collinearity.

⁴⁵We note the exception of a negative effect for PLUvRvarW on the slopes at points $k = 2$ and 5 (significant at the 5% level).

⁴⁶For both the bootstrapped baseline results (col. 2) and the weighted kernel based specification (col. 3).

⁴⁷Results available from the authors.

2.5 Discussion

In this section we reflect on the results and use the opportunity to address a few issues, drawbacks as well as qualities of the research conducted. We first discuss the findings of the paper and their internal and external validity. We briefly review the design of the empirical strategy and lend particular focus to how we deal with the issue of endogeneity.

2.5.1 Findings

In this paper, we investigate whether uncertainty affects supplier bidding as predicted by the theory. We find that uncertainty from weather forecasts indeed affects the suppliers' bid function as expected. The aggregate supply function steepens when the level of uncertainty increases. We take this as evidence that firms take dynamic cost considerations into account and adjust their behaviour when facing increased expected dynamic costs.

We also find significant results for the effect of the level of uncertainty about the realisation of market demand on the suppliers' behaviour. However, we observe a strong discrepancy between the effect for uncertainty as measured on price volatility and the effect of uncertainty as measured on volume volatility. While the former is attributed a negative effect, the latter is attributed a positive effect on the slope of the aggregate supply function. The differing opposing results are robust in all specifications and seems to be of too much importance to be neglected.

The two proxies in question ($PLU^{D,P}$ and $PLU^{D,Q}$) are two variables designed to measure the same information, namely the prediction error of the demand function. As such, they are identical with respect to the set-up, computation as well as point at which they are extracted. They only differ with respect to the dimension in which the variation of the demand function is measured, the former in the price dimension and the latter in the volume dimension.

A theory using linear functions would predict that these measures of the shifts of the demand line are identical and interchangeable (modulo a translation by the slope). Also our data, i.e. the observed bid functions, suggests that, at least locally at the point $k = 3$, the bid functions are linear⁴⁸. Furthermore, our demand estimation models for both price and volume variation⁴⁹ indicate that the prediction model used works well in

⁴⁸Recall the graph in figure 2.2.2.

⁴⁹Precisely look at columns 3 of tables 2.3 and 2.4.

both dimension. In particular at $k = 3$, significance and equal signs on coefficients for all terms included as well as similar explanatory power⁵⁰ in both regressions confirms the similar nature of the two proxies.

Our recovered $\text{PLU}^{D,P}$ and $\text{PLU}^{D,Q}$ are, as expected, collinear⁵¹. While OLS remains unbiased in the presence of collinearity between two regressors, its precision is reduced. We correct for the collinearity by dropping one proxy or the other, but the individual results remain unchanged - the coefficients of the two proxies keep opposite signs.

Assuming that our empirical strategy is valid to test the relationship of interest, a possible reason for our intriguing observations could be that the slope of the demand function, which relates $\text{PLU}^{D,Q}$ and $\text{PLU}^{D,P}$, is endogenous on the uncertainty. Uncertain demand does not only unilaterally shift the demand function in one dimension (either P or Q), but also affects the shape and thus the slope of the curve. This effect is not accounted for in our research design and could drive the opposing results for both proxies. The endogeneity of the slope of the demand curve could be accounted for in our model by extracting the residuals from a regression of $\text{PLU}^{D,P}$ on $\text{PLU}^{D,Q}$ in an analysis to see if endogeneity exists and then reusing the residuals to control for slope effects of the demand curve in the final regression. We leave this avenue for further research.

Without having resolved the empirical discrepancy in the results, the stark contrast between the two could also hint at the fact that we need new theories to explain both demand and supplier bidding behaviour on the electricity market. This calls for new theoretical models to better explain the shape of aggregate bid functions, which are S-shaped overall. Special attention in these models should be placed on the effect of uncertainty and its importance for bidders via the link of dynamic costs.

Finally, our analysis relies strongly on the analysis of the point of inflection ($k = 3$), but the functional analysis is important, too. While results on the whole bid function are broadly speaking in line with the point-specific analysis on the point of inflection, the significance of the results is weaker and the results less clear. Furthermore, we often observe varying effects on low and high volume points⁵². We conclude that the impacts of variations in exogenous factors on the shape of the bid functions are not

⁵⁰R² of 0.463 for the price and 0.478 for the volume regression.

⁵¹Not perfectly, but with a correlation coefficient of 0,62

⁵²We refer specifically to the strengthening or weakening effects of exogenous variables on different points as shown in demand level estimation tables 2.3 and 2.4 as well as in the slope regressions tables 2.6 - 2.9.

uniform. Non-linear effects are neither predicted by our linear theory nor have been shown in previous studies (with the exception of [Wolfram, 1999]). Our results hint at more intricate mechanisms which drive the shape of these bid functions.

2.5.2 Internal and external validity

We believe that the work is credible due to many aspects of the research design.

First, our set-up is based on rather intuitive relations which we test exclusively using simple OLS regressions. These regressions are econometrically unbiased given the data impurities that we observe. To guarantee precision of our estimates, we use bootstrapping techniques.

Second, considerable effort has gone into the treatment of the information that goes into the right hand side of our regressions. We do not only refer to the final PLUs used, but also point at the precise use of our controls. See for example the treatment of the variable RteBlackBox (details see page 101), which proxies for the information contained in the day ahead demand estimates (PrevConsoH) given out by the grid operator RTE. In order to extract the marginal information of the PrevConsoH estimate, which is not explained by other controls variables that we include in our analysis, we compute the residuals from a regression of PrevConsoH on our other controls, e.g. daytime controls such as suncycle. These residuals (called RteBlackBox) enable us to achieve a more sophisticated understanding of our regression output⁵³.

We also emphasize the aspect that we understand our dataset as a cross-sectional dataset rather than a time-series. While we do segment our dataset into weekday and weekend days and only run our analysis on the former, there is no reason why demand on a Tuesday afternoon should not be comparable to demand on a Thursday afternoon. We therefore ignore weekday dummies to increase our sample size. Furthermore, we avoid the use of dummy variables to control for the hour of the contracts in our regressions in order to further increase the sample size. However, we cannot compare electricity consumption between 4am and 4pm within a day. Neither can we compare two 4pm hours of a day in winter and another in the summer. Using dummies would first restrict our sample size, plus make our interpretation more difficult since the dummy variable aggregates the effect over all conditions that change between samples. We use a bottom

⁵³See for example the regression output of the demand estimation in tables 2.3 and 2.4.

up approach that allows us to circumvent the sample size restriction and interpretation difficulties from daytime or seasonality dummies. Instead, we use continuous variables to control for the daytime and season by means of short and longer term temperature averages or other weather characteristics such as luminosity , which generates controls like deltasun^{54} .

Finally, we point at the empirical framework that allows us to run reduced form regressions on multiple regions of bid functions to better understand functional responses of those bids to variation in exogenous factors. We use 5 points for our analysis and refer to appendix 2.7 for the full details on this choice and the evaluation of the point selection. With hindsight, we feel that an additional two points would have been useful to better understand functional behaviour of the part of the bid functions, which is more relevant in equilibrium, i.e. on the centre part⁵⁵. We note the computational demands of more points.

The methodology developed for our exercise on data from the French electricity market has applications in other domains. This is valid for the non-parametric point selection mechanism (section 2.3.1), the mechanism to aggregate local geographic data to a national level (appendix 2.8) as well as the identification strategy based on purely ex-ante data.

In particular, we note that the possibility to run reduced form estimation strategies for the analysis of markets which make access to functional data available. This includes all markets which use a multi-unit, uniform (or discriminatory) auction mechanism.

2.5.3 Endogeneity

The set-up of this work is specifically aimed at circumventing problems of endogeneity. For that sake, we keep a strict separation of ex-post and ex-ante information to the left and right hand sides, respectively, of any regression.

To achieve this separation of ex-ante and ex-post information, both newly developed methodologies are highly useful. The point selection methodology from section 2.3.1 allows us to extract proxies for the level of uncertainty about the realisation of market demand, which are unaffected by the equilibrium interaction with the market supply. The weather data treatment methodology from appendix 2.8) enables us to base our proxies

⁵⁴See section 2.3.2 for full details on our set of control variables for both demand and supply.

⁵⁵For that we would recommend the points representing half of the maximum curvature between the current points $k = 2, 4$ and $k = 3$.

for the level of uncertainty from renewables on measures of the expected homogeneity of weather forecasts. Both methodologies allow us to recover ex-ante information on the prevailing uncertainty that firms have at their hands at the time of bidding. The information contained in all other controls used is also available at the time of bidding.

However for data availability reasons, we are not able keep this strict separation at all times in practice and revert to using ex-post data to compute some variables that should ideally be computed on ex-post information only. This is the case twice in this work: (i) we use observed weather data to compute the variable Solar⁵⁶ and (ii) we use the pooled data over all auctions for the demand estimation and subsequent uncertainty forecast of equations 2.3.2 - 2.3.5.

In both cases, we do not believe that this choice compromises our results. For the case of Solar, we use realised luminosity instead of forecast data. This is as if weather forecasts were perfectly accurate. Given that solar production only accounts for a small fraction of total electricity generation and that we extract the very informative component of the Solar variable by using the variable suncycle (which is arguably very well predictable), we do not see the use of ex-post data as problematic.

For the case of the PLU^D computation, we run the demand estimation pooled over all observed auctions (i.e. past and future) and say that firms have this level of information when bidding in each auction of our sample. We do so because, we do not have the necessary data before 01.01.2011 and thus cannot calibrate our forecasting model on a “learning” dataset. Instead, we assume that demand patterns conditional on the explanatory variables has remained constant over our 2.5 years time period of analysis. The estimation based on pooled data then yields, on average, the same insights as an analysis conducted purely on past data.

We could test robustness of our pooled approach by investigating the effect of a restriction on using only past data in the demand estimation. A learning effect could arise from more precise estimations of demand functions. However, due to the long experience of most firms on the market in reality, this learning effect would be artificial and not represent a real insight. We therefore accept the possibility of a (small) endogeneity concern in this paper and further work could fully circumvent this issue by extending the database appropriately.

⁵⁶Contrary to Wind1DA and Tempeff15, which we are able to compute purely on forecast data.

2.6 Conclusion

This paper is a sophisticated proof of concept of our methodology applied to the electricity market. We observe that bidders take uncertainty from renewables generation as well as uncertainty from demand realisation into account. The results indicate that electricity suppliers react to an increased level of uncertainty by bidding more volume elastically (steeper supply functions in the dimension Q (x-axis) - P (y-axis)) in order to minimise expected dynamic costs, which increase with the uncertainty. The results also indicate that not only supplier bidding is affected by uncertainty, but that the level of uncertainty also impacts bidding from the demand side of the market.

Future empirical work should focus on investigating the endogeneity of the demand function on uncertainty as well as better understand frictions in the bidding (e.g. focal price points). Concurrently, the results also call for more advanced theoretical work on the shape of bid functions of players, in particular to explain non-linear shapes. This is also suggested by our bid functional analysis which hints at non-unilateral effects of exogenous variables on the shape of the functions. The economic insight hidden in full bid functions is vast and a better understanding of these could be applied to address important welfare questions⁵⁷.

⁵⁷Such an application, which the authors currently focus on is the question of the optimal choice of the geographic installation of renewable electricity generation units (solar panels and wind turbines) with respect to minimising the intermittency of renewables generation. A clear understanding of the effects of uncertainty on the market is vital to close the analysis on organisational questions of the market. This is outside of the focus of this paper

2.7 Results of the point selection methodology

2.7.1 Precision of point selection

We have selected $K = 5$ types of comparable points for each of the 37'500 demand and supply functions. This section details the results of the point selection methodology and presents evidence why the point selection algorithm has produced comparable points reliably.

The graphs in figure 2.7.1 show the local density of selected points in the price - quantity space for the demand (left) and supply (right) curves. The fact that the groups of data points are disjoint from one another indicates that the points selected are distinctly different across groups.

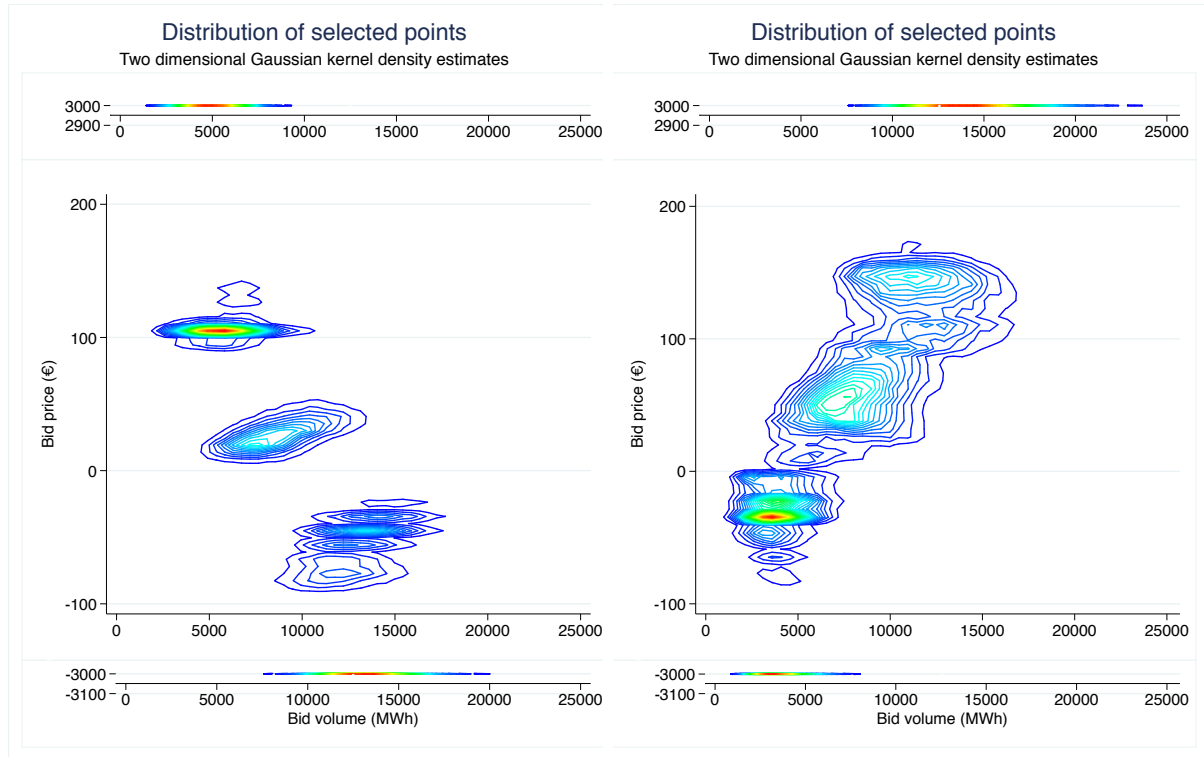


Figure 2.7.1: Heat map on selected, comparable demand and supply points

Note: Please note the discontinuity in the scale of the y-axis. The three separate graphs are arranged to be understood as a single one. The warmer the colours of the heat map, the higher the frequency of selected price-quantity pairs. The colour legend is omitted for brevity, density changes between contours are of the order of 10^{-4} .

In figure 2.7.1, selected points of type $k = 1$ manifest at the bottom of the graph with prices fixed at $-3000\text{€}/\text{MWh}$. Similarly, $k = 5$ points appear at the top of the graph with prices fixed at $+3000\text{€}/\text{MWh}$. The three distinct groups of data points refer to

points of type $k = 4$, $k = 3$ and $k = 2$, respectively, when reading the zoomed, center part of the graph from top to bottom.

In appendix 2.7.7, tables 2.10 and 2.11 allow to match data frequencies in the left graph of figure 2.7.1 with their types. Tables 2.12 and 2.13 relate to the data of the right graph in figure 2.7.1.

We note that the point selection for the demand curves has produced groups of points that are more distinct (and thus more robustly attributed to a certain type k) than for the supply function. While the smooth logistic function approach was unable to cope with the variations in the data from the electricity market, our more flexible non-parametric approach is more robust. Our methodology only relies on assuming that the first derivative is uni-modal and that sufficient variation exists in the data to distinctly identify the regions of different slope⁵⁸. Overall, this is strong evidence that the algorithm is able to distinctly differentiate between points of different types.

2.7.2 Observations of bidding frictions

Distinct point selection is further supported by the evidence in figure 2.7.2. These graphs show the distribution in the price-quantity space of the selected points separately for the demand and supply function. Distinct clouds are an indication that selected points are different across types k .

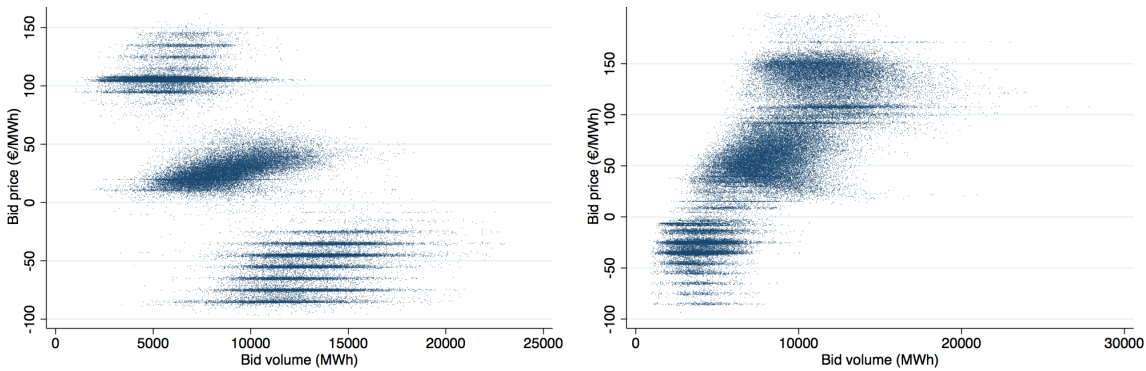


Figure 2.7.2: Distribution of selected demand (left) and supply (right) points

⁵⁸On very rare occasions, our algorithm was unable to distinctly select between neighbouring point types, because the original bid function was linear for a large part. E.g. point $k = 4$ cannot not be identified if the bid function is linear between points $k = 3$ and $k = 5$. *****We therefore dropped two observations in the dataset - CHECK!.

However, a feature of the graphs is striking: patterns (horizontal lines) seem to exist for the selected points of type⁵⁹ $k = 2$ and $k = 4$. Many selected points accumulate at certain prices of regular intervals of 10€/MWh, i.e. there seem to be focal price points for the bidders at the curvature points of the bid functions. The pattern is present for selected points of both the supply and demand functions, although the selected points from the supply function exhibit this pattern slightly less.

The points following the pattern (types $k = 2, 4$) represent the points of maximum curvature of the aggregate bid functions, i.e. the region where the aggregate bid function transitions from a price elastic center portion to the price inelastic extremities of the bid function.

Without prioritising any explanation⁶⁰, we acknowledge the existence of bid point patterns in the values (i.e. prices and quantities) of selected points.

We are, however, interested in S' , the slope at each selected point - an information measured at the selected point. We therefore investigate whether the values of the first derivative at the selected points display a pattern. Figure 2.7.3 shows the histograms of slopes of supply functions for the points $k = 2, 3$ and 4 . No pattern in the values of the derivatives is apparent.

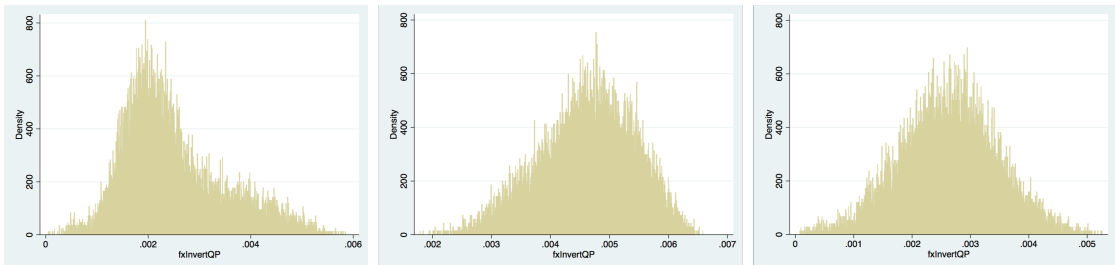


Figure 2.7.3: Histogram of slopes per point type

Note: Histograms of extracted slopes at points of type $k = 2$ (left), $k = 3$ (middle) and $k = 4$ (right).

Although values of the selected points are possibly biased due to focal price points, we do not observe patterns in the variable of interest (i.e. the first derivatives of the

⁵⁹Types $k = 1$ and $k = 5$ do not exhibit variation in price, because bidding at the extreme prices of +3000€/MWh is imposed by the auction rules. We thus neglect their analysis here.

⁶⁰We do not investigate the origins of bidding frictions in this section, which focuses purely on the methodology. For the electricity market, a few possible explanations are that (1) bid functions are driven by marginal costs consideration towards the extremes of the bid curve, (2) bidders bid coarsely since they have used up much of their bid point allowance (256 points) on the center portion of the curve, (3) bidders spend less effort on adequately bidding at extremes since the likelihood of the market outcome occurring at the extremes is much lower.

selected points) and deem the methodology adequate for our purposes.

Finally, we emphasize that the observed patterns are not caused by the point selection mechanism since the algorithm can only choose between explicitly bid points or linearly interpolated points, that could be part of a market equilibrium under the reigning price setting algorithm. The pattern arises from many horizontal steps occurring at the same prices in different auctions.

2.7.3 Value of selected points (determining K)

We remind the reader that the aim is to recover points that summarize well the behaviour of the full aggregate bid functions in different auctions. Our technique allows us to extract representative and comparable points across bid functions of different auctions. From the selected points, we can also go back to infer the original bid function from which the points were selected. In order to evaluate the utility of our methodology, we investigate the added benefit of an additional point in our point selection.

By selecting $K = 5$ points per curve, rather than fewer points per curve, we are able to significantly reduce the degrees of freedom for inferring the original bid function. In other words, our information (as captured by the selected points) of the original bid function is more precise.

In order to investigate the marginal gain of information for additional points, we first recover the master curve (the mean expectation of a demand curve) and its confidence interval⁶¹ for $K = 0$ to $K = 5$ points. Then, we look at the decrease in uncertainty achieved by including an additional point, obtained using our technique. Figure 2.7.4 shows the master curves (red line) and the expected error (pink shaded interval above and below the master curve) as a function of the number of reference points⁶².

Without any reference point, the uncertainty on the inferred bid function would lie in the interval shown in graph A of figure 2.7.4. With two reference points (namely the minimum and the maximum quantity), the uncertainty is reduced as shown by the smaller error interval in graph B. Graph C adds a third point (the point of inflection)

⁶¹To compensate for asymmetric variation above or below the master curve, we do not use the standard deviation to compute the confidence interval. Instead our upper (or lower) bounds are given by the mean of all curves below (or above) the expected master curve respectively.

⁶²The master curve in A is obtained by rescaling all demand functions by their mean value. The master curves in B - D are obtained by rescaling the reference points, such that they coincide with corresponding point on the master curve in A plus rescaling all points between the reference points by a vector obtained as a linear combination of the displacement vectors of the closest reference points.

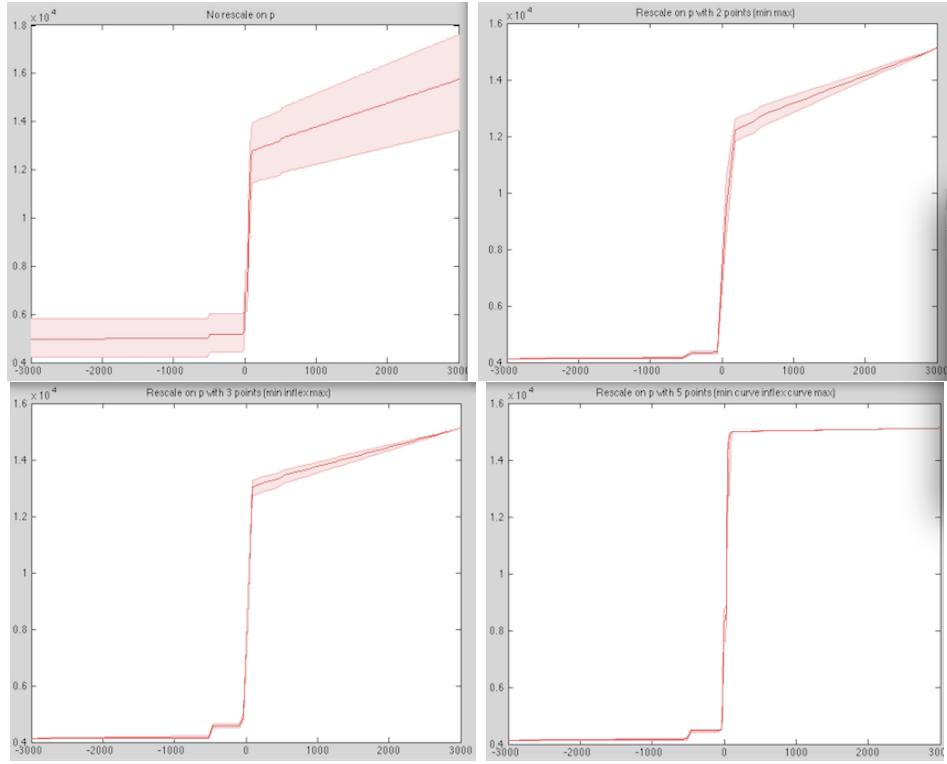


Figure 2.7.4: Error bars as a function of the number of extracted points

Note: The graphs represent the master curve with the error interval for inferring the original bid function, conditional on the number of extracted, reference points (RP). Top left (A): Computed without any RP. Top right (B): Computed using 2 RP. Bottom left (C): Computed using 3 RP. Bottom right (D): Computed using 5 RP.

and Graph D adds another two points (the two points of maximum curvatures). Figure 2.7.4 shows clearly that with an increasing number of reference points, we obtain a more precise information about the original bid function. We quantify the gain in precision by measuring the pink shaded area in each graph A to D. The result is shown in figure 2.7.5 and reveals decreasing marginal information for each additional point. By selecting $K = 5$ points, we are able to reduce the uncertainty about the original curve by a factors of about 50 (see figure 2.7.5). We see this insight as support for using $K = 5$ points for further work.

While the graphs in figure 2.7.4 are displayed on inverted axes and rescaled units, we show the final master curve and uncertainty interval on the original axes and units in figure 2.7.6.

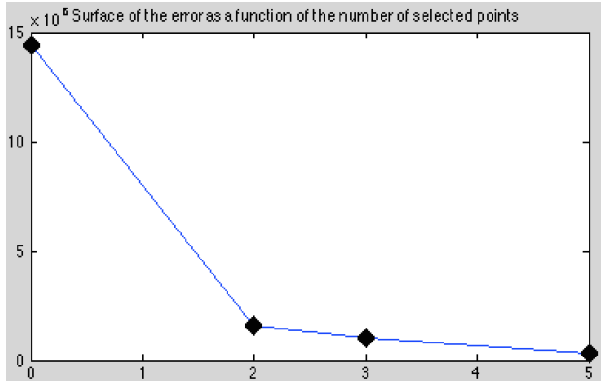


Figure 2.7.5: Proxy for degrees of freedom on master curve

Note: The graph plots a proxy for the number of degrees of freedom for the inference of the original bid function on the number of reference points. Specifically, it plots the size of the pink shaded area in figure 2.7.4 against the number of points.

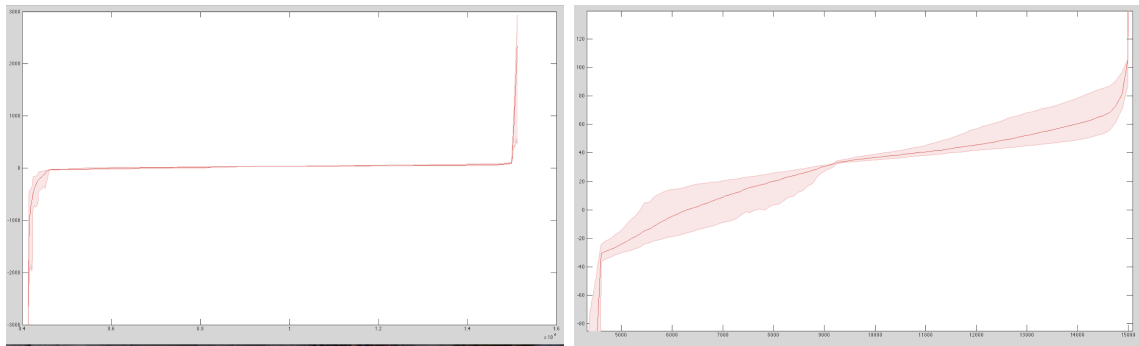


Figure 2.7.6: Overall (left) and zoomed (right) Mastercurve with confidence interval

Note: Master curve in the quantity - price dimension.

2.7.4 Discussion and Conclusion

In this article, we have developed an alternative technique to run a cross-section reduced form model on data generated by a market that keeps track of the full aggregate demand and/or supply functions. While in this paper we apply it to aggregate demand functions, the methodology is fit for the analysis of aggregate supply functions and individual bid functions of either market side.

The methodology is inspired by the techniques used in the literature on Treasury auctions, but has been set up from scratch to allow treatment of more heterogeneous data. Furthermore, the hard assumption of an underlying logistic function is relaxed and our non-parametric point selection avoids the storing of bid function information in the form of estimated function parameters, which are difficult to interpret.

Smoothing of the original bid functions is a component in both the traditional logistic

function approach and our comparable point selection methodology. The smoothing enables the user to abstract of small bid function particularities and imprecision, e.g. steps in the function. However, in the traditional approach, the reduction of plus 1000 bid points into very few parameters resulted in the mixing up of “local” bid function information from all parts of the function at once. Our non-parametric approach allows specifically to control the smoothing parameter and thus enables the researcher to choose the smoothness of a bid function when extracting the points of interest. In any case, the smoothing range of the new technique is merely a fraction of that of the traditional approach and, hence, we do not mix up information of different parts of the bid function.

The results of the comparable point selection are encouraging. We show that each type of point is distinctly chosen and that patterns of the original bid functions do not influence the quality of derivative information extracted at the selected points. We acknowledge the existence of bidding frictions in the original data and highlight this observation for further work. Overall, we deem the selection of points to be of sufficient precision for a detailed study of the behaviour of the slope at all points. For immediate values (prices or quantities) of the bid functions at the selected points, we deem the methodology sufficient for, at least, the point of inflection ($k = 3$).

2.7.5 Technical details

Using the kernel density estimation (KDE) in our setting

In order to estimate the first and second derivatives of the bid functions, we use a kernel density estimation. The estimator is essentially a smooth version of a histogram and counts the number of points in moving intervals (called a window) of predefined width along a dimension of the data. In our case, it counts bid points per price interval. In addition, the KDE assigns a weight to each observation based on the distance from the observation to the center of the window. The weighing function is called the kernel.

The observed bid functions are each a multitude of price-quantity combinations. However, a kernel density estimation on the observed points of the bid function would be useless since the number of points per price interval does not vary much with the slope of the curve.

We use a characteristic of the auction mechanism (the linear interpolation between consecutive bid points, for details see 2.2) to our advantage and are able to transpose

the observed bid function to one that suits our needs. This is done by adding linearly interpolated points at the unit cent level (corresponding to the minimum bidding unit). The kernel density estimation is then able to estimate the slope of the function by simply counting the points in an interval since the number of points per price interval of constant width varies proportionally with the slope of the function over that interval.

Hard choices in the code of the KDE

A few specific choices have been made in the code and are detailed here.

Kernel choice: First, we use the default Epanechnikov kernel for simplicity. It is generally considered that the kernel choice has significantly less impact than the choice of the bandwidth. The use of the kernel is to weigh more the observations close to the centre of the moving window. The performance of a kernel is judged on the trade-off between variance and bias. The used Epanechnikov kernel is optimally efficient. However, even simplistic kernel functions, such as the rectangular, have a relative efficiency of 93%. Thus, kernel choice is not important and other factors may influence the decision, such as computational effort [Salgado-Ugarte et al., 1994, Silverman, 1986].

Bandwidth choice: Second, we hard code the bandwidth selection for computational reasons. The bandwidth of the kernel (and thus the width of the price interval over which points are counted) is determined on the basis of a trade-off between smoothing the original bid function and mixing up information of different parts of the bid function. By smoothing the original bid function, we obtain estimates of the information that our KDE measures (i.e. points in the interval and thereby the slope) that are less sensitive to local specificities of the bid functions. The larger the selected bandwidth, the larger the interval over which points are counted and the stronger the smoothing of the estimates. However, as the width of the interval increases, we mix up more information of a selected point of interest with the information of its neighbouring points. Therefore, in setting the bandwidth we aim to achieve smoothed estimates with a reasonable compromise between respecting local curve information, while not being fragile to steps in the bid function.

For estimates of the first order derivative, these considerations are minor and we could use the default bandwidth, optimal for a Gaussian distribution, to extract the point of maximum slope from the distribution. However, one reason we slightly increase it is

to ensure that the distribution of the first derivatives is uni-modal⁶³. Furthermore, the selection of the bandwidth in the first stage density estimation impacts both the precision and speed of the second stage estimation. A better smoothing in the first stage gives a large advantage in the second stage estimation⁶⁴, thus we have a further incentive to increase the bandwidth.

For the second derivative the trade-off is more critical: We want to obtain a reasonably broad smoothing to obtain a meaningful selection of points that is not driven by random noise. On the other hand, a large bandwidth reduces the importance of local information of a part of the curve as a consequence of which, selected points (points $k = 2$ and $k = 4$) are pushed towards the point of inflection ($k = 3$). This is due to the maximum point of the first derivative gaining more weight in the second derivative's estimation. The fact that first derivative estimates are already smoothed rather strongly, we can choose a narrow bandwidth in the second stage KDE.

In the end, we select a rather broad bandwidth of 45 units in the first estimation. This gains robustness of the point selection mechanism against noise in the data and estimation speed in the second stage. The bandwidth in the second stage is set more narrowly at a level of 2 units to keep as much information as possible from the first stage estimation and allow sufficient variation to select the k points.

To support our choice, we illustrate the impact of different bandwidths on the first and second stage estimation in figures 2.7.7 and 2.7.8. Our choice is based on an adequate point selection and the fastest runtime.

In these graphs, the top row shows the first stage KDE, over the whole function on the left and zoomed on the right. The large bandwidth in figure 2.7.7 shows the impact of smoothing on the estimates of the first derivative as compared to figure 2.7.8. The second row in both graphs shows the second stage KDE in two versions: Using a wide kernel bandwidth on the left and a tight bandwidth on the right. Again, we disclose the result as seen over the whole function (left) and zoomed on the central price range (right). The third row details the original demand function with the final point selection given

⁶³Uni-modal at the point of inflection in the price-quantity dimension. The smoothing ensures that the selected point is not mistaken due to steps in the bid function that have a very large slope locally, but which is not representative of the neighbouring portion of the bid function.

⁶⁴The gain in computation in the second stage arises from the fact that a stronger smoothing in the first stage produces a more homogenous dataset for the second stage estimation. By more homogenous, we mean that fewer monotone regions of the graph of first derivatives must be interpolated at the unit cent level to ensure that our algorithm works correctly.

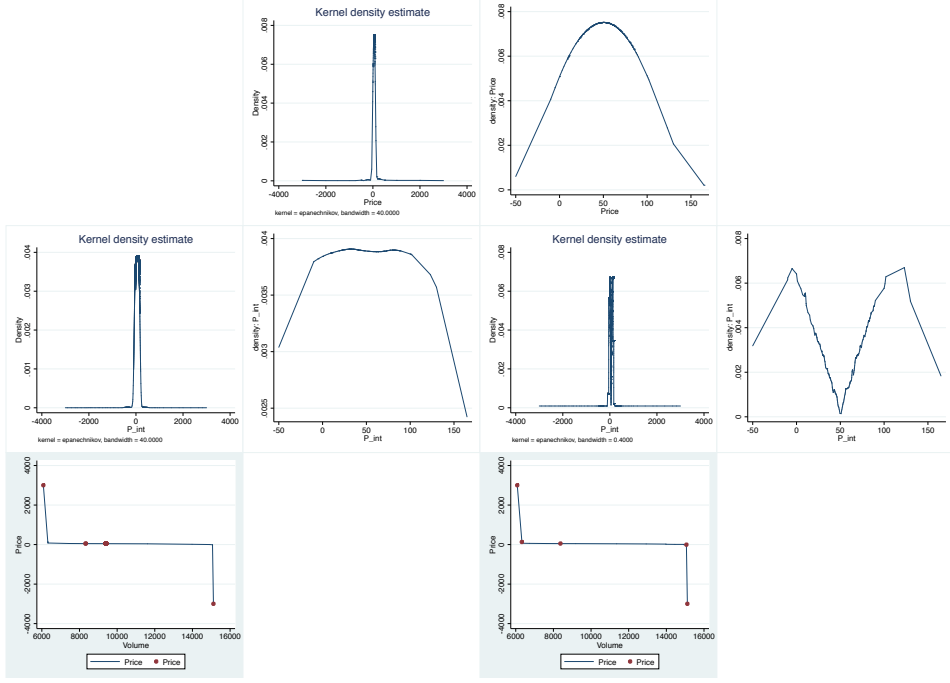


Figure 2.7.7: Comparison of bandwidths: Large bandwidth in first stage

Note: Large bandwidth in first stage (top row), large bandwidth in second stage (second row left), small bandwidth in second stage (second row right), Resulting selection of points for large bandwidth in stage one and two (bottom row left, A) and selection of points for large bandwidth in stage one and small bandwidth in stage two (bottom row right, B).

the bandwidth selection as given by the two rows above. Regardless of the first stage bandwidth, we see that a large bandwidth in the second stage KDE easily distorts the point selection. Selected points of type $k = 2, 4$ are either two centred or too wide as a result of the second derivatives being smoothed excessively and not precisely representing the local specificities of the curve. The right hand side of both figures show that a tighter bandwidth on the KDE can easily mistake large slope changes due to steps in the bid functions as the appropriate points of maximum curvature of the full bid function and thereby make an error. Therefore, we apply a sensitive second stage KDE on rather smooth estimates of the first derivatives, which yields an adequate point selection in our setting (figure 2.7.7B).

The bandwidth selection received much attention in this work in order to obtain a reasonable selection of points based on local information of the curves, while achieving a satisfying robustness to noise in the bid function. We are aware that this subjective setting of the bandwidth is not without consequence for our work. However for computational

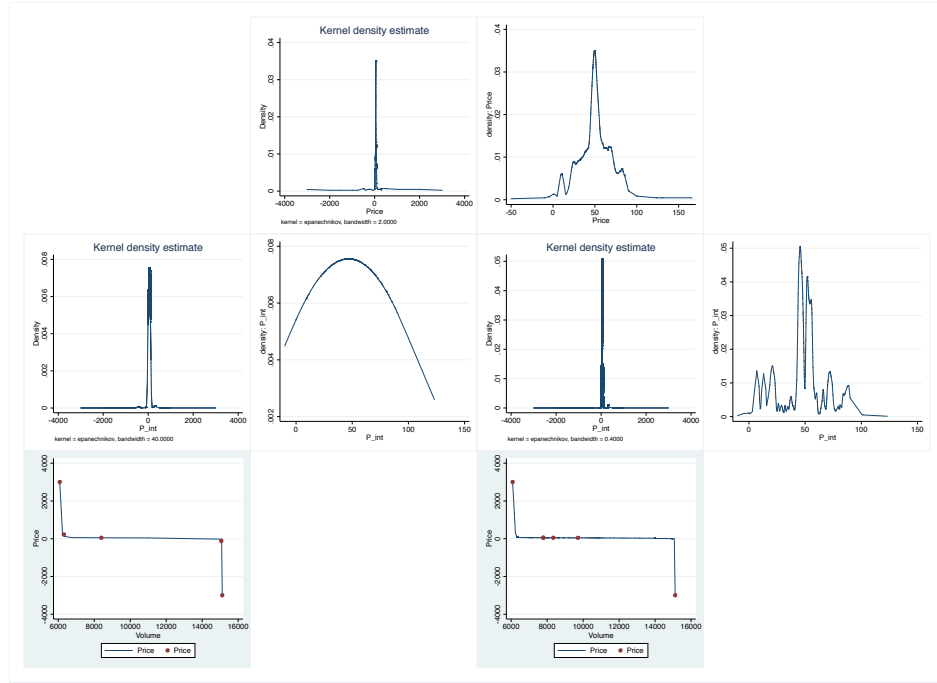


Figure 2.7.8: Comparison of bandwidths: Small bandwidth in first stage

Note: Small bandwidth in first stage (top row), large bandwidth in second stage (second row left), small bandwidth in second stage (second row right), Resulting selection of points for large bandwidth in stage one and small bandwidth in stage two (bottom row left, C) and selection of points for small bandwidth in stage one and two (bottom row right, D).

reasons⁶⁵, we do not run a full robustness test on this choice ex-post.

2.7.6 Outlier detection and removal

In some rare cases, our point selection mechanism does not work. This is the case when curves have very small number of points at a kink and it is thus very difficult to detect their curvature. As a result, the selected points are then quasi in-differentiable from the next selected point type, i.e. a point of type $k = 2$ is almost identical to the selected point $k = 3$. The code is unable to select the right points due to a data lack on the original curve (second derivative on a constant slope up to POI is zero).

We screen for adjacent points that display quasi no variation in volumes. Figure 2.7.9 shows a histogram of volumes differences over 2 selected points (from $k = 2$ to $k = 4$) and reveals a positive mass point at zero, indicating outliers that do not display any volume variation between points of the same bid function. We use the histogram to identify and drop those outliers from our dataset.

⁶⁵The point selection algorithm ran for more than two weeks in the current setting.

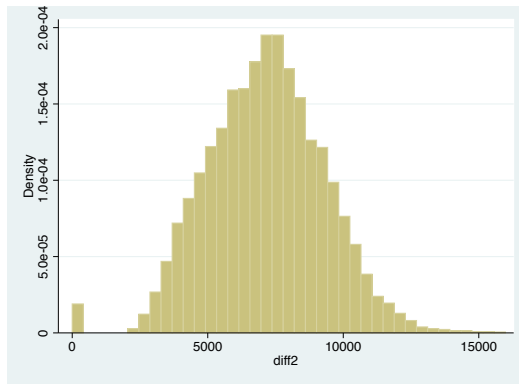


Figure 2.7.9: Histogram of volume variation between points

Note: The histogram shows the volume difference between points $k = 2$ and $k = 4$ of the same bid functions.

2.7.7 Summary statistics of selected points

	Mean	Median	StdDev	Min	Max
Prices for $k = 1$	-3,000.0	-3,000.0	0	-3,000	-3,000
Prices for $k = 2$	-56.7	-55.0	19	-97	70
Prices for $k = 3$	27.6	26.8	11	-27	93
Prices for $k = 4$	120.2	105.4	193	-11	2,999
Prices for $k = 5$	3,000.0	3,000.0	0	3,000	3,000

Table 2.10: Prices of selected demand points

	Mean	Median	Std. Dev	Min	Max
Volumes for $k = 1$	13,328	13,222	2,213	4,990	23,254
Volumes for $k = 2$	12,919	12,824	2,238	3,321	23,001
Volumes for $k = 3$	8,779	8,664	2,028	1,958	18,335
Volumes for $k = 4$	5,777	5,730	1,558	987	12,773
Volumes for $k = 5$	5,031	4,968	1,467	914	11,301

Table 2.11: Volumes of selected demand points

	Mean	Median	Std. Dev.	Min	Max
Prices for $k = 1$	-3,000.0	-3,000.0	0	-3,000	-3,000
Prices for $k = 2$	-30.3	-25.0	219	-2,999	439
Prices for $k = 3$	61.3	58.6	24	11	526
Prices for $k = 4$	133.9	136.3	32	36	626
Prices for $k = 5$	3,000.0	3,000.0	0	3,000	3,000

Table 2.12: Prices of selected supply points

	Mean	Median	Std. Dev.	Min	Max
Volumes for $k = 1$	3,721.7	3,526.0	1,344	618	10,594
Volumes for $k = 2$	4,432.8	4,226.0	1,602	844	11,765
Volumes for $k = 3$	8,467.2	8,365.5	1,814	3,431	20,932
Volumes for $k = 4$	11,849.5	11,717.7	2,411	3,641	27,810
Volumes for $k = 5$	14,390.6	14,142.0	3,052	6,580	35,356

Table 2.13: Volumes of selected supply points

2.8 Appendix: Technical details on PLU^R

2.8.1 Methodology to aggregate geographically dispersed information on a national level

We have two types of meteorological data: observations and forecasts. The methodology for each differs slightly.

Dealing with meteorological data

Interpolation methodology on weather observations Observations are obtained from MétéoFrance for three parameters of particular interest: temperature, wind speed and light intensity. These observations take the form of tables of hourly observations for a given set of weather stations. Each parameter is observed on a different set of stations.

Due to their hourly nature, the analysis of the electricity market's sensitivity to weather requires a very high number of observations. Therefore we select between one and two stations per Département⁶⁶, a French administrative unit of roughly 6000 km^2 ,

⁶⁶There are 95 Département in France

i.e. of a typical lengthscale of about 75 km. We have 161 stations for temperature, 113 stations for wind speed and 106 for light intensity, as shown in Fig 2.8.1.

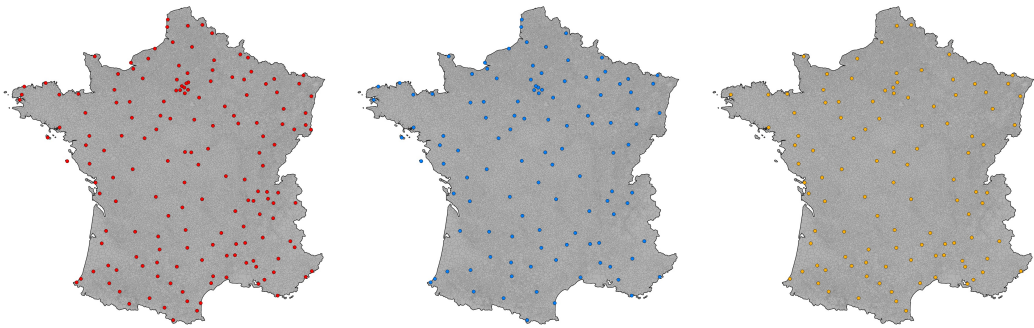


Figure 2.8.1: Stations for which we have hourly data. Left : temperature, center : wind speed, right : light intensity.

For each hour, we select the corresponding observations and interpolate them in order to reconstruct the weather on the entire french territory. An interpolation consists on inferring the value of a variable at query points using a reference data set of known values. The easiest interpolation method is the linear interpolation: think about a dataset of hourly observations with one missing value; to reconstruct the missing value, take the average of the value of the preceding and following hour. There are numerous methods of interpolation, even more so when the data is spatial in nature, all revolving around two main steps. First, given a query point at which one would like to infer the value of the variable, there needs to be a selection rule to know which of the points from the reference data set should be used (in our example the preceding and following values). Second, once these points are selected, one needs a weighting function to know their relative importance in order to obtain the interpolated value (in our example it is a simple averaging, that is weights of 0.5).

We use the natural neighbour interpolation method, well known for its good balance between speed and accuracy. In short, through the use of a Voronoi algorithm (a method that divides the plane in regions "belonging" to certain points), one is able to define the natural neighbours of a point, that are then used to perform the interpolation using a ratio of surfaces as weights (see Fig 2.8.2 for more details).

Picture treatment to recover weather forecasts Forecasts are obtained from the Global Forecast System (GFS), and come in the form of colormaps, as shown in Fig

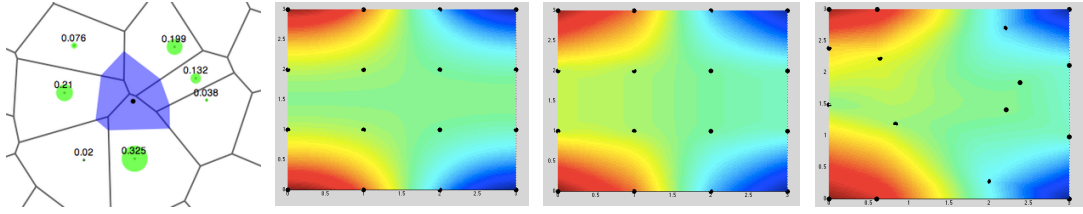


Figure 2.8.2: Left: Voronoi's algorithm is applied once on the reference points highlighted in green to obtain the white surfaces, and a second time on the same points to which is added the query point in the center to obtain the new blue cell. The green circles, which represent the interpolating weights, are generated using the ratio of the shaded area to that of the cell area of the surrounding points.

Center left: example of a reference surface (color mapped) to be reconstructed through a natural neighbour interpolation. Center right: interpolated surface with a reference set of 16 evenly organised points, represented in black. Right: interpolated surface with a reference set of 16 unevenly organised points, represented in black. From 16 points one is able to reconstruct the color mapped surfaces which aim at being able to reproduce the reference one, represented in the center left image.

2.8.3. We are going to illustrate our methodology on temperature data, but the same exact approach is performed on wind speed data. The general idea is that the pointwise precision is low (2°C per color) but the overall map contains more precise topological data than a few tens of precise but sparse stations.

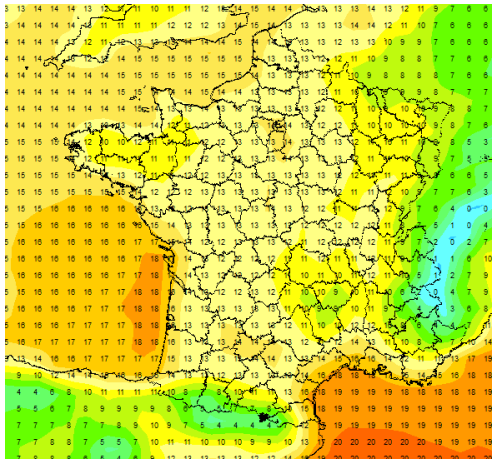


Figure 2.8.3: Temperature forecast from a simulation run by the GFS at 6 a.m. on the 3rd of november 2011, for a forecast at 22 p.m.

To extract the relevant data we first clean the color map from its irrelevant information, namely the temperature in numbers and the borders. Note that this step introduces a small amount of high spatial frequency noise, see Fig 2.8.4 left and center left.

Second, a lot of information is lost from the actual GFS simulations by using a color map representation, as temperature is described as a discontinuous variable: each color

has a precision of $2^{\circ}C$. In order to correct for this, we leverage the fact that all the information contained in this color map, that is the color at each pixel, is actually contained in a smaller set of points. Consider the value at the boundaries between different color regions: by knowing that the interior of a constant color region has a constant value, one is able to represent all the information contained in the original image by keeping only track of the values at the boundaries. To recognise those boundaries we perform image analysis, more precisely we use edge recognition methods based on finding high gradient regions, thus obtaining Fig 2.8.4 center right.

Once we represent the information in this denser form we can perform the last step, which consists in fitting a surface to our newly defined dataset, i.e. the temperature values at the boundaries. We could perform an interpolation, but these methods are not well suited to such organised reference sets, here data points on curves representing iso-temperatures. In addition the first step introduced some spatial noise which we want to correct to some extent. We allow here our fitted surface to take different values than our data points. This allows us to define the rigidity of our fitted surface, i.e. a cost associated to spatial noise, and therefore reduce the importance of the high frequency noise introduced in the first step. The end result is presented in Fig 2.8.4 right. It is key to understand that this image is displayed using a colormap close to the one in the original picture to facilitate comparison but that its underlying data is continuous whereas the original image describes temperature by bins of $2^{\circ}C$.

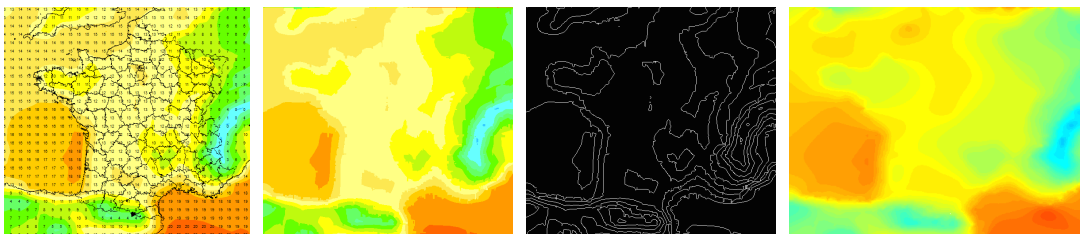


Figure 2.8.4: Left: reference image. Center left: borders and numbers are removed. Center right: edge recognition. Right: final fitted surface.

Autocorrelation lengthscale We also use this dataset to build measures of the weather uncertainty. To do so we measure the autocorrelation lengthscale of our three weather variables of interest : temperature, wind speed and light intensity. This lengthscale measures how much are the weather variables correlated spatially. We consider

that the autocorrelation lengthscale is inversely proportional to uncertainty about the variable we are interested in. When it is small, the variable is less spatially correlated, leaving more room for noise to blur the anticipation of the impact of this variable on a national level. Conversely, when the autocorrelation lengthscale is large, the variable is very correlated spatially, that is that the informational content of one datapoint is higher for the prospect of using it for the evaluation of a national effect.

Take two points on a plane and a finitely spatially correlated bounded variable. If those points are infinitely distant, the value of the variable at these points should be uncorrelated. That is that the absolute difference between the variable taken at those two points should have a given average value. Conversely, two points infinitely close should have the same value, i.e. a zero absolute difference between the variable taken at those two points. The question is how fast is the transition between those two limit cases. First, we define the average absolute difference between two points when distant of a given value. Second we extract a typical lengthscale.

To define the average absolute difference between two points when distant of a given value, we consider every possible pair of points in our dataset at a given point in time. For a given pair we compute its distance and its absolute difference in value (in black in Fig.2.8.5). For 100 datapoints we obtain 4950 pairs. We then use a kernel smoother in order to obtain the average non parametric autocorrelation function (in blue in Fig.2.8.5).

To recover a typical lengthscale we make the parametric assumption that the autocorrelation is exponential in nature. We fit an exponential function through our smoothed data (in red in Fig.2.8.5), and recover the exponential decay parameter as our lengthscale (in green in Fig.2.8.5). We perform this operation for every hour in our dataset and every weather variable. The results are timeseries for the characteristic lengthscale of the weather parameters.

Aggregation of local information

Wind1DA *Wind speed (average speed in km/h):* Wind speeds influence the productivity of wind turbines, which are a source of unpredictable electricity generation. In general, renewable technologies benefit from a feed-in guarantee by the state. That is, regardless of the trading outcome on all markets, renewable energies will be the first to be fed into the power grid at a guaranteed price.

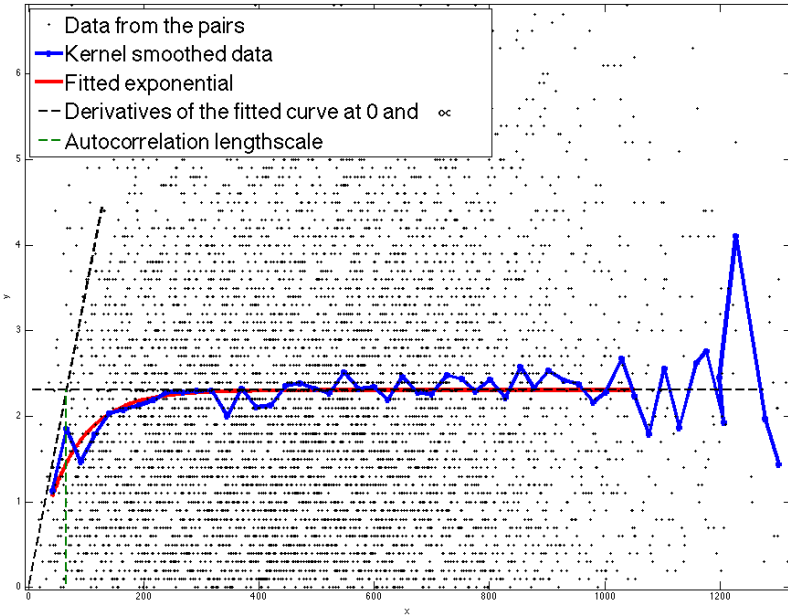


Figure 2.8.5: Autocorrelation lengthscale computation. In black are the points obtained from all the pairs from our original data, that is absolute wind speed differences as a function of the distance between the two points. In blue is the kernel smoothed function from those points. In red is the exponential fit. In black are the derivatives of the fit at 0 and ∞ . In green is the recovered autocorrelation lengthscale. The unit for the lengthscale is in km.

Consequently, the electricity production of renewable technologies represents a production shock for all actors on the market. The production shock means that the demand to be served by traditional electricity producing firms is reduced by the amount that is serviced by the electricity gained from renewable sources.

In the case of wind turbines, the average speed of the wind per hour allows to proxy for the size of the production shock due to the electricity generation from wind energy.

We use hourly windspeed forecast in the form of color maps from the Global Forecast System (GFS), giving the speed by bin of 5 km/h at 10m above ground, and the location and production capacity of the wind turbines present on the french territory, given by the SOeS (service d'observations et d'études statistiques - observations and study department) a department of the french environment ministry.

We consider that all turbines in France are of the same type, that is that they have the same response curve and height.

A typical response curve is represented in Fig. 2.8.6. It has three main characteristics : the wind speed at which the turbine starts to produce electricity, called the cut-in speed,

the speed at which the turbine reaches its rated output, called the rated ouput speed, and the speed at which the turbine has to stop to avoid damage, called the cut-out speed. We use data publicly available⁶⁷ to obtain a rough estimate of the french average wind turbine characteristics. We use a cut-in speed of 2.5 m/s, a rated output speed of 14 m/s, and reduce arbitrarily the cut-out speed from an estimate of 24 m/s to 20 m/s to account for the fact that a turbine is shut down not when the average speed is too high but when the maximal speed becomes dangerous for the turbine.

Wind speed also increases with height, and turbines are typically between 60 and 80m high. We therefore apply a multiplier to the reconstructed wind speed at 10m.

We seek to reconstruct the french wind energy production from meteorological data. The two adjusted values, the cut-out speed and the speed multiplier, are adjusted by hand to obtain reasonable fits. The reason for this is that the reconstruction of wind speed and aggregate production is computationally intensive, therefore we cannot perform a full blown estimation. We choose these values with a precision of roughly 10% with respect to their admissible range of values.

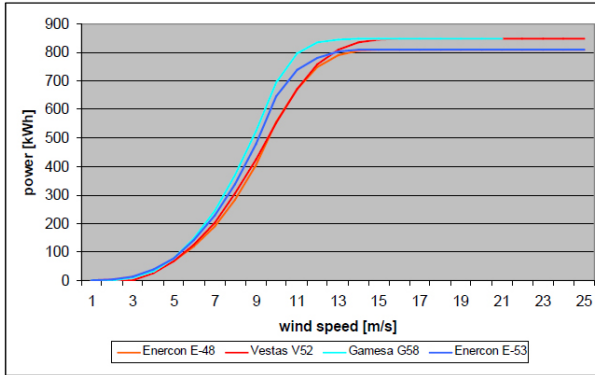


Figure 2.8.6: Typical response curves of different wind turbines

We obtain a reconstruction of wind production from day-ahead wind speed forecasts that we compare to actual observed production and to day-ahead wind production forecast computed by RTE, the french grid operator as shown in Fig.2.8.7. We stress here that our aim is two-fold: to link wind production to weather data and to use forecast data as the market actors only possess this information when bidding. We do not aim at producing better forecasts than the grid operator, the figure is only displayed to show that our methodology produces reasonable estimates (we obtain a correlation coefficient

⁶⁷<http://www.thewindpower.net>

between our forecast and the observation of 0.85 where the grid operator obtains 0.97).

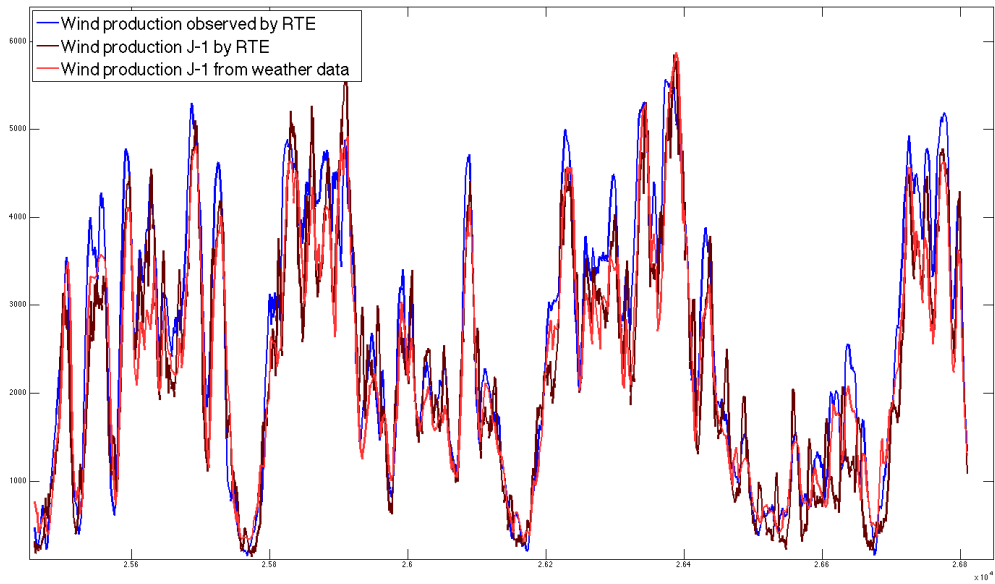


Figure 2.8.7: All curves are hourly production data. The origin of the hours is the first of January 2011, and the production is in MWh. In blue: the observed wind production. In dark red: the day-ahead predictions from the grid operator. In light red: the day-ahead predictions from weather data.

Tempeff15 We focus on the effect of temperature on the demand of electricity first. In France, a high percentage of the population heats their housing with electricity, therefore cold waves have a high impact on electricity consumption: 2300MW of additional power consumption for every drop of 1°C below 15°C , as shown in Fig.2.8.8 sourced from [RTE, 2014], the French grid operator.

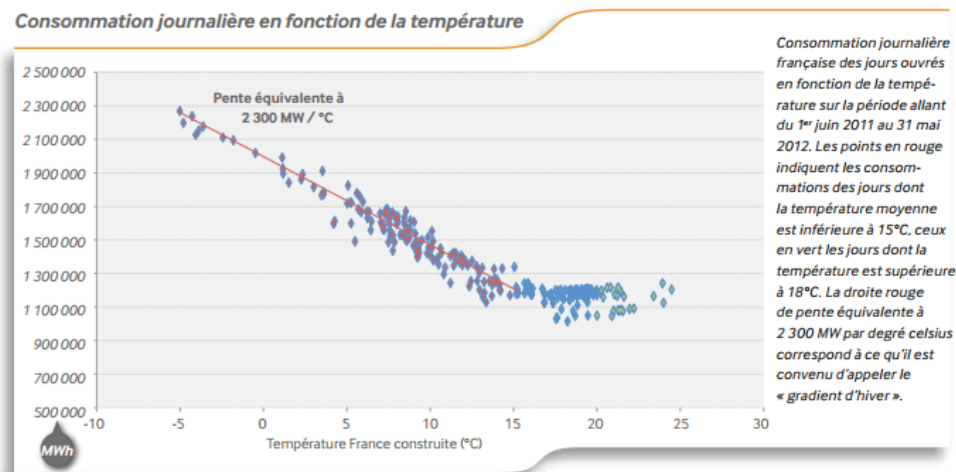


Figure 2.8.8: Daily electricity consumption in France as a function of the temperature

We apply this information to our observed meteorological data in order to build an effective temperature for France aimed at capturing its effect on consumption. To do so, we reconstruct temperature data for every french *commune*. We consider population as being a good proxy for potential heat consumption, therefore we apply it as a weight to the *commune* temperature. Lastly, we consider that temperatures saturate at 15°C. This allows us to build an effective temperature taking into account where the population is located and the nonlinearity of heat start up which allows us to account at the country-level for the local impact of temperature on the electricity consumption.

Tempeff We also build an effective temperature that does not account for the non-linearity at 15°C following the same methodology otherwise as a control.

Roll_Temp H Variable capturing seasonal trends by using the rolling average temperature on effective temperature (Tempeff15) over the last H hours, i.e. the last $H/24$ days.

Solar Light intensity (in $W.m^{-2}$) impacts the electricity market through multiple channels. The most obvious one is the associated electric production from photovoltaic panels. But there is another channel through which lighting can be seen as impacting electricity consumption : more sunlight decreases artificial light usage. In France, annually, the electric consumption that can be attributed to lighting represents roughly 50 TWh where solar production is roughly 4 TWh⁶⁸.

We have photovoltaic production data, which in itself is a blackbox. As we aim to link meteorological data to consumption we first want to validate the quality of our meteorological data. To do so we reconstruct the photovoltaic production from weather data. We know what are the hourly luminosity conditions on the french territory but also where is installed the photovoltaic production capacity. The SOeS (statistical observation and study department), a branch of government, publishes each year a file containing the installed capacity of renewable energy sources per communes, a french administrative unit with a typical size of roughly 3 km. France is formed of a little bit more than 36 000 of those communes.

⁶⁸These estimates are computed by the authors based on numbers coming from [Bertoldi and Atanasiu, 2007], INSEE and EDF

We use observed luminosity data from MétéoFrance, as there is no hourly forecast of luminosity, and assume a sigmoid response from photovoltaic panels to light intensity with a saturation towards high light intensity, that is approximately a linear response up to a certain threshold. The results are shown in Fig.2.8.9.

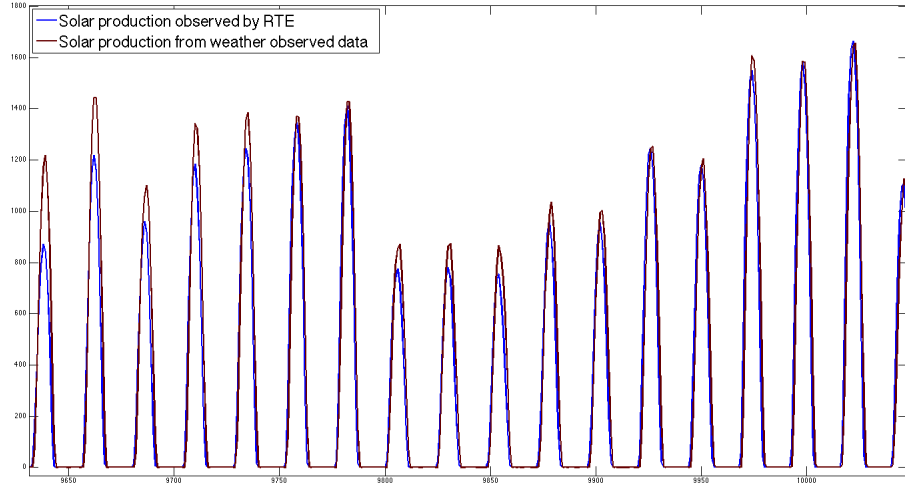


Figure 2.8.9: Hourly solar production in MWh. The time origin is the first January 2011. In blue: observed production by RTE. In dark red: reconstructed production from observed weather data.

We observe that solar production is much more regular than wind production, therefore it is not possible to build a proxy for lighting consumption that would allow us to decorrelate the effects from production and lighting. We therefore stick to this proxy to capture the net effect of both channels.

SolarRest Solar represents estimates of solar production. Therefore, it is highly collinear to the daily suncycle variable since solar production is light dependent. SolarRest is the residual from a regression of Solar on suncycle and captures the unexplained part of solar production on top of pure light intensity considerations. Table 2.14 gives the results of the regression.

	(1)	
	Solar	SE
suncycle	1,500***	3.903
Constant	0.876**	0.383
Observations	150,959	
R^2	0.702	

*** p<0.01, ** p<0.05, * p<0.1

Table 2.14: Regression of Solar on suncycle

RteBlackBox RTE, the French grid operator gives day ahead predictions of the total hourly consumption, which are available at the time of bidding. This variable is called PrevConsoH.

We do not have access to the exact definition of the index and it is thus a black box. However, it is available to the firms at the time of bidding and we want to include it in the demand estimations.

At the same time, it is evident that the Index uses much of the information that we explicitly control for in the regressions, therefore collinearity is an issue. In order to have correct coefficient estimates, we adopt an instrumental variable approach by regressing the RTE prediction on our exogenous factors, extracting the residuals and only including the unexplainable component of the RTE prediction in the demand estimation in the form of a separate variable called RteBlackBox.

Formally, RteBlackBox is equal to the predicted residuals (u) of the following regression, where X stands for the vector of explanatory variables: Tempeff15, Roll_Temp24 , Roll_Temp240, suncycle, morning, deltasun and EWH.

$$\text{PrevConsoH} = a + bX + u \quad (2.8.1)$$

In table 2.15 we give the output of regression 2.8.1 in column 1, which is strong support that our prepared data for exogenous variables is of very high quality. We highlight the significance of all explanatory variables at the 1% level and the R^2 statistic of 85.3%.

The signs and interpretation of the coefficients are exactly in line with the results

of the demand estimation (in both the price and quantity dimension) for the point of inflection $k = 3$.

Furthermore, we highlight that the comparison of columns 1 and 2 gives very strong support to our adjusted measure of effective temperature (Tempeff15 instead of Temp-eff), which takes into account the demand behaviour as a function of the temperature. Temperatures above 15°C are considered not to impact demand behaviour [RTE, 2014].

2.9 Appendix : Computational details and descriptive

2.9.1 Hard choices in the PLU computation

In computing the multi-variate kernel based prediction of the uncertainty for a given auction, we select auctions of a sufficient degree of similarity. We base the forecast equation 2.3.5 on this subsample dataset. We thereby consider that firms use the forecasting equation only *locally* in the neighbourhood of the auction of interest.

In order to define the size of the neighbourhood of an auction, we have to explicitly specify the width of the kernel window used in selecting the respective subsamples.

The trade-off involved is that we want to have small kernels for a precise computation of the PLU, while we want large kernels to make sure that we have a sufficient sample size in each kernel in order to derive meaningful statistics.

We choose to use a constant kernel window length with respect to each conditioning variable. We set the length of the window for each variable equal to $\frac{1}{3}$ of the variation of that variable. E.g. for Tempeff15, we observe a range of values from -10°C to 14°C . The subsample used to compute the PLU^D corresponding to a specific observation will consist of all observations that are within a range of $\pm 4^{\circ}\text{C}$ of that observation for Tempeff15. The same logic is applied to selecting the neighbourhood with respect to all other conditioning variables.

Table 2.16 gives descriptive statistics about the conditioning variables for the kernel and the explicit choice m , which determines the length of the kernel window for a variable X_e using the formula $b_{X_e} = \frac{2}{m_{X_e}}$.

2.9.2 Descriptive Statistics

On realised market equilibria

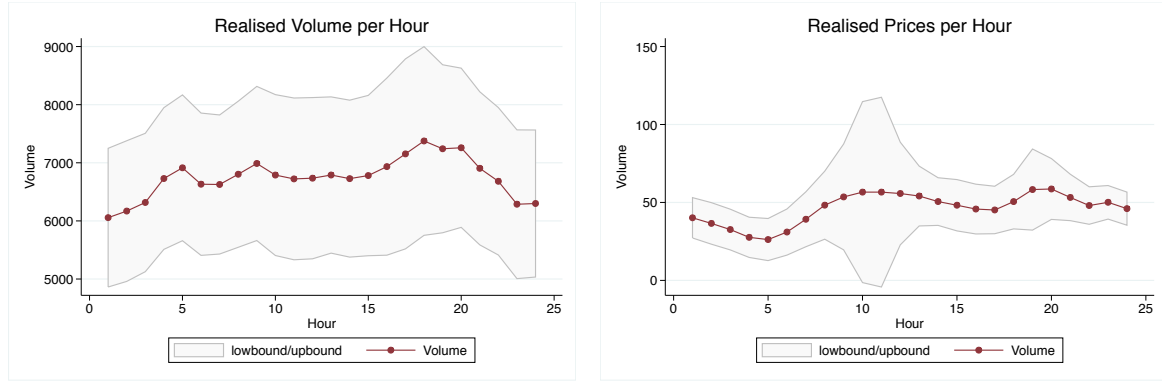


Figure 2.9.1: Plotted average realised Volume (left) and Price (right) per Hour with 95% confidence intervals.

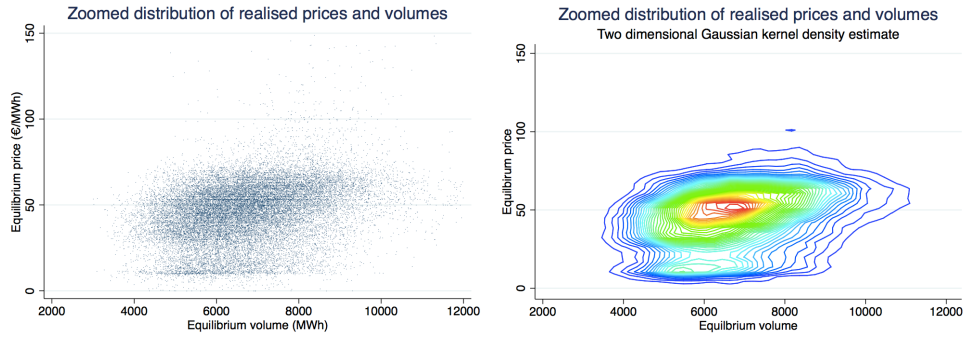


Figure 2.9.2: Distribution of observed market equilibria

Note: The warmer the colours of the heat map, the higher the frequency of realised price-quantity schedules. The colour legend is omitted for brevity, density changes between contours are of the order of 10^{-4} .

On player bid functions

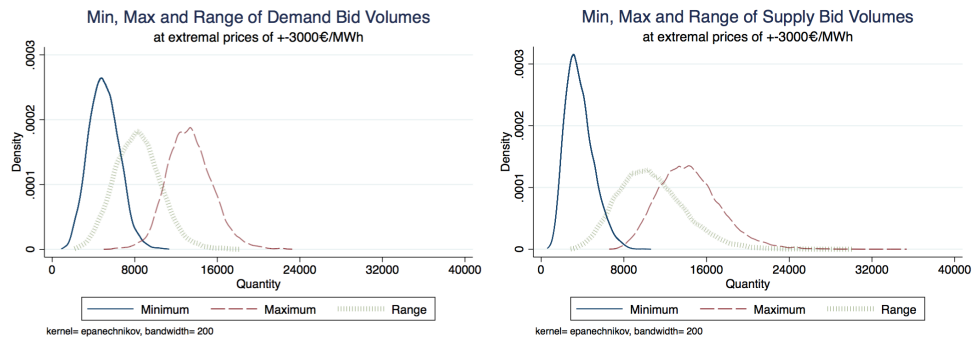


Figure 2.9.3: Distribution of minimum and maximum production volumes (and corresponding range) bid in an hourly auction.

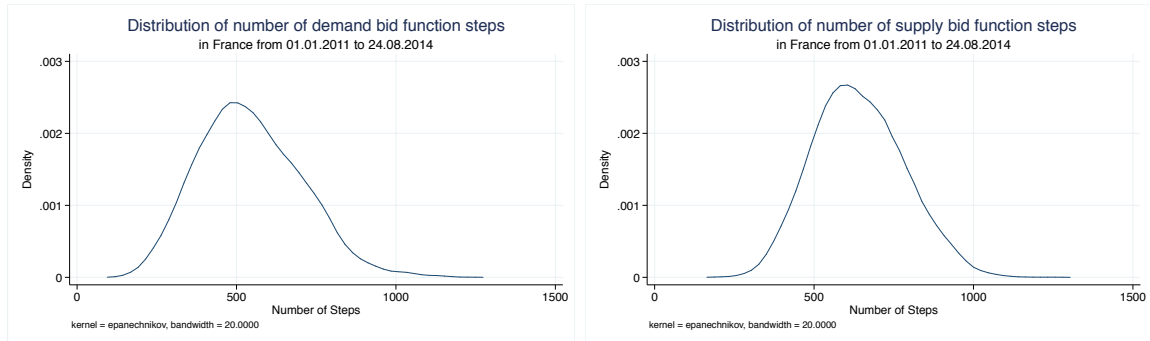


Figure 2.9.4: Distribution of number of bid function steps

On exogenous factors

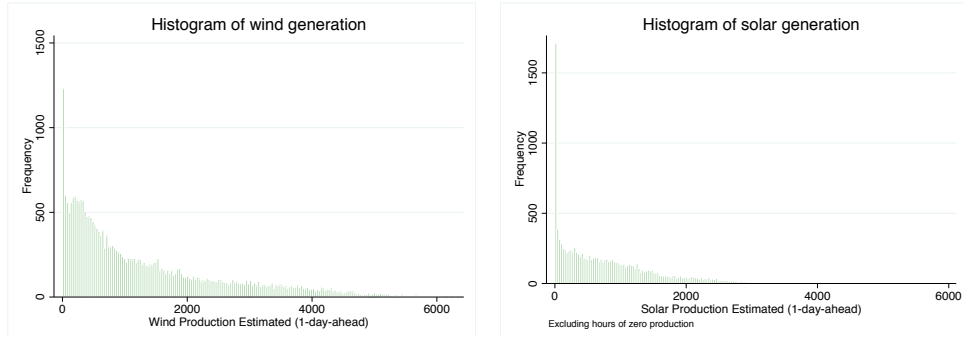


Figure 2.9.5: Histogram of predicted wind (left) and predicted solar (right) generation

For k=3 (Point of inflection)

	(1) fxInvertQP	(2) fxInvertQP	(3) fxInvertQP	(4) fxInvertQP
PLUvRvarT	0.000882 (0.00152)	0.000882 (0.00415)	0.00374** (0.00155)	0.00508 (0.00354)
PLUvRvarTsq	-0.000529 (0.000584)	-0.000529 (0.168)	-0.00161*** (0.000603)	-0.00215 (0.183)
PLUvRvarW	0.00790*** (0.00123)	0.00790*** (0.00257)	0.00647*** (0.00121)	0.00574*** (0.00207)
PLUvRvarWsq	-0.00235*** (0.000373)	-0.00235 (0.0644)	-0.00192*** (0.000370)	-0.00170 (0.0479)
PLUvRvarS	-5.20e-10 (2.68e-09)	-5.20e-10 (3.58e-08)	-2.28e-09 (3.16e-09)	-2.23e-09 (3.69e-08)
PLUvRvarSsq	0 (0)	0 (0)	0 (0)	0 (0)
Coal	6.90e-06*** (4.35e-07)	6.90e-06*** (4.64e-07)	5.18e-06*** (4.39e-07)	6.29e-06*** (6.87e-07)
Brent	-2.36e-05*** (1.51e-06)	-2.36e-05*** (1.96e-06)	-1.18e-05*** (1.53e-06)	-1.40e-05*** (2.01e-06)
Gas	-2.82e-07 (1.89e-06)	-2.82e-07 (9.41e-06)	1.37e-05*** (1.67e-06)	1.36e-05*** (2.46e-06)
IT2	-2.71e-05*** (2.17e-06)	-2.71e-05 (1.80e-05)	-1.73e-05*** (1.34e-06)	-1.99e-05*** (1.69e-06)
EUA	7.20e-05*** (2.31e-06)	7.20e-05*** (4.49e-06)	2.62e-05*** (3.34e-06)	2.71e-05*** (6.84e-06)
Wind1DA	1.04e-07*** (6.45e-09)	1.04e-07*** (1.03e-08)	1.18e-07*** (6.51e-09)	1.25e-07*** (7.63e-09)
Hydro	-7.55e-06*** (8.33e-07)	-7.55e-06*** (2.24e-06)	-4.08e-06*** (8.61e-07)	-5.88e-06*** (1.11e-06)
PLUvDvarP	-0.000219*** (4.57e-05)	-0.000219 (0.000203)		
PLUvDvarQ	0.000567*** (9.44e-05)	0.000567 (0.000585)		
PLUvDvarKP			-0.000600*** (2.69e-05)	-0.000462*** (4.24e-05)
PLUvDvarKQ			0.000151*** (3.39e-05)	0.000170** (6.80e-05)
Constant	0.00651*** (0.000208)	0.00651*** (0.000789)	0.00513*** (0.000195)	0.00538*** (0.000257)
Observations	11,702	11,702	11,702	11,702
R ²	0.200	0.200	0.233	0.234

(Standard errors in parentheses)

*** p<0.01, ** p<0.05, * p<0.1

Table 2.5: Regressions of slope on PLU^R and PLU^D and PLU^D at k = 3

Note: Standard errors are reported in parenthesis. Column 1 refers to the baseline specification. Column 2 reports bootstrapped results for the baseline model. Column 3 reports the results for the (weighted) regression on the kernel based PLU^D. Column 4 reports bootstrapped results of the model in column 3.

For k=1 (Left extremal point)

	(1) fxInvertQP	(2) fxInvertQP	(3) fxInvertQP
PLUvRvarT	-4.14e-05***	-4.14e-05	0.000277*
PLUvRvarTsq	1.56e-05***	1.56e-05	-0.0122
PLUvRvarW	-6.04e-06	-6.04e-06	-0.000138
PLUvRvarWsq	1.71e-06	1.71e-06	0.00738
PLUvRvarS	0	0	-5.70e-05
PLUvRvarSsq	-0	-0	0.00172
Coal	-8.54e-09***	-8.54e-09***	(omitted)
Brent	8.64e-08***	8.64e-08***	(omitted)
Gas	-6.20e-08***	-6.20e-08***	(omitted)
IT2	4.95e-08***	4.95e-08***	3.50e-08
EUA	-3.14e-08***	-3.14e-08***	4.43e-06***
Wind1DA	-3.38e-10***	-3.38e-10***	2.48e-10
Hydro	4.69e-08***	4.69e-08***	(omitted)
PLUvDvarQ	-3.87e-06***	-3.87e-06***	
PLUvDvarKQ			-7.21e-10***
Constant	2.11e-06***	2.11e-06**	-6.00e-05***
Observations	11,702	11,702	50
R ²	0.152	0.152	0.681

Standard errors available from the authors

*** p<0.01, ** p<0.05, * p<0.1

Table 2.6: Regressions of slope on PLU^R and PLU^D and PLU^D at k = 1

For k=2 (Left point of maximum curvature)

	(1) fxInvertQP	(2) fxInvertQP	(3) fxInvertQP
PLUvRvarT	-0.00252	-0.00252	0.292
PLUvRvarTsq	0.00106	0.00106	-17.27
PLUvRvarW	-0.00549***	-0.00549**	0.339
PLUvRvarWsq	0.00158***	0.00158	-21.86
PLUvRvarS	-6.82e-10	-6.82e-10	0.0669
PLUvRvarSsq	0	0	-1.968
Coal	2.36e-06***	2.36e-06***	(omitted)
Brent	-1.86e-05***	-1.86e-05***	(omitted)
Gas	-8.94e-06***	-8.94e-06***	(omitted)
IT2	1.98e-05***	1.98e-05***	6.92e-05
EUA	8.69e-05***	8.69e-05***	-0.000439
Wind1DA	6.13e-09	6.13e-09	6.70e-07
Hydro	-5.82e-06***	-5.82e-06***	(omitted)
PLUvDvarP	-4.81e-05***	-4.81e-05***	
PLUvDvarQ	0.000442***	0.000442***	
PLUvDvarKP			-9.62e-07*
PLUvDvarKQ			-4.27e-07
Constant	0.00319***	0.00319***	0.00279
Observations	11,702	11,702	50
R ²	0.158	0.158	0.414

Standard errors available from the authors

*** p<0.01, ** p<0.05, * p<0.1

For k=4 (Right point of maximum curvature)

	(1) fxInvertQP	(2) fxInvertQP	(3) fxInvertQP
PLUvRvarT	-0.00442***	-0.00442	0.000559
PLUvRvarTsq	0.00149**	0.00149	-0.000368
PLUvRvarW	-0.000137	-0.000137	-0.00205
PLUvRvarWsq	0.000173	0.000173	0.000739*
PLUvRvarS	2.59e-09	2.59e-09	2.40e-09
PLUvRvarSsq	-0	-0	-0
Coal	2.22e-07	2.22e-07	1.48e-06***
Brent	-7.46e-06***	-7.46e-06***	-1.30e-05***
Gas	9.04e-06***	9.04e-06***	2.04e-05***
IT2	-1.96e-05***	-1.96e-05***	-2.61e-05***
EUA	4.71e-05***	4.71e-05***	3.19e-05***
Wind1DA	1.64e-08**	1.64e-08**	1.50e-08**
Hydro	-8.73e-06***	-8.73e-06***	-1.33e-05***
PLUvDvarP	-0.000212***	-0.000212***	
PLUvDvarQ	0.000110	0.000110**	
PLUvDvarKP			-0.000163***
PLUvDvarKQ			4.08e-05
Constant	0.00370***	0.00370***	0.00406***
Observations	11,701	11,701	11,701
R ²	0.086	0.086	0.117

Standard errors available from the authors

*** p<0.01, ** p<0.05, * p<0.1

Table 2.8: Regressions of slope on PLU^R and PLU^D and PLU^D at k = 4

For k=5 (Right extremal point)

	(1) fxInvertQP	(2) fxInvertQP	(3) fxInvertQP
PLUvRvarT	-0.000252	-0.000252	0.000734***
PLUvRvarTsq	9.10e-05	9.10e-05	-0.000280***
PLUvRvarW	-0.000555***	-0.000555**	-0.000545***
PLUvRvarWsq	0.000169***	0.000169	0.000163***
PLUvRvarS	-4.17e-10	-4.17e-10	-3.07e-10
PLUvRvarSsq	0	0	0
Coal	-8.70e-07***	-8.70e-07***	-4.90e-07***
Brent	1.72e-06***	1.72e-06***	4.90e-07**
Gas	4.53e-06***	4.53e-06***	2.96e-06***
IT2	2.23e-06***	2.23e-06***	2.47e-06***
EUA	2.89e-06***	2.89e-06***	8.35e-06***
Wind1DA	-5.41e-10	-5.41e-10	3.49e-09***
Hydro	1.78e-06***	1.78e-06***	1.19e-06***
PLUvDvarQ	4.29e-05***	4.29e-05***	
PLUvDvarKQ			5.56e-05***
Constant	-0.000494***	-0.000494***	-0.000351***
Observations	11,702	11,702	11,702
R ²	0.128	0.128	0.131

Standard errors available from the authors

*** p<0.01, ** p<0.05, * p<0.1

	(1)	(2)
	PrevConsoH	PrevConsoH
Tempeff15	-682.6***	
Roll_Temp24	-802.0***	
Roll_Temp240	-1,175***	
SolarRest	-0.860***	-0.345***
suncycle	7,849***	7,418***
morning	-4,759***	-4,398***
deltasun	10,108***	9,010***
EWH	-1,245***	-1,254***
Tempeff		-301.4***
Roll_avgT24		-687.3***
Roll_avgT240		-918.2***
Constant	77,701***	76,651***
Observations	146,909	146,909
R^2	0.853	0.816

*** p<0.01, ** p<0.05, * p<0.1

Table 2.15: "Black box" regression on RTE predicted consumption

Note: The dependent variable PrevConsoH is the day ahead prediction by RTE of the total consumption in France.

X_e	m	Mean	Median	Std. dev.	Min	Max
Tempeff15	6	7.7	8	5	-10	14
Roll_Temp24	6	7.7	9	4	-8	14
Roll_Temp240	1	7.6	8	4	-7	13
suncycle	6	0.3	0	0	0	1
morning	6	0.5	1	0	0	1
deltasun	6	0.1	0.1	0	0	0.4
EWH	6	0.3	0	0	0	1
SolarRest	6	5.4	-1	364	-1,337	2,241
RteBlackBox	6	-0.0	37	4,755	-16,966	18,209

Table 2.16: Variables used in the kernel based PLU^D computation

Note: For the PLUv51, we have excluded the variable Roll_Temp240 from the conditioning in order to increase the size of each subsample used for the calculation of the observation specific PLU^D. Version 52 also conditions on the variable Roll_Temp240 using $m = 6$.

References

- [Anderson and Xu, 2005] Anderson, E. J. and Xu, H. (2005). Supply function equilibrium in electricity spot markets with contracts and price caps. *Journal of Optimization Theory and Applications*, 124(2):257–283.
- [APX, 2017] APX (2017). Type of orders on the epex day-ahead auction, uk. <https://www.apxgroup.com/trading-clearing/uk-half-hour-day-ahead-1530-auction/>.
- [Arima, 2012] Arima, K. (2012). Dispatch modelling: Quantifying long term benefits via high resolution analysis. Technical report, Wärtsilä Power Plants.
- [Berg et al., 1999] Berg, S. A., Boukai, B., and Landsberger, M. (1999). Bid functions for treasury securities; across countries comparison. Technical report, Citeseer.
- [Bergès and Martimort, 2014] Bergès, A. and Martimort, D. (2014). Dynamics of the electricity day-ahead market : Supply function equilibria and ramping costs. Technical report, Paris School of Economics.
- [Bertoldi and Atanasiu, 2007] Bertoldi, P. and Atanasiu, B. (2007). Electricity consumption and efficiency trends in the enlarged european union, status report. Technical report, Institute for Environment and Sustainability, European Commission.
- [Boiteux, 1960] Boiteux, M. (1960). Peak-load pricing. *The Journal of Business*, 33(2):157–179.
- [Bolle, 1992] Bolle, F. (1992). Supply function equilibria and the danger of tacit collusion: the case of spot markets for electricity. *Energy economics*, 14(2):94–102.
- [Borenstein et al., 2002] Borenstein, S., Bushnell, J. B., and Wolak, F. A. (2002). Measuring market inefficiencies in california’s restructured wholesale electricity market. *American Economic Review*, 92(5):1376–1405.
- [Boukai and Landsberger, 1998] Boukai, B. and Landsberger, M. (1998). Market bid functions for treasury securities as logistic growth curves. Technical report, Working Paper, Indiana University–Purdue University, Indianapolis, Indiana.
- [Boyle, 2007] Boyle, G. (2007). *Renewable Electricity and the Grid, the Challenge of Variability*. Routledge.
- [EPEX, 2014] EPEX (2014). Website of the european power exchange.
- [EPEX, 2015] EPEX (2015). Type of orders on the epex day-ahead auction, france. <https://www.epexspot.com/en/product-info/auction>.

- [GE, 2015] GE (2015). Heavy-duty gas turbine operating and maintenance considerations. Technical report, General Electrics Energy.
- [Green, 1991] Green, R. (1991). Reshaping the cegb: electricity privatization in the uk. *Utilities Policy*, 1(3):245–254.
- [Green, 1999] Green, R. (1999). The electricity contract market in england and wales. *The Journal of Industrial Economics*, 47(1):107–124.
- [Green and Newbery, 1992] Green, R. J. and Newbery, D. M. (1992). Competition in the british electricity spot market. *Journal of political economy*, 100(5):929–953.
- [Hobbs, 2001] Hobbs, B. F. (2001). *The next generation of electric power unit commitment models*, volume 36. Springer.
- [Hortacsu and Puller, 2008] Hortacsu, A. and Puller, S. L. (2008). Understanding strategic bidding in multi-unit auctions: a case study of the texas electricity spot market. *The RAND Journal of Economics*, 39(1):86–114.
- [Kastl, 2011] Kastl, J. (2011). Discrete bids and empirical inference in divisible good auctions. *The Review of Economic Studies*, 78(3):974–1014.
- [Klemperer and Meyer, 1989] Klemperer, P. and Meyer, M. (1989). Supply function equilibria in oligopoly under uncertainty. *Econometrica*.
- [LaCommare and Eto, 2004] LaCommare, K. H. and Eto, J. H. (2004). Understanding the cost of power interruptions to us electricity consumers. *Lawrence Berkeley National Laboratory*.
- [Meibom et al., 2009] Meibom, P., Weber, C., Barth, R., and Brand, H. (2009). Operational costs induced by fluctuating wind power production in germany and scandinavia. *Renewable Power Generation, IET*, 3(1):75–83.
- [Newbery, 1998] Newbery, D. M. (1998). Competition, contracts, and entry in the electricity spot market. *The RAND Journal of Economics*, pages 726–749.
- [Özcan, 2004] Özcan, R. (2004). The logistic function approach to discriminatory and uniform price treasury auctions.
- [Préget and Waelbroeck, 2005] Préget, R. and Waelbroeck, P. (2005). Treasury bill auction procedures: Empirical perspectives from french market bid functions. *Journal of International Money and Finance*, 24:1054–1072.
- [Reguant, 2011] Reguant, M. (2011). The welfare effects of complementary bidding mechanisms: An application to electricity markets. Technical report, Working paper.
- [Reichl et al., 2013] Reichl, J., Schmidthaler, M., and Schneider, F. (2013). Power outage cost evaluation: Reasoning, methods and an application. *Journal of Scientific Research & Reports*, 2(1):249–276.
- [REN21, 2013] REN21, S. C. (2013). Renewables 2013, global status report.
- [RTE, 2014] RTE (2014). Website of rte, the french grid operator.

- [Salgado-Ugarte et al., 1994] Salgado-Ugarte, I. H., Shimizu, M., and Taniuchi, T. (1994). Exploring the shape of univariate data using kernel density estimators. *Stata Technical Bulletin*, 3(16).
- [Seierstad and Sydsæter, 1987] Seierstad, A. and Sydsæter, K. (1987). *Optimal Control Theory with Economics Applications*. North-Holland.
- [Sewalt and De Jong, 2003] Sewalt, M. and De Jong, C. (2003). Negative prices in electricity markets. *Commodities Now*, 2:74–79.
- [Silverman and Ramsay, 2005] Silverman, B. and Ramsay, J. (2005). *Functional Data Analysis*. Springer.
- [Silverman, 1986] Silverman, B. W. (1986). *Density estimation for statistics and data analysis*, volume 26. CRC press.
- [White, 1980] White, H. (1980). A heteroskedasticity-consistent covariance matrix estimator and a direct test for heteroskedasticity. *Econometrica: Journal of the Econometric Society*, pages 817–838.
- [Wolak, 2007] Wolak, F. A. (2007). Quantifying the supply-side benefits from forward contracting in wholesale electricity markets. *Journal of Applied Econometrics*, 22(7):1179–1209.
- [Wolfram, 1998] Wolfram, C. D. (1998). Strategic bidding in a multiunit auction: An empirical analysis of bids to supply electricity in england and wales. *The Rand Journal of Economics*, pages 703–725.
- [Wolfram, 1999] Wolfram, C. D. (1999). Measuring duopoly power in the british electricity spot market. *American Economic Review*, pages 805–826.

List of Figures

1.1	a b	22
1.2	This graph plots $S^*(p)$ for different values of the ramping cost parameter, and compares them to the set of equilibria obtained in KM's framework. Four optimal supply schedules are plotted. The black curve (full line) corresponds to the case where $\gamma \rightarrow 0$. As before, as γ increases the optimal schedules get steeper and steeper until in the limit of $\gamma \rightarrow \infty$, the optimal schedule attains a vertical slope. In addition, we show the set of available equilibria in KM's model in light green, and the extremal demand schedules in dashed black.	25
1.3	This graph plots an envelope of constant average value but varying width $\omega(t)$. By comparing regions of increasing or decreasing width, respectively the left or right side of a lobe, one sees that the informativeness of the envelope is being respectively reduced or increased with respect to a situation where the width would be kept constant. The change in informativeness is represented by the area between the (full) green arrows (observed level of informativeness) compared to the area between the (dashed) red arrows (level of informativeness had the width been constant). In addition, by comparing the left lobe to the right one, it is possible to see why the relative variation of the width, and not the absolute variation of the width, matters. For a larger width (right lobe) and the same rate of change in the width, there is less change in informativeness than for a smaller width (left lobe), i.e. the same rate of change matters less for the right lobe than for the left lobe.	28
2.0.1	Illustrating the effect of increased uncertainty.	42
2.1.1	Traded volume plotted against total annual consumption	43
2.2.1	Example aggregate demand and supply bid functions	46
2.2.2	Aggregate bid functions for 20 consecutive days	47
2.3.1	Selected points on original bid functions	49
2.3.2	Example of an assymetric aggregate supply function. In red is the actual aggregate function, in green is an estimated logistic function showcasing the large discrepancies that can arise with this parametric approach. The blue point is the market outcome.	51
2.3.3	Comparison of two aggregate demand functions for the same hour . . .	53
2.3.4	Steps of the point selection process	53
2.3.5	Temperature based seasonality controls	61
2.3.6	Continuous controls for daily patterns	62
2.7.1	Heat map on selected, comparable demand and supply points	79
2.7.2	Distribution of selected demand (left) and supply (right) points	80
2.7.3	Histogram of slopes per point type	81
2.7.4	Error bars as a function of the number of extracted points	83

2.7.5	Proxy for degrees of freedom on master curve	84
2.7.6	Overall (left) and zoomed (right) Mastercurve with confidence interval	84
2.7.7	Comparison of bandwidths: Large bandwidth in first stage	88
2.7.8	Comparison of bandwidths: Small bandwidth in first stage	89
2.7.9	Histogram of volume variation between points	90
2.8.1	Stations for which we have hourly data. Left : temperature, center : wind speed, right : light intensity.	92
2.8.2	Left: Voronoi's algorithm is applied once on the reference points highlighted in green to obtain the white surfaces, and a second time on the same points to which is added the query point in the center to obtain the new blue cell. The green circles, which represent the interpolating weights, are generated using the ratio of the shaded area to that of the cell area of the surrounding points. Center left: example of a reference surface (color mapped) to be reconstructed through a natural neighbour interpolation. Center right: interpolated surface with a reference set of 16 evenly organised points, represented in black. Right: interpolated surface with a reference set of 16 unevenly organised points, represented in black. From 16 points one is able to reconstruct the color mapped surfaces which aim at being able to reproduce the reference one, represented in the center left image.	93
2.8.3	Temperature forecast from a simulation run by the GFS at 6 a.m. on the 3rd of november 2011, for a forecast at 22 p.m.	93
2.8.4	Left: reference image. Center left: borders and numbers are removed. Center right: edge recognition. Right: final fitted surface.	94
2.8.5	Autocorrelation lengthscale computation. In black are the points obtained from all the pairs from our original data, that is absolute wind speed differences as a function of the distance between the two points. In blue is the kernel smoothed function from those points. In red is the exponential fit. In black are the derivatives of the fit at 0 and ∞ . In green is the recovered autocorrelation lengthscale. The unit for the lengthscale is in km.	96
2.8.6	Typical response curves of different wind turbines	97
2.8.7	All curves are hourly production data. The origin of the hours is the first of January 2011, and the production is in MWh. In blue: the observed wind production. In dark red: the day-ahead predictions from the grid operator. In light red: the day-ahead predictions from weather data.	98
2.8.8	Daily electricity consumption in France as a function of the temperature	98
2.8.9	Hourly solar production in MWh. The time origin is the first January 2011. In blue: observed production by RTE. In dark red: reconstructed production from observed weather data.	100
2.9.1	Plotted average realised Volume (left) and Price (right) per Hour with 95% confidence intervals.	103
2.9.2	Distribution of observed market equilibria	103
2.9.3	Distribution of minimum and maximum production volumes (and corresponding range) bid in an hourly auction.	104
2.9.4	Distribution of number of bid function steps	104
2.9.5	Histogram of predicted wind (left) and predicted solar (right) generation	104

Table of Contents

Remerciements—Acknowledgements	i
General introduction	1
Summary	5
Chapter 1: Dynamics of the Electricity Day-Ahead Market : Supply Function Equilibria and Ramping Costs	9
1.1 Introduction	11
1.2 Heuristic Description of the Model	14
1.3 Stochastic Dynamics	16
1.3.1 The stochastic process	16
1.3.2 The ramping costs	17
1.3.3 Discussion of the approximations	19
1.3.4 The maximisation program	19
1.4 The Monopoly	20
1.5 The Symmetric Oligopoly	23
1.6 Dynamic behavior of the bids	25
1.6.1 Results	26
1.7 Discussion	29
1.8 Concluding Remarks	29
Appendix	30
Appendix 1.A Proof of Proposition 1.4.1	30
Appendix 1.B Proof of Proposition 1.5.1	32
Appendix 1.C Proof of proposition 1.6.1	34
Appendix 1.D Proof of proposition 1.6.2	34
Chapter 2: Investigating the Impact of Uncertainty on Firms with Dynamic Costs : A Case Study of the French Electricity Market	35
2.0.1 Literature review and contribution	39
2.0.2 Theoretical prediction	41
2.1 The EPEX spot market	43
2.1.1 General background	43
2.1.2 Auction rules and mechanism	44
2.2 Our data explained	45
2.3 Methodology	48
2.3.1 Point selection	50
2.3.2 Regression methodology	54
2.4 Results	64
2.4.1 Demand estimation	64

2.4.2	Final regression	69
2.5	Discussion	73
2.5.1	Findings	73
2.5.2	Internal and external validity	75
2.5.3	Endogeneity	76
2.6	Conclusion	78
2.7	Results of the point selection methodology	79
2.7.1	Precision of point selection	79
2.7.2	Observations of bidding frictions	80
2.7.3	Value of selected points (determining K)	82
2.7.4	Discussion and Conclusion	84
2.7.5	Technical details	85
2.7.6	Outlier detection and removal	89
2.7.7	Summary statistics of selected points	90
2.8	Appendix: Technical details on PLU ^R	91
2.8.1	Methodology to aggregate geographically dispersed information on a national level	91
2.9	Appendix : Computational details and descriptives	102
2.9.1	Hard choices in the PLU computation	102
2.9.2	Descriptive Statistics	103
References		109
List of Figures		112